Characterization of Additively Manufactured All-Aromatic Polyimide as a Dielectric Substrate for Conductive Direct-Write Silver Inks

Thomas Edward Oja

Thesis submitted to the faculty of Virginia Polytechnic Institute and State University in partial fulfillment of the requirements for the degree of

Master of Science

In

Mechanical Engineering

Christopher B. Williams

Bradley A. Davis

Michael D. Bartlett

October 1, 2020
Blacksburg, VA

Keywords: Additive Manufacturing, 3D Printing, Printed Electronics, Materials

Characterization of Additively Manufactured All-Aromatic Polyimide as a Dielectric Substrate for Conductive Direct-Write Silver Inks

Thomas Oja

Academic Abstract

Hybridizing additive manufacturing (AM) structures and direct write (DW) deposition of conductive traces enables the design and physical creation of integrated, complex, and conformal electronics such as embedded electronics and complex routing on a fully AM structure. Although this hybridization has a promising outlook, there are several key AM substrate-related limitations that limit the final performance of these hybridized AM-DW electronic parts. These limitations include low-temperature processability (leading to high trace resistivity) and poor surface finish (leading to electronic shorts and disconnections). Recently discovered ultraviolet-assisted direct ink write (UV-DIW) all-aromatic polyimide (PI) provides an opportunity to address these previous shortcomings previously due to its high-temperature stability (450C) and superior surface finish (relative to other AM processes).

The primary goal of this thesis is to characterize the integration of this UV-DIW PI with DW-printed conductive inks as a means for obtaining high-performance hybrid AM-DW electronics. This goal has been achieved through an investigation into the increased temperature stability of AM PI on the conductivity and adhesion of DW extrusion and aerosol jet (AJ) silver inks, determining the dielectric constant and dissipation factor of processed UV-DIW PI, and determining the achievable microwave application performance of UV-DIW PI. These performance measurements are compared to commercially-available PI film and relative to existing AM substrates, such as ULTEM 1010.

The temperature stability of UV-DIW PI enabled higher-temperature post-processing for the printed silver traces, which decreased DIW trace resistivity from 14.94±0.55 times the value of bulk silver at 160 °C to 2.16±0.028 times the resistivity of bulk silver at 375 °C, and AJ silver trace resistivity from 5.27±0.013 times the resistivity of bulk silver at 200 °C to 1.95±0.15 times the resistivity of bulk silver at 350 °C. The adhesion of these traces was not negatively affected by higher processing temperatures, and the traces performed similarly on UV-DIW PI and commercial PI. Furthermore, at similar thicknesses, UV-DIW PI was found to have a similar dielectric constant and dissipation factor to commercial Dupont Kapton PI film from 1 kHz to 1 MHz, indicating its ability to perform highly as a dielectric electronics substrate. Finally, the decrease in resistivity was able to decrease the gap in microwave stripline transmission line performance when compared with ULTEM 1010 processed at 200°C, with peak 10 GHz S21 loss differences decreasing from 2.46 dB to 1.32 dB after increasing the UV-DIW processing temperature from 200 °C to 400°C.

Characterization of Additively Manufactured All-Aromatic Polyimide as a Dielectric Substrate for Conductive Direct-Write Silver Inks

Thomas Oja

General Audience Abstract

Due to the extensive potential benefits and applications, researchers are looking to hybridize additive manufacturing (AM) processes with direct write (DW) techniques to directly print a 3D part with integrated electronics. Unfortunately, there are several key substrate-related limitations that hinder the overall performance of a part fabricated by hybrid AM-DW processes. Specifically, typical AM materials are not capable of providing an electronics substrate with combined sufficient surface resolution, surface finish, and high-temperature processing stability. However, the recent discovery of a novel AM-processable all-aromatic polyimide (PI) presents an opportunity for addressing these limitations as its printed form offers a high surface resolution, superior surface finish, and mechanical stability up to 400 °C.

The primary goal of this thesis is to evaluate the benefits and drawbacks of this PI, processed via ultraviolet-assisted direct ink write (UV-DIW) AM, as an AM-DW electronics substrate. Specifically, the author characterized the effect of the increased temperature stability of the printed PI on the resultant conductivity and adhesion of silver inks printed via direct ink write (DIW) and aerosol jetting (AJ) DW processes. These results were also compared to the performance of the inks on commercial PI. Furthermore, the dielectric performance of printed PI was evaluated and compared to commercial PI. To demonstrate and evaluate the hybridized approach in a potential end-use application, the author also characterized the achievable microwave application performance of UV-DIW polyimide relative to the existing highest performance commercially available printed substrate material.

The experiments in this thesis found an 83% and 66% decrease in resistivity from extrusion and AJ printed inks due to the ability of the printed PI to be processed at higher temperatures. Furthermore, UV-DIW PI was found to have similar dielectric properties to commercial PI film, which indicates that it can serve as a high-performance dielectric substrate. Finally, the high-temperature processing stability was able to decrease the performance gap in microwave application performance between the higher performing dielectric substrate, ULTEM 1010. These results show that UV-DIW could serve as a dielectric substrate for hybridized AM-DW electronic parts with higher performance and the ability to be deployed in harsher environments than previous AM-DW electronic parts explored in literature.

Table of Contents

Table of Figures

Chapter 1

Chapter 2

Chapter 3

Chapter 4

Chapter 5

Appendix B

Table of Tables

Chapter 2

Chapter 3

Chapter 4

Chapter 5

Appendix A

1. Introduction to Additive Manufacturing and Direct Write Electronics

Like the name suggests, AM technologies employ a process in which layers are added one by one to build a desired geometry from the ground up. This ground-up approach minimizes waste and allows for complex geometries to be created in computer aided design (CAD) software and exported to an AM system in rapid fashion with seemingly limitless design complexity. Direct-write is a class of deposition methods which stands out as a means to directly deposit conductive inks for electronics purposes (detailed in Section 1.2). With these methods, structural AM technologies have the ability to be hybridized with direct write electronics printing. This hybridization enables the design and physical creation of integrated, complex, and conformal electronics housed in a spatially efficient and structurally sound product [1].

Hybridizing AM and direct write (DW) electronics has a promising outlook, boasting the ability to create embedded electronics, conformal passive electronics, and complex active electrical signal routing in and on a fully additively manufactured structure. Robinson and coauthors took advantage of this hybridization through combining a form of sheet lamination AM, ultrasonic consolidation (UC), and direct write of silver based ink to create an integrated circuitry within a honeycomb-based structure, as seen in Figure 1.1 [2]. Many other examples of novel AM-DW electronics structures have been studied in literature, as documented in Section 2.3

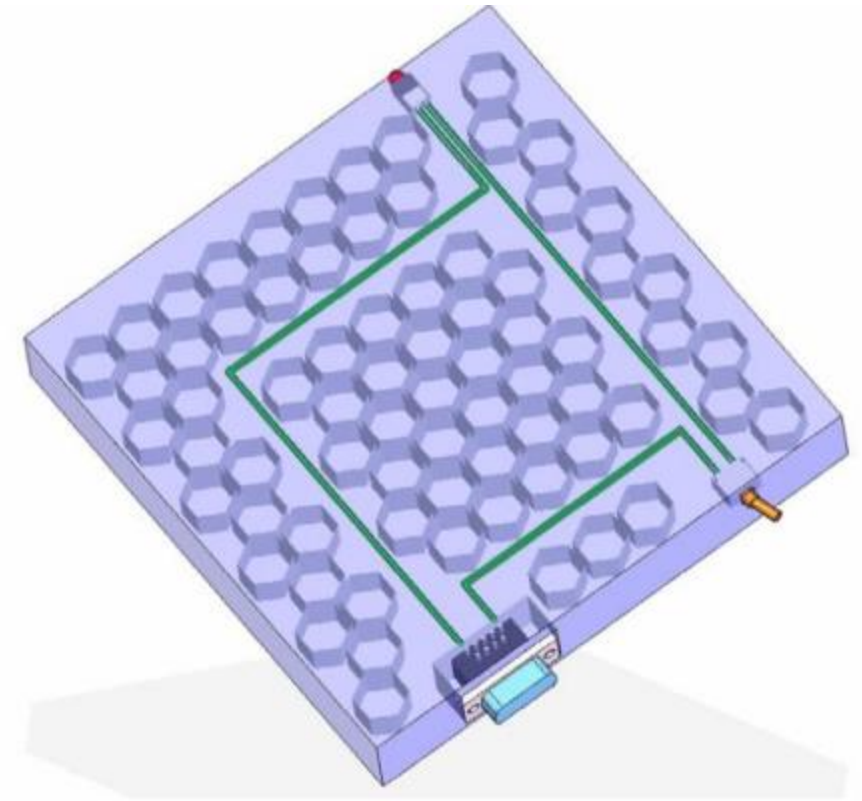

Figure 1.1: CAD model showing the hybridizing of UC and DIW to create an embedded circuit within an AM honeycomb structure [2].

While the hybridization of AM and DW electronics seems to possess limitless potential, there are drawbacks that must be considered. As stated by Espalin and coauthors, AM materials and methods must possess high performance dielectric substrate properties, high spatial resolution, superior surface finish, and DW ink with bulk level conductivities [3]. Unfortunately, there are currently no widely available commercial AM materials capable of fulfilling all of these performance targets.

Recently, scientists and engineers at Virginia Tech have developed multiple methods for the additive manufacturing of all-aromatic polyimide, similar in chemistry and properties to commercial Dupont Kapton, using multiple AM methods [4] [5]. This all-aromatic polyimide AM material provides a high-performance dielectric substrate, high spatial resolution, superior surface finish, and a high-temperature processing limit allowing for post-processing of conductive inks at higher temperatures than allowed by typical AM substrates, leading to higher conductivity traces. **The primary goal of this thesis is to**

characterize the integration of this all-aromatic polyimide with the direct write of electronics as a viable means for obtaining high-performance hybrid AM-DW electronics, previously unexplored in literature. To achieve this goal, the following **research objectives are pursued:**

(i) characterize the effect of increasing the processing temperature of commercially available direct write conductive inks on the ink resistivity and adhesion on Dupont Kapton substrate

(ii) evaluate the resistivity and adhesion of these DIW conductive inks processed at higher temperatures on the all-aromatic polyimide substrate and compare to that on Dupont Kapton

(iii) characterize the dielectric performance of the AM all-aromatic polyimide

(iv) demonstrating how the dielectric properties and high-temperature processing capabilities of all-aromatic polyimide affect its RF performance compared to other high-performance dielectric substrates.

1.1 Additive Manufacturing

As AM technology field advances and expands, researchers and large manufacturers and are now viewing AM technologies as a feasible method for obtaining high-performance parts with tunable material properties, rather than just an interesting concept with promising potential. With a wide array of modern technologies ranging from friction stir metal alloy extrusion to continuous liquid interphase photopolymeriziation, modern AM systems are classified in seven modalities: vat photopolymerization, powder bed fusion, material extrusion, sheet lamination, binder jetting, direct energy deposition, and material jetting. [6] [7] [8].

The generic AM process begins with a 3D model with a final AM printed part. The software creates a full structure geometry and then outputs the 3D model file, typically an STL file, so that either another software built-in or separate from an AM system can manipulate the file. This manipulation typically

involves slicing the STL file into layers of predetermined thickness. Thinner layers provide a more accurate representation of the original design intent and a better surface finish. The AM system then takes this layer-by-layer information and builds the part with little to no monitoring.

In this thesis, the AM process used will focus on ultraviolet assisted direct ink write (UV-DIW) to produce the all-aromatic polyimide substrate. This technology is represented by the red line on the morphological matrix in Figure 1.2. This unique AM process represents a functional combination of vat photopolymerization and material extrusion, wherein photopolymer resin is selectively extruded through a pneumatic syringe nozzle and then photocured in a layer-by-layer fashion. After printing the photocured polyimide precursor requires post-processing drying and thermal imidization to chemically convert it to the fully-aromatic polyimide structure and achieve the desired high-performance properties. Rau and coauthors explain this process using the diagram shown in Figure 1.3 [5]. Although this material can also be printed using traditional vat photopolymerization, UV-DIW has an advantage in its ability to print materials simultaneously, within the same layer, to achieve multimaterial parts. Unlike vat photopolymerization, UV-DIW also allows for the all-aromatic polyimide to be printed directly onto a preexisting material or structure [9]. This ability could be useful for printing a dielectric electronics substrate part onto a preexisting surface or part.

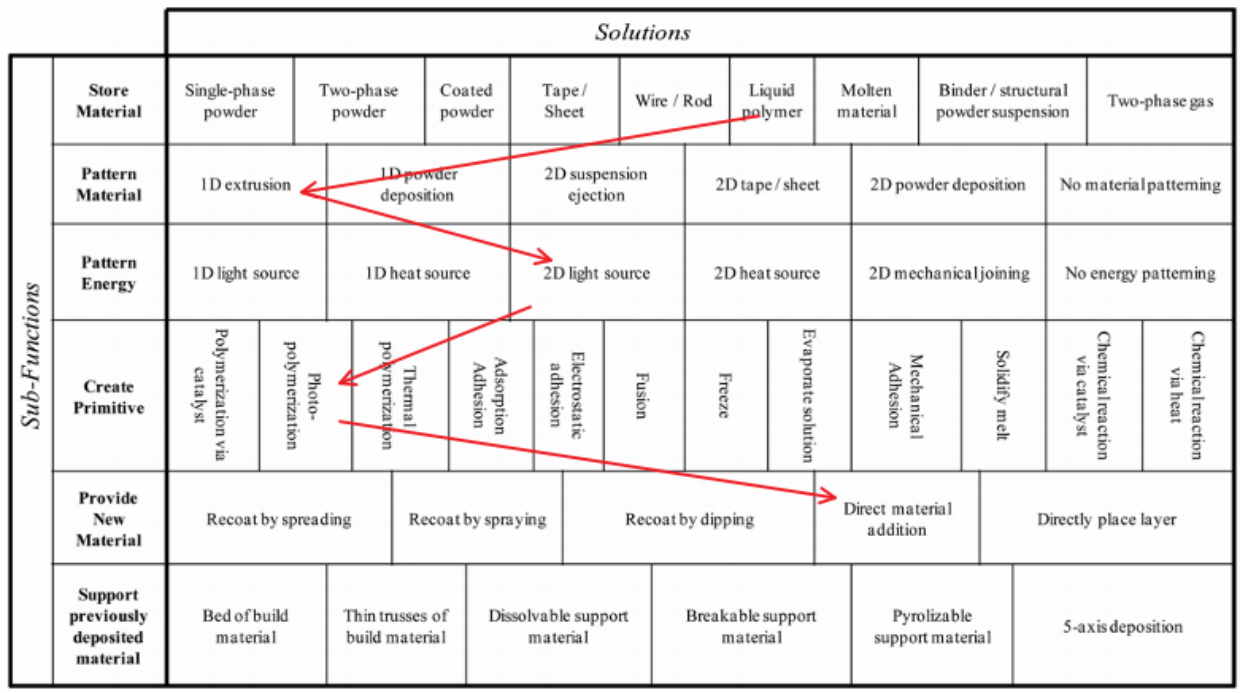

Figure 1.2 AM morphological matrix detailed AM systems desired subfunctions and chosen solutions. [10]. The UV-DIW AM process is shown by the red line.

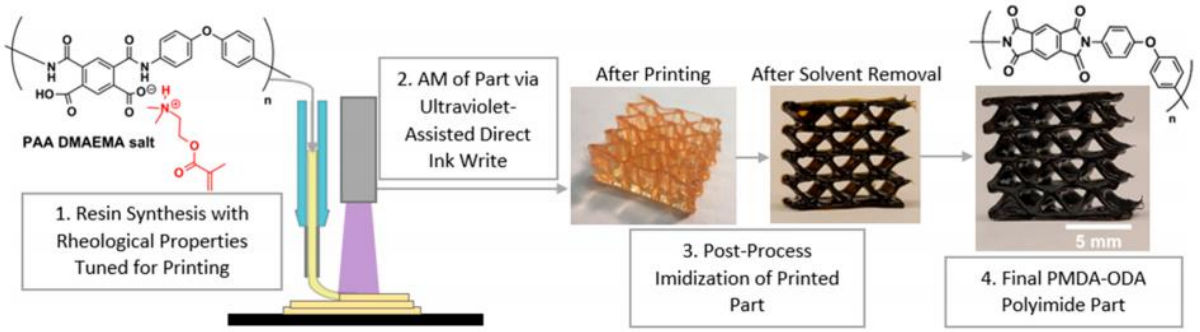

Figure 1.3 Process summary diagram of printing all-aromatic polyimide using UV-DIW and drying and thermal post-processing [5].

1.2 Direct Write of Electronics

Direct writing is a form of material deposition techniques broadly describing a variety of technologies that selectively deposition of functional materials, such as conductive inks, on flat or conformal substrates to, produce simple patterns or complex structures [11]. Hon and coauthors review and classify direct writing into the methods shown in Figure 1.4. The methods 'Flow' and 'Droplet' will be utilized in this thesis as a means to selectively deposit conductive traces on a polyimide substrate and

will be explained in detail in Chapter 2. 'Energy' beam DW involves the deposition of materials through laser or focused ion beams. 'Tip' DW involves dip-pen lithography with molecules diffusing onto a substrate through micro-capillary or micro-pipette action between the tip and the surface to create an ordered pattern [11].

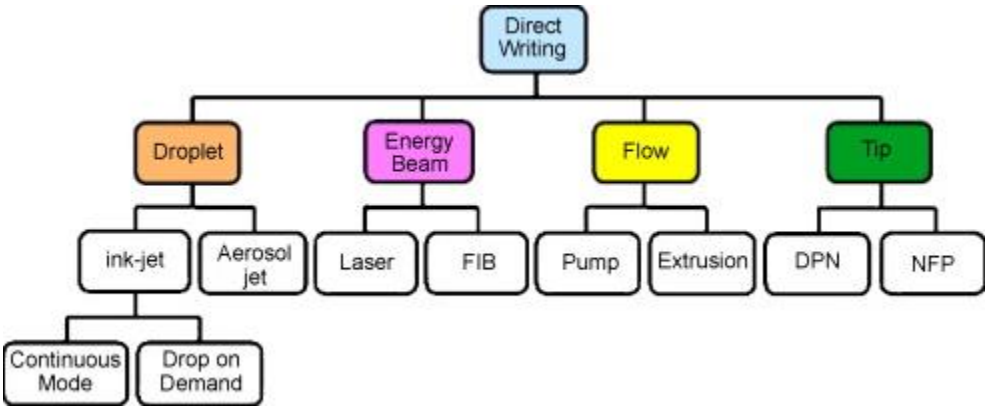

Figure 1.4: Direct writing classification of methods extensively reviewed by Hon and coauthors [11].

The methods 'Flow' and 'Droplet' will be utilized in this thesis as a means to selectively deposit conductive traces on a polyimide substrate and will be explained in detail in Chapter 2. 'Energy' beam DW involves the deposition of materials through laser or focused ion beams. 'Tip' DW involves dip-pen lithography with molecules diffusing onto a substrate through micro-capillary or micro-pipette action between the tip and the surface to create an ordered pattern [11].

The wide array of available technologies also allows a variety of direct write material formulations to be used for forming conductive traces. Hoey and coauthors assert that direct write technologies, specifically aerosol jetting, have advantages over traditional lithography-based processes for depositing conductive traces. These advantages include serving as a maskless, time reducing, lower cost, higher material utilization, and more environmentally friendly method for producing microelectronics on a variety of conformal and non-conformal surfaces [12].

Combining direct write technologies with additive manufacturing systems allows for the design and creation of highly complex and spatially efficient high-performance electronics with a wide array of

applications (discussed further in Section 2.3). However, as briefly discussed earlier, to achieve high performance this combination must feature substates with high special resolution and superior surface finish. While some AM processes are capable of depositing materials at high resolution and surface finish, the materials feature low processing temperature limits which decreases the conductivity of the direct write inks. This thesis will investigate the potential of additively manufactured all-aromatic polyimide to serve as a high-temperature capable substrate with high special resolution and superior surface finish to provide a high-performance electronic multifunctional 3D structure, previously unachievable with traditional AM materials.

1.3 Thesis Road Map

This thesis will discuss and demonstrate the feasibility and applications of combining AM all-aromatic polyimide with aerosol jetting and flow pump direct write of silver particle ink for the creation of high-performance conformal electronics. The additive manufacturing of all-aromatic polyimide provides a novel material, similar to commercial Dupont Kapton, with physical and chemical properties desirable for multifunctional electronic parts. These properties (discussed further in Section 2.5) provide the means to eliminate some of the limitations encountered commonly found when combining AM materials with direct write electronics, which include low spatial resolution, undesirable surface finish causing shorts between conductive traces, and low temperature processing capabilities causing low conductivity traces (discussed further in Section 2.4). To demonstrate this concept, silver particle inks will be directly printed on both the AM-produced all-aromatic polyimide and commercial Dupont Kapton film as a point of comparison. Their integration feasibility, advantages, disadvantages, and applications will be investigated and compared.

The ultimate goal and application of the all-aromatic polyimide discussed in this thesis involves hybridizing the printing AM structural polyimide substrate and conductive traces in one system. However, this hybridization presents some challenges giving the printed solvent-laden gel of the

polyimide precursor. As a result, this thesis is scoped to characterize only the printing of conductive traces onto an already imidized polyimide substrate. This investigation will provide valuable findings regarding the possible advantages and limitations involving the ultimate goal of hybridized printing of a UV-DIW polyimide precursor structure with DW conductive traces.

In Chapter 2, a review of the integration of direct write electronics and additively manufactured parts is discussed in detail. This review includes an in-depth look at conductive direct write inks, aerosol jetting, and extrusion pumping. Previous examples and applications of direct write electronics integration with additively manufactured parts is discussed along with the current limitations regarding the combination of the two technologies. High-performance AM dielectric substrates, with an emphasis on novel AM all-aromatic polyimide, are also discussed.

Chapter 3 and Chapter 4 present the research questions to be answered in this thesis along with the experimental methods, results, and explanation required to answer those questions. More specifically, the experiments required to characterize the feasibility, advantages, disadvantages, and possible applications of combining direct write electronics and AM all-aromatic polyimide are presented and their results are documented. The research questions which guides this work include:

i. How does increasing the processing temperature of silver-loaded conductive inks printed onto Dupont Kapton affect conductivity and adhesion?
ii. How does the silver-loaded conductive trace conductivity and adhesion performance compare when printed on AM all-aromatic polyimide versus commercial Dupont Kapton?
iii. How does the dielectric performance of additively manufactured all-aromatic polyimide compare to commercial Dupont Kapton and similar high-performance AM polymer substrates?
iv. How does the dielectric performance and high temperature processing limit effect the RF performance of the all-aromatic polyimide and how does its performance compare to ULTEM 1010?

Conclusions to the topics discussed in Chapter 3 and Chapter 4 are presented in Chapter 5. These conclusions include the possible further applications of combining AM all-aromatic polyimide with direct write electronics. Future research questions regarding investigating the potential of direct write electronics along with novel AM materials such as all-aromatic polyimide is also presented.

2. Review of Direct Write Electronics for Additive Manufacturing

To gain a full understanding of the current state of the art with integrating direct write and additive manufacturing technologies for the sake of fabricating integrated structural electronics, a review of the relevant direct write technologies, systems, integration, application, limitations, and high-performance dielectric substrates is necessary. This review also provides some of the necessary background knowledge and identification of gaps in literature required to formulate and answer the research questions presented in discussed in Chapter 3 and Chapter 4. Specifically, this review discusses current direct write of electronics systems, aerosol jet (AJ) and flow DIW of electronic materials (Section 2.2), previous integration and application of AJ and DIW electronics with AM (Section 2.3), limitations integrating AM and DW electronics (Section 2.4), and currently available high-performance AM dielectric substrates (Section 2.5).

2.1 Conductive Ink Direct Write Technologies and Materials

The direct write technologies focused on by this review must be compatible with additive manufacturing technology, allowing for possible embedding and layer by layer circuit building. The DW technologies must have high resolution XYZ positioning capable of depositing high conductivity inks over surfaces. Among the direct write technologies reviewed by Hon et al. and Teh et al., the aerosol jet, extrusion, and inkjet direct write methods are most compatible with AM [11] [13]. This claim is asserted by Perez and Williams in their AM-DW integrated electronics review, in which they state that other direct write technologies are characterized by incompatible reaction environments and tools difficult to integrate with AM processes [1].

2.1.1 Aerosol Jetting DW

Aerosol jetting is a broad term used to describe the contactless selective deposition of accelerated aerosolized suspended ink particles. A broad array of customizations on the concept have

been developed including single nozzle deposition [14], multi nozzle deposition [15], lens-focusing deposition [16], and microcold spray deposition [17], as reviewed by Hoey and coauthors [12]. Typically, the particles are atomized using either an ultrasonic or pneumatic atomizer and then carried by nitrogen gas to the deposition head and focused by a secondary stream of nitrogen 'sheath' gas to create very fine lines and prevent particle clogging at the deposition tip. A diagram showing this process using an ultrasonic atomizer is shown in Figure 2.1 [18]. With this system, the dispensing tip remains stationary while the platen holding the substrate moves in the XY plane at a customizable speed. As illustrated, the nitrogen carrier gas and sheath gas are independently varied depending on the desired print qualities. Increasing the carrier gas increases the volume of material deposited on the substrate. Alternatively, increasing the sheath gas decreases the diameter of the deposited material, altering the resulting material line width [19].

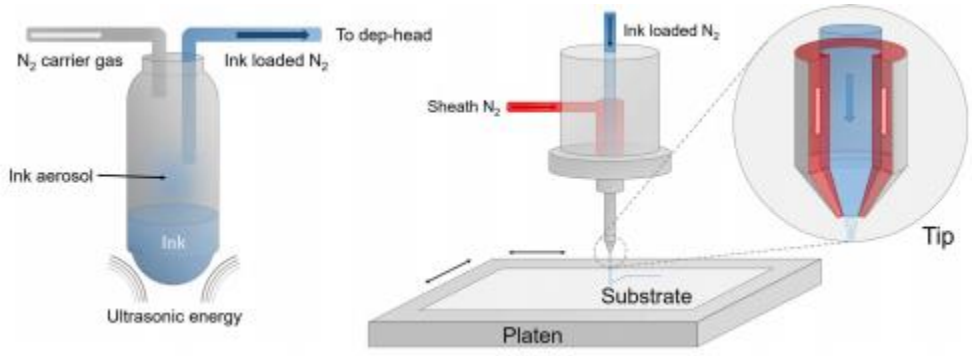

Figure 2.1: Diagram of aerosol jet printing using an ultrasonic atomizer to atomize the ink particles [18].

One of the main advantages of the aerosol jet (AJ) system is its ability to print high resolution features with a wide variety of inks. The AJ is capable of depositing features with 10µm resolution, making it ideal for microelectronic applications [18].

Compared to other DW methods, the AJ system is not limited by an ink's viscosity, rather it is only limited by the ink's ability to be atomized, making it capable of printing inks with viscosity typically ranging from 1 to 1000 cP. Depending on the ink, atomization process, and deposition head size, AJ printing systems are typically capable of these high resolution inks at up to 300mm/s allowing for rapid

printing of desired geometries [12]. Additionally, the standoff of the dispensing tip to the substrate is variable from 1 to 5mm without sacrificing print quality, allowing for simple conformal printing on non-uniform or curved surfaces [20]. This flexibility warranted by the AJ process, has allowed the printing of a wide array of materials including metals [21], carbon nanotubes and graphene [22] [23], polymers [24], and biological materials [25]. Often, these materials can be printed in the form of suspended nanoparticles due to the aerosolization process allowing for solvent to be evaporated in the heatable tube and platen.

The material flexibility, high print speeds, and variable deposition standoff distance make the aerosol jet system well-suited for integration with AM systems. The high resolution of the printed traces has the potential to print complex arrays of microelectronics, allowing for a wide scope of integration applications.

2.1.2 Material Extrusion DIW

Material extrusion direct ink write (DIW) is achieved through continuous flow of ink through a syringe under positive mechanical pressure. This positive mechanical pressure can be achieved through air pressure, mechanical extrusion pressure, or a positive displacement pump. The two most common methods to achieve this include syringe and micro-dispensing systems, commercialized by MicroPen and nScrypt, respectively [11]. Figure 2.2 shows a syringe and micro-dispensing DIW system [26] [27].

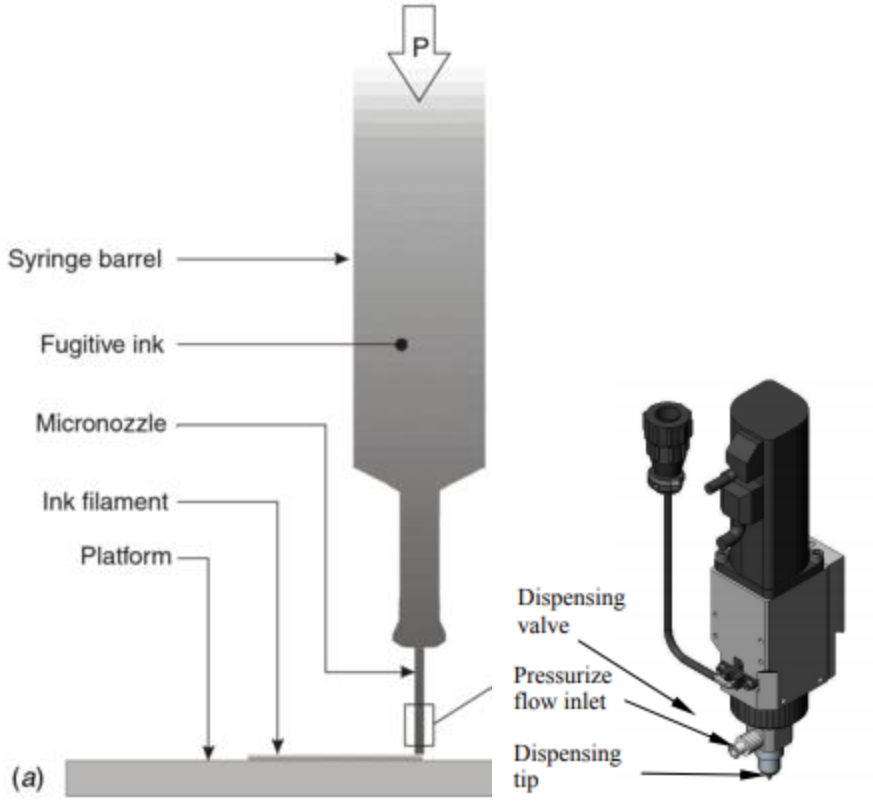

Figure 2.2: An example illustration of a syringe (left) and micro-dispensing (right) DIW system [26] [27].

The mechanical pressure dependency of these two systems allows for variable operation characteristics including variable volume dispensing and precise geometry control from the XY movement system. Changing the mechanical pressure can be taken advantage of to customize line width depending on the desired application. The size of the micronozzle and dispensing tip can also be changed depending on the ink used and desired line width.

The flexibility of extrusion-based direct write allows for a wide array of materials to be dispensed. Simple syringe-based extrusion samples are largely limited in material choice by the pressure capability, nozzle diameter, and syringe configuration. More complex systems are able to print a wider array of materials with a higher degree of control. The micro-dispensing Smart Pump, developed by nScrypt, demonstrates a higher degree of complexity. The Smart Pump can accurately control air pressure, valve opening timing, and dispensing height. These highly controlled and accurate settings give

the Smart Pump the ability to print materials from 1 cPs to 1,000,000 cps with speeds up to 500 mm/s and line width generally as all as 20 μm [27].

Due to the simple positive mechanical force dispensing principles, the array of materials able to be printed by extrusion based DIW is seemingly limitless. Moreover, the high upper limit of ink viscosity with extrusion based direct write systems make them ideal for dispensing highly loaded metal particle conductive inks with high volume. Additionally, the dispensing tip can be oriented out of plane with more complex movement systems to allow for conformal printing onto 3D structures, discussed further in Section 2.3.

2.1.3 Inkjet DW

Inkjet-based direct writing involves the ordered deposition ink/fluid droplets on a flat plane in a desired pattern or geometric shape. As discussed by Hon and coauthors, the two main methods of inkjet printing are called continuous inkjet (CIJ) and drop-on-demand (DOD). CIJ, like the name suggests, consists of ink droplets being dispensed continuously with some droplets hitting the substrate and others being recycled back into the ink storage unit. The droplets are selectively chosen to be deposited on the substrate or recycled, most commonly through electrostatic deflection. Unlike CIJ systems, DOD systems deposit ink only when desired; this ink is deposited through a pressure pulse typically controlled by a piezoelectric or thermal (bubble-jet) actuator [11]. These two processes are shown in Figure 2.3 [11].

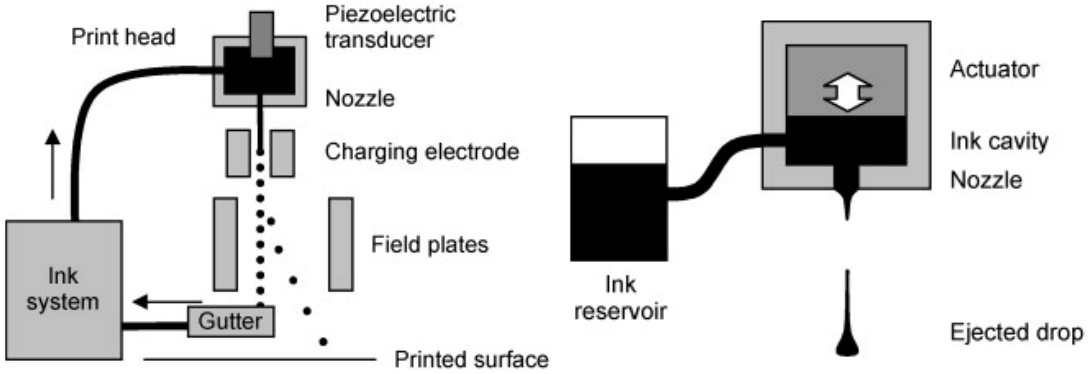

Figure 2.3: Illustrations of CIJ (left) and DOD (right) inkjet systems [11].

One primary benefit of using an inkjet based DW system for material deposition is their relatively high write speed. Inkjet heads can be linked in series for the rapid deposition of inks covering large print areas in a short amount of time [28]. Depending on the technology utilized, inkjet printing can also create line widths as small as 10μm, comparable to aerosol-based DW and slightly smaller than extrusion-based DIW [29].

However, the process also introduces challenges not found in the other DW methods discussed. To be jettable, an ink's viscosity must be limited to 100 cP, as higher viscosity inks can obstruct the nozzle and require higher, often unachievable, pressures to deposit material [29] [30]. These viscosity limitations also introduce issues with printing highly conductive lines since inks with higher solids loadings will be more viscous and more difficult to print using inkjet technology, an issue not faced with aerosol jet and extrusion based DIW [31]. Although these viscosity limitations can be overcome using nozzle-free approaches such as photoacoustic actuation [32]and laser-induced forward transfer technologies [33], these processes present their own limitations and are not compatible with AM integration.

In order to combat some of these limitations regarding the printing of highly loaded metal-based inks, metalorganic decomposition (MOD) inks were developed as an alternative. MOD inks have proven to be a viable alternative for highly loaded conductive metal nanoparticle inks in inkjet systems, which require a strict material properties band to be followed for successful printing [34]. MOD inks do not contain any particles, rather a solution of metal particles is dispersed in a solvent such as xylene or mixed alcohols depending on the metal precursor. After post-processing evaporation of the solvent, the metal particles collect on the substrate; however, due to about 80% volume loss from this evaporation, disconnections in conductive patterns often occur and need to be fixed using other techniques such as sintering [35]. A figure showing the processing of MOD inks compared to traditional metal particle dispersed inks is shown in Figure 2.4 [35].

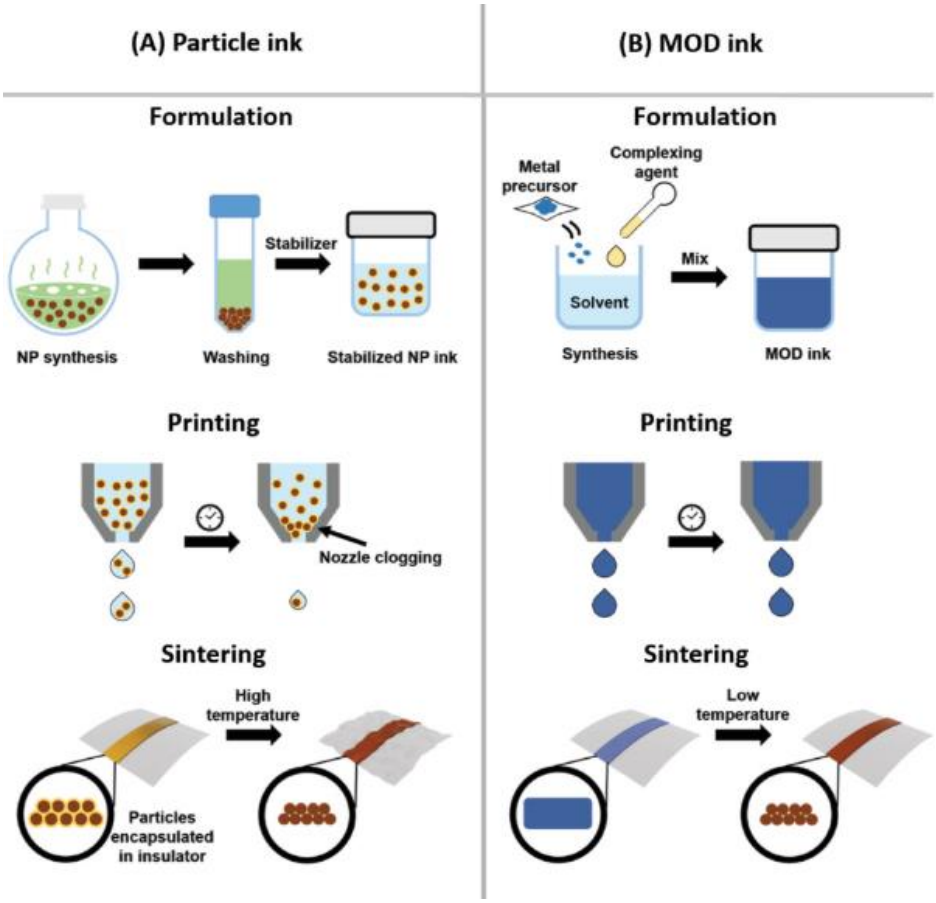

Figure 2.4: An illustration showing the processing differences between particle-based and MOD ink deposition [35].

Inkjet systems' ability to print conductive inks in highly precise geometries with a maneuverable, noncontact, and conformally onto substrates makes them a respectable candidate for integration with AM. However, the narrow band of material properties of which it can successfully print gives it a slight disadvantage compared to the aerosol jet and extrusion DIW approaches. This also prevents the conductive highly metal-loaded inks from being printed, which result in lower conductivity traces, even when using the MOD ink approach [35].

2.1 Aerosol jetting and Extrusion DIW of Electronics

Based on the material limitations of inkjetting systems, aerosol jetting and extrusion DIW are deemed the most viable electronics DW process for integration with UV-DIW polyimide resin. Aerosol jetting can deposit a wide array of inks in a variety of orientations over conformal surfaces with very

high-resolution traces. Extrusion based DIW is able to use very simple to complex technologies to deposit highly viscous inks with high resolution and very high metal solids loading viscous inks, resulting in lower resistivity conductive traces. Inkjetting, while able to match these processes in resolution, is limited in its ability to dispense inks with its narrow band of operation. For these reasons, aerosol jetting and extrusion DIW are considered in this thesis for depositing conductive traces on AM substrates. In this section, previous application of aerosol jetting and extrusion DIW are discussed as a precursor to the integration of these technologies in printing electronics on AM parts, discussed in Section 2.3.

2.2.1 Extrusion based DIW of conductive inks

Due to the high precision and wide ink printability band of extrusion DIW, there are many instances of the technology being used to print conductive inks. Many scientists have taken advantage of this simple technology that extrudes continuous streams of materials through a nozzle, enabling the manufacturing of conformal and embedded electronic devices. With the wide material property printability band offered by extrusion based DIW (Section 2.1.2) there are a wide array of DIW based extrusion conductive inks that have been demonstrated as effective conductors for electronics applications. These materials include, but are not limited to, silver-based ink [36] [37] [38], copper-based ink [39], electrodes [40], and carbon-based nanomaterials [41].

Silver-based inks are perhaps the most popular and widely available inks for direct write extrusion due to their high conductivity, lower price than gold inks, and resistance to oxidation (found in copper inks). Shen and coauthors demonstrated the ability to print 15µm wide silver lines that reached a resistivity of $5.29 \cdot 10^{-8}$ Ω·m (about 3 times the resistivity of bulk silver) after sintering the lines at 625°C in air [36]. They studied the direct write printing of five separate commercially available silver inks, featuring solids loading around 80 wt%, and characterized their various material properties with respect to DIW extrusion. Although these inks demonstrated resistivity only three times bulk silver, this resistivity would not be achievable in hybridized AM applications, as typical printable substrates cannot

withstand such high temperatures. Zhou and coauthors demonstrated the ability to use this silver-based DIW extrusion technology to create a broad array of RF passive antennas and discrete transistors, as shown in Figure 2.5 [42].

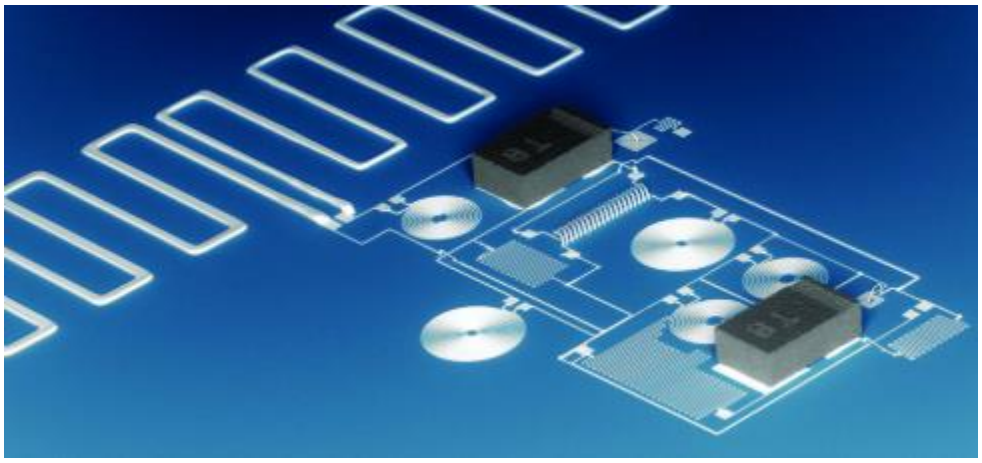

Figure 2.5: A variety of RF passive antennas and transistors made using silver-based DIW [42]. Each black transistor features a contact surface measurement of 1 mm x 0.6 mm.

DIW extrusion has also been used in 3D electronics applications rather than just in deposition of 2D traces. Fu and coauthors demonstrated the ability to 3D print graphene oxide electrode inks to fully print fuel cells, demonstrated in Figure 2.6 [40]. These lithium-fuel cells were entirely 3D printed using a three-stage process with three separate inks using extrusion DIW. Although this method only shows the 2D layer by layer application of DW extrusion for electronics, various 3D applications have been demonstrated also. Using extrusion DIW, Adams and coauthors were able to conformably print silver traces over a glass hemisphere to create small 3D antennas, as shown in

Figure 2.7 [43].

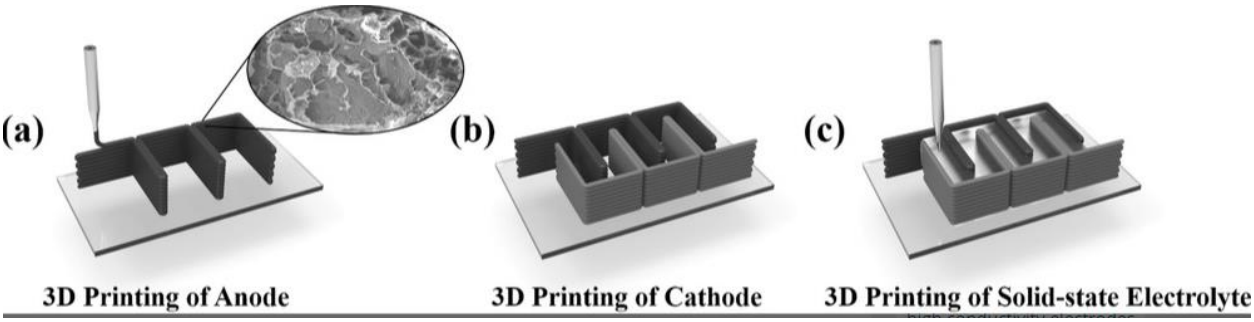

Figure 2.6: Process diagram showing the creation of a fuel cell using DIW [40].

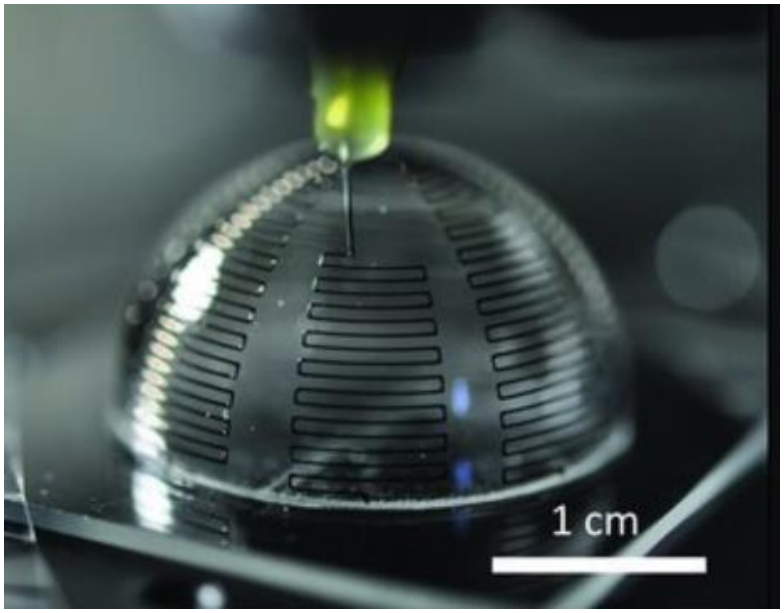

Figure 2.7: Conformal printing of DW silver ink to create a 3D antenna [43].

The wide material property printability range and 2D and 3D applications of extrusion based DIW demonstrate the ability this technology to be utilized in a wide array of integrated AM electronics applications. The high solids loading of conductive inks provide a viable option for creating high conductivity electronic traces as the building block for complex AM integrated electronic parts.

2.2.2 Aerosol Jet DW of conductive inks

Aerosol jetting (AJ) is a broad term used to describe the contactless selective deposition of accelerated aerosolized suspended ink particles. AJ is capable of printing very high resolution features with a wide variety of inks, making it perfect for microelectronic applications [18]. Due to the only limitation in the material choice for AJ being the ink's ability to being aerosolized, many conductive inks for electronic applications have been created and studied. The broad array of AJ inks for electronics applications include silver particle inks [44] [45], carbon nanotube and graphene particle inks [22] [46], copper and copper-nickel alloy particle ink [47], gold particle ink [48], and organic materials [48] [49]. Like extrusion DIW, silver-based inks are the most prevalent found in literature. This is due to silver having similar high conductivity like gold and copper-based inks, with copper being the least expensive

of the three. However, copper ink remains a lower tier contender due to oxidation in ambient conditions of printed traces lowering conductivity over time [50].

Although aerosol jetting is able utilize a wide variety of inks to obtain high performance electronic traces with high resolution, obtaining quality lines remains a problem. This is due to the inherent design of the machine, in which a quality balance between line thickness and line edge roughness must be found [51]. Often times, to achieve high resolution lines with acceptable dimensions and quality, manufacturers or researchers must go through an optimization process in which they vary the atomization parameters, carrier gas, sheath gas, and tube/platen temperatures. Zhang and coauthors created a novel hybrid multi-objective optimization approach for achieving desired high-quality silver traces [51]. This optimization approach was able to achieve a desirable balance of low line edge roughness and sufficient line thickness, and offers a proven statistical approach optimize printed line properties rather than the common trial and error method.

Aerosol jet printing of functional electronics using conductive inks has been widely demonstrated in literature. The studied printed electronics includes solar cells [49], electrical interconnects [52], antennas [53], strain gauges[54], and a wide array of other applications as reviewed by Wilkinson and coauthors [55]. Figure 2.8 shows a phased array antenna conformally printed on a curved substrate using silver nanoparticle ink. This was achieved without using AJ deposition rotation since the AJ process is able to print on surfaces rotated up to 45° from the deposition head [56]. Gu and coauthors demonstrated a technique for printing AJ UV-curable polymer fillets between different leveled surfaces and then subsequently printing silver nanoparticle ink over the fillets for well-formed electrical connections between the two surfaces [57]. Illustrated in Figure 2.9, this shows yet another example of utilizing aerosol jet deposition technology to create conformal electrical traces over nonplanar surfaces.

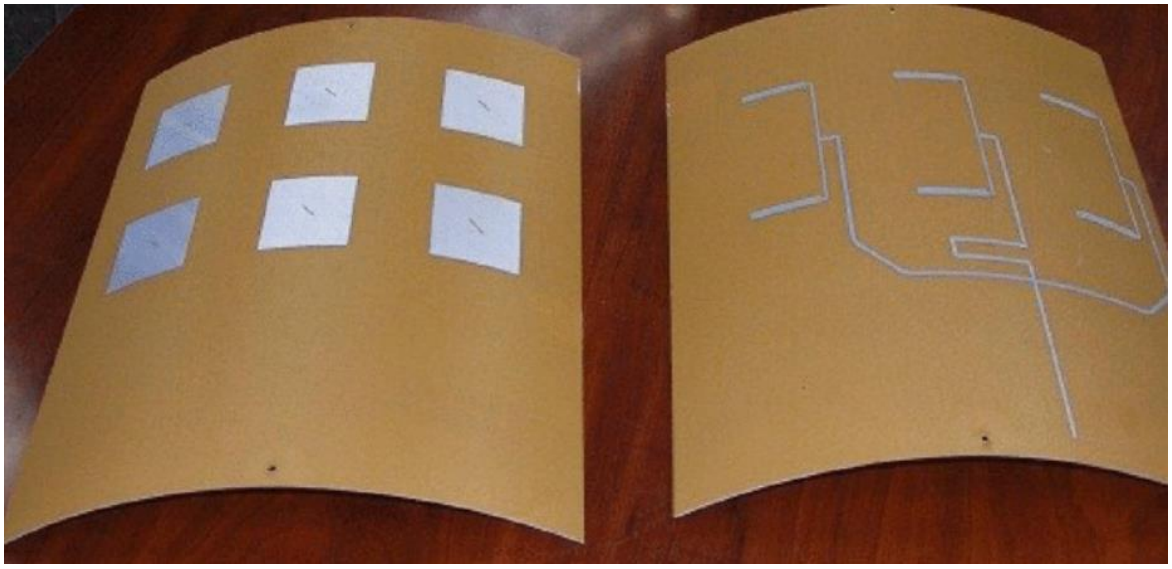

Figure 2.8: Phased array antenna conformally aerosol jetted over a curved surface [56].

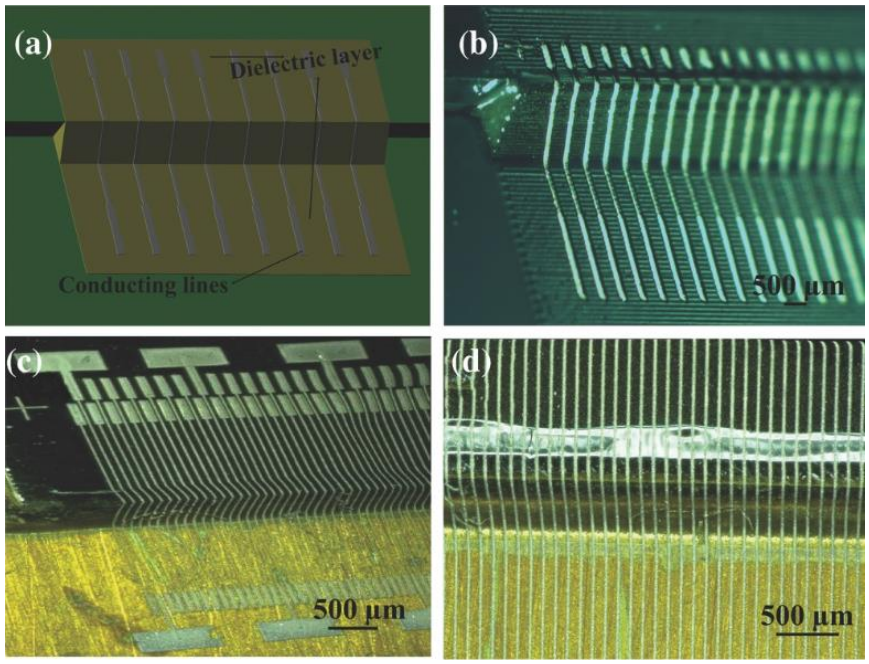

Figure 2.9: Aerosol jetted UV-curable polymer fillets with aerosol jetted silver particles printed on top to create conductive connections between multilevel surfaces [57].

To further expand on the idea of using AJ DW of conductive inks to print electronics on conformal surfaces, the idea of tilting the deposition head or equivalently tilting the part to achieve printing over curved surfaces must be considered. This concept could be applied to creating three-dimensional antenna arrays for better special navigation. Figure 2.10 shows a 19 mm ceramic cube that

was tilted 45° while an aerosol jet printing silver nano-particles was translated in the X direction along the surface while also altering its height in the Z direction [56]. Technology utilizing five axis rotation of the part while being printed on with the AJ has been developed by Optomec with their Optomec 5x printer with an example application shown in Section 2.3.3.

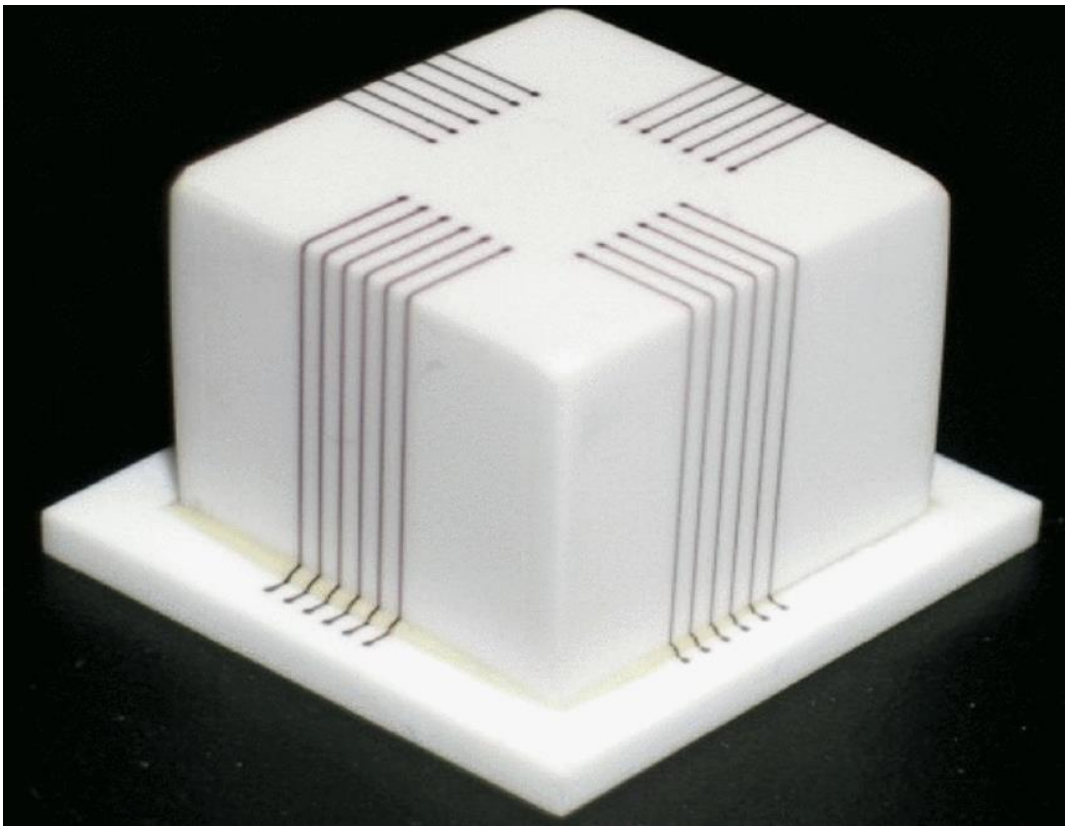

Figure 2.10: Ceramic cube with aerosol jetted silver nanoparticles continuously printed on surfaces of varying orientation [56].

As discussed, this section, aerosol jet technology has the ability to print a wide array of conductive materials with high resolution over conformal and non-planar surfaces. This makes it an appropriate option to utilize for integrating DW of electronics and additive manufacturing processes and parts. Current integration and application of these technologies will be discussed in Section 2.3.

2.3 Integration and Application of AJ and Extrusion DIW and AM

In Section 2.2, the use of extrusion and aerosol jetting direct ink write of conductive materials to create a wide array of functional electronics was discussed. Combining these conductive inks with the

ability of these DW systems to print highly precise patterns on conformal and non-planar surfaces along with the ability of AM systems to print an infinite amount of different shaped structures enables the design and creation of integrated, complex, and conformal electronics housed in a spatially efficient and structurally sound product [1]. This section will discuss the previous integration and application of DW conductive inks with additively manufactured parts to create complex functional electronics.

2.3.1 Hybrid AM DW Electronics systems

In order to prevent the need for separate system printing of AM parts and DW electronic traces, companies and labs have developed fully homogenous systems combining the two technologies into one hands-free process in which the system produces embedded functional electronics. This technology has progressed over time with a start/stop integrated stereolithography and direct extrusion of conductive inks system developed at the University of Texas at El Paso in 2012 [58]. This system, shown in

Figure 2.11, featured a 250/50 SLA machine with a nScrypt ink dispensing system. Utilizing laser conductive ink curing, this system was able to successfully create functional 2D and 3D 555 timer circuits formed via DIW extrusion conductive ink traces onto SLA-printed structure. Although this process was able to demonstrate the capabilities of hybrid AM-DIW electronics systems, the required subprocesses were manual and its products featured low power application due to high trace resistivity.

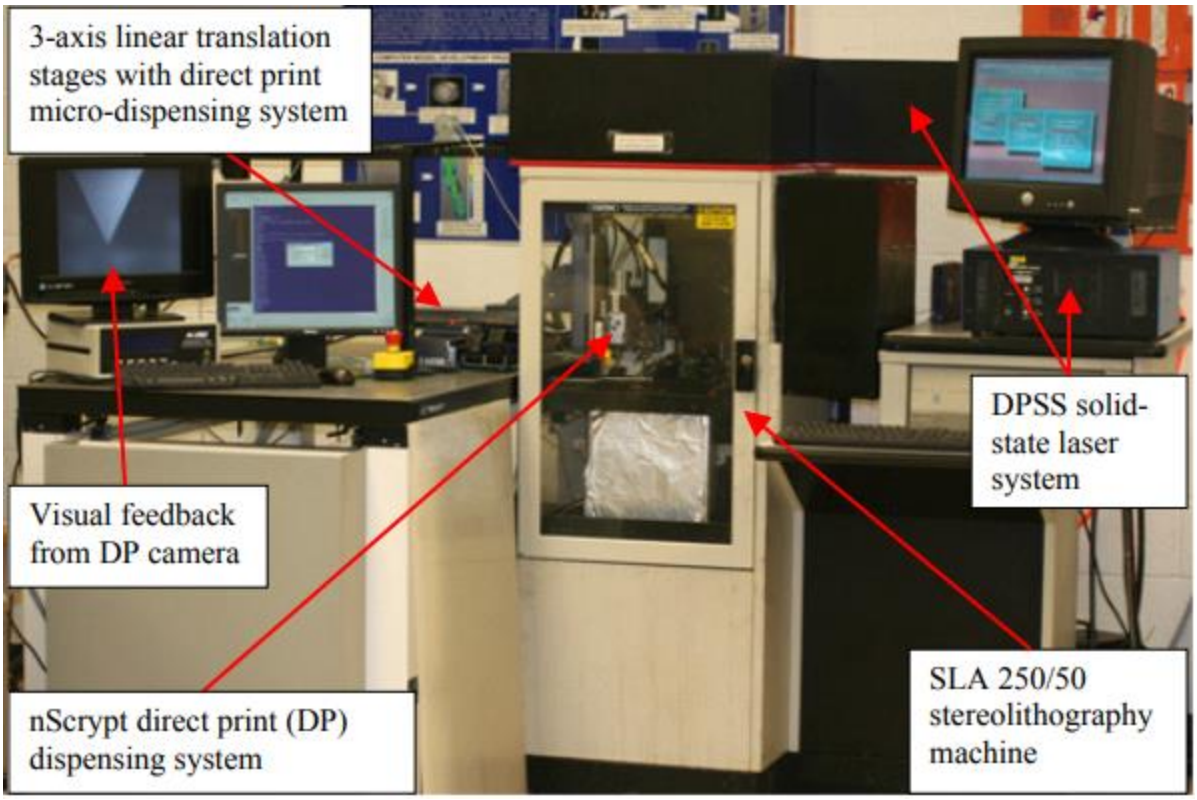

Figure 2.11: Combined stereolithography and DIW system developed at UTEP for creating complex AM electronic devices [58].

Researchers at UTEP have since progressed in their electrically functional AM device research with the creation of a robotic multi-process system. This system features a six-axis robot working as the centerpiece combining two fused filament fabrication printers with separate materials for multi-material printing as well as a gantry with subtractive machining, copper wire embedding, DIW fluid extrusion, electrical component placing, and conductive foil application [59].

In 2013, researchers at The University of Akron published their progress on hybridizing the direct write of electronics and projection microstereolithography [60]. Their process involved dispersing carbon nanotubes in a photocurable polymer to create a conductive path within the rest of a photocurable part to create a 3D structure with embedded electronics. This process photocured the conductive photocurable polymer while it was being printed to create 3D thin conductive 'wires'. These wires would maintain their shape while non-conductive photopolymer was cured around them to create

3D electronic AM structures, as shown in Figure 2.12. Information regarding the resistivity of the polymer carbon nanotube structure was not reported; however, it can be assumed that it was much higher than typical metal loaded inks.

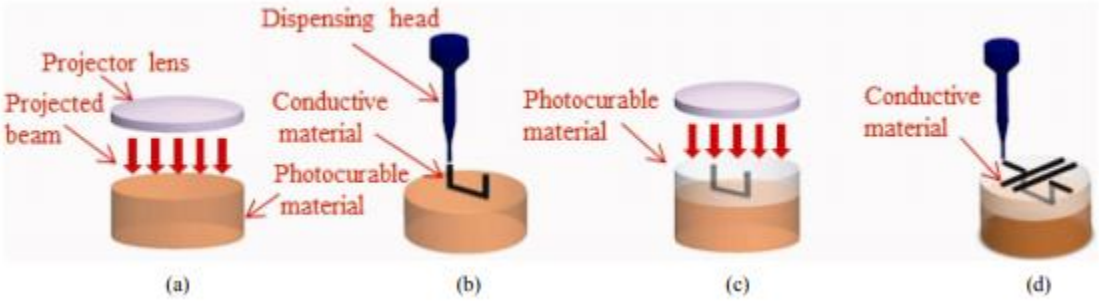

Figure 2.12: System for combining nonconductive photocurable polymer with photocurable conductive material to create complex 3D electronic structures [60]

In 2015, Jang and coauthors documented their process integrating vat photopolymerization (VP) and direct write extrusion to create 3D circuits. Their process involved creating a partial structure using VP, removing the structure, cleaning and drying the structure, depositing/curing conductive inks and components, and then repeating until completion [61]. Although this process demonstrated a good proof of concept for integrating AM and DIW of conductive inks, the ink used featured a resistivity almost four orders of magnitude higher than bulk silver. This relatively high resistivity was a product of the photopolymer not being able to withstand a processing temperature of 190°C, required by the other ink option presented in the study. The researchers also had to insert separate electronic components into the structure rather than only using conductive inks to achieve 3D functionality, as shown in Figure 2.13. The process also featured a separate manual cleaning/drying phase for the partial VP structure which created a long and non-automated process. However, the researchers were able to create a 3D light sensing LED circuit using their integrated process.

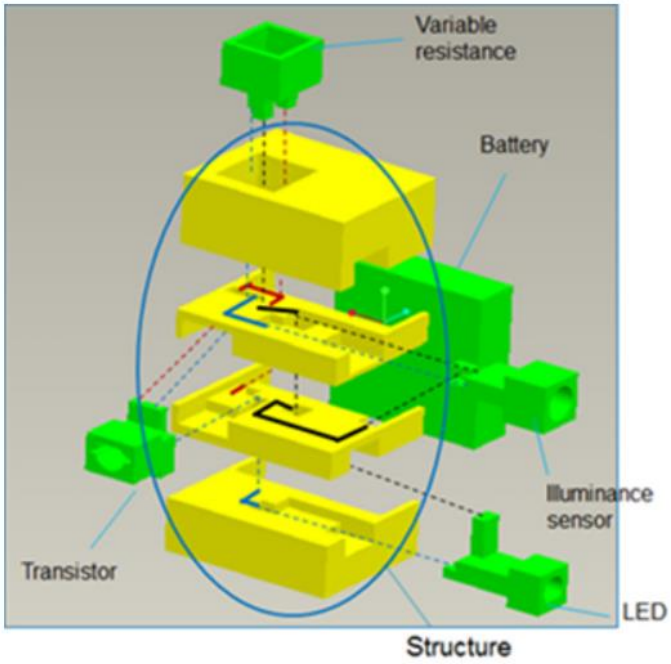

Figure 2.13: Process for integrating AM and DIW to create complex electronics utilizing the removal and cleaning of VP parts [61].

In 2017, researchers at Duke University were able to break the mold of using separate processes for combining creating 3D electronics using AM through employing the fused filament fabrication (FFF) of dual-materials with conductive thermoplastic filaments. The researchers utilized copper-based, graphene-based, and carbon black-based conductive filament in combination with typical PLA as a dielectric. Utilizing these filaments to create smaller electrical subcomponents, researchers were able to create a high-pass filter, embedded component, and free-standing conductive structures. Figure 2.14 illustrates the process of combining dielectric and conductive FFF to create a 3D embedded LED structure [62].

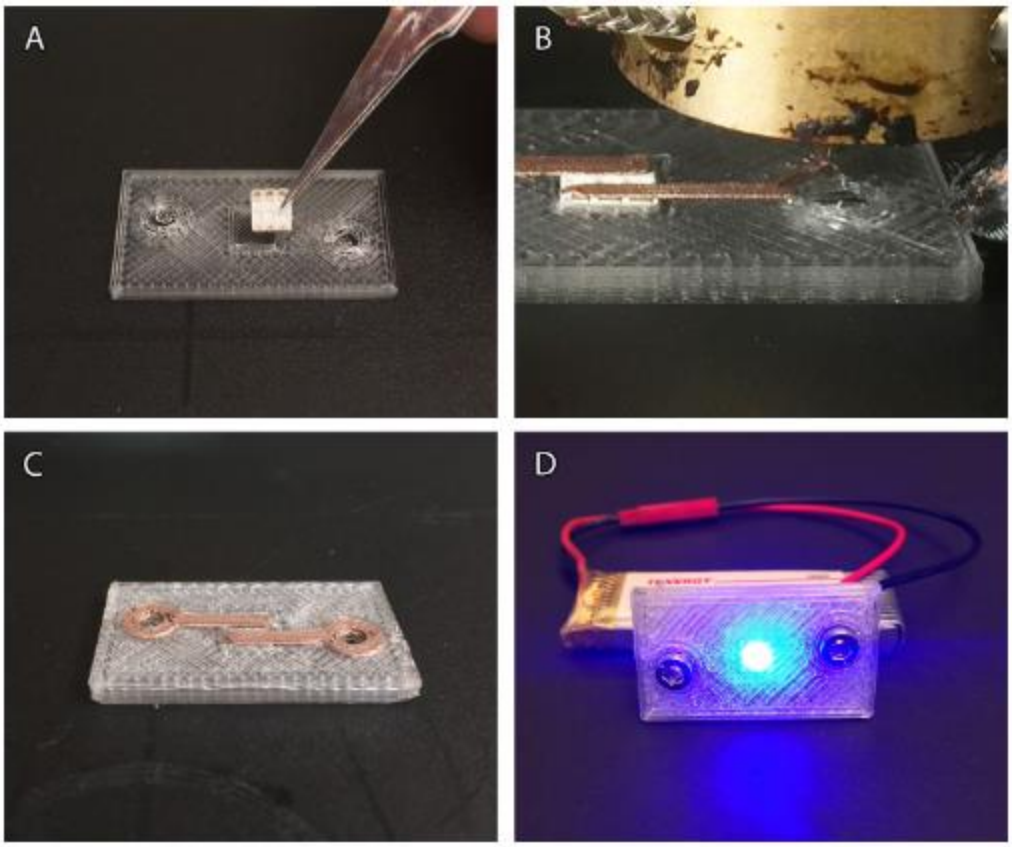

Figure 2.14: Embedded LED created through the FFF of conductive and nonconductive polymer-based filaments [62].

As a final example of non-commercial 3D electronics AM systems, researchers at Georgia Institute of Technology created the m^4 3D printer combining inkjet, fused filament fabrication, direct ink writing, and aerosol jetting technologies [63]. This printer utilized these AM processes along with pic-and-place robotics and intense pulsed light sintering to create complex devices including those with electrical functionality. Utilizing the combined AM capabilities in an uninterrupted process, the researchers were able to create a stretchable LED light ribbon with embedded conductive ink, as shown in Figure 2.15. To demonstrate 3D conductive trace functionality the researchers created a structure with vertical vias that were cured in-situ using the heated bed and a post-printing oven cure; the final product is shown in Figure 2.15 as well. The process also featured the ability to utilize pre-fabricated

electronic components, such as a LED chip, in combination with the AM processes which utilized a FFF structure and DIW silver electrodes as shown in Figure 2.16 [63].

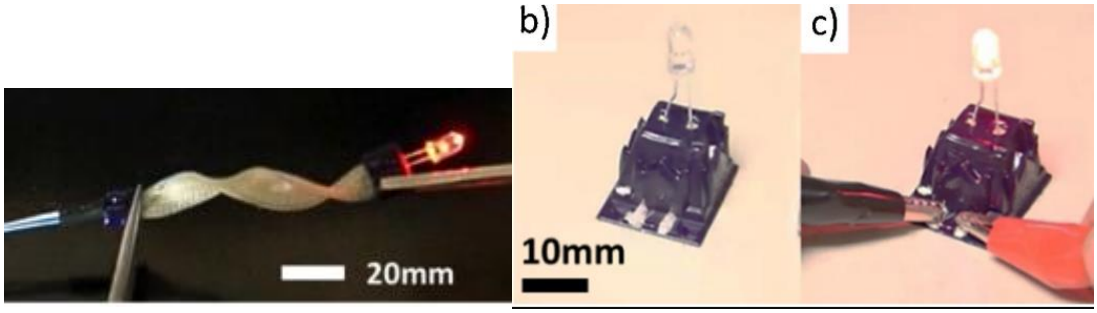

Figure 2.15: AM produced stretchable LED ribbon(left) and vertical LED connecting via's (right) produced using four-in-on additive manufacturing system [63].

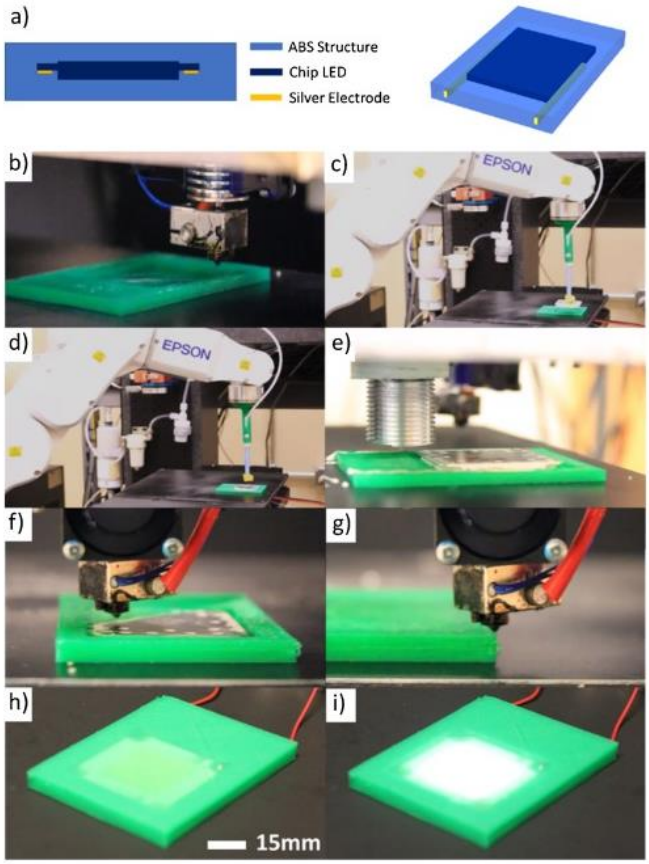

Figure 2.16: Four-in-one AM system used in conjunction with pre-fabricated chip LED to create an embedded electronic LED structure [63].

Companies aiming to commercialize the combined AM-electronics capabilities have created printers with integrated AM structures and DW conductive traces. Voxel8 created an affordable printer

combining FFF and DIW conductive inks. The printer utilizes a pneumatic extrusion process do deposit an ink that cures at room temperature to allow for the designing and rapid prototyping of electrically functional AM parts. This technology has been demonstrated on functional products such as a drone with embedded electrical interconnects as shown in Figure 2.17. However, this process results conductive interconnects featuring a resistivity of approximately 31 times the value of bulk silver. Additionally, the DragonFly 2020 printer, by Nano Dimension, is a multimaterial jetting AM process that jets both dielectric materials and conductive nanoparticle inks. Nano Dimension advertises the ability to rapidly prototype RF active devices, sensors, multilayer PCBs, and molded interconnect devices [64]. The silver nanoparticle ink is typically cured via infrared and heat treated during post-processing to achieve a resistivity of 5% to 30% of bulk Copper [65]. Although this resistivity demonstrates an improvement upon Voxel8, there is still room for improvement. An example PCB printed using the DragonFly Pro is shown in Figure 2.18 [66].

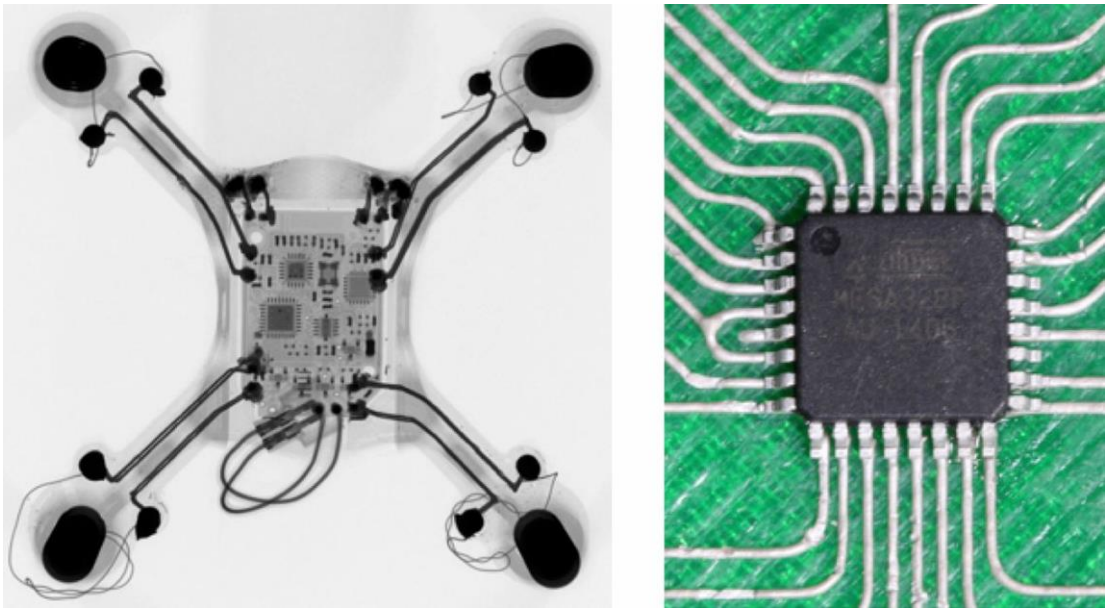

Figure 2.17: Drone with IC chip made functional through combining FFF and DIW of conductive inks in the Voxel8 printer [59].

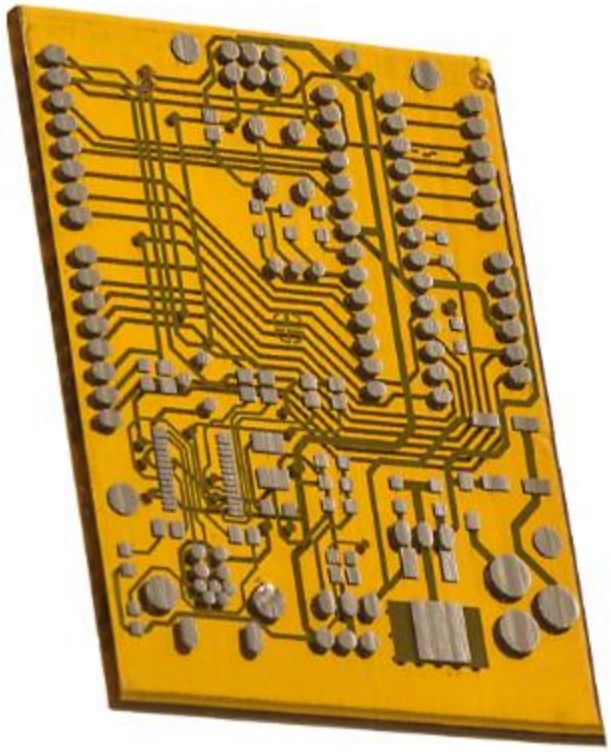

Figure 2.18: Fully AM produced PCB produced throught the inkjetting of conductive and non-conductive materials in the DragonFly Pro AM system [66].

2.3.2 Embedded Electronics

Embedded electronics are perhaps the most promising application of integrating AM structures with functional conductive elements. Embedded electronics offer a spatially efficient structure with multiple layers of conductive elements integrating for complex electronics. In this subsection, various examples of AM embedded electronics are discussed including sensors, antennas, and microelectronics.

In 2013 researchers were able to utilize the idea of AM embedded electronics to create an 3D printed bionic ear, shown in Figure 2.19, merging biologic and electronic functionalities. The ear is capable of capturing inductively-couples signals from cochlea-shaped printed conductive electrodes enabling for auditory sensing of RF signals and even humanoid left/right stereo music [67]. This product was printed via syringe DIW extrusion using a Fab@Home 3D printer of structural, biological, and electronic materials including an alginate hydrogel matrix (structural) with ‘viable chondrocytes’

(biological) and a silver nanoparticle infused silicone solution (electrical). This AM-electronics integration shows the biological application potential of this electrically functional 3D printed product concept.

Figure 2.19: 3D printed bionic ear created using the syringe extrusion of structural, biological, and conductive materials [67].

AM-produced embedded antennas provide a very logical application of AM structural and electronic integration due to their wide variety of functional geometries. In 2015 a significant contribution to this concept was published by a variety of authors who fabricated antennas via AM structural and electrical integration [68-71]. Ketterl and coauthors integrated fused filament fabrication (FFF) and extrusion-based direct ink write to create a seven-layer passive phased array connected with conductive vias [68]. Liang and coauthors were able to print patch antenna via FFF and ultrasonic wire mesh embedding using the system discussed in [59]. Using this method, the researchers were able to construct the antenna with no sintering due to the very high conductivity of the embedded copper wire [69]. Furthermore, this wire embedding technique was also used to create an Archimedean spiral antenna documented by Shemalya and coauthors [71]. As a final example, Pa and coauthors were able to fabricate a low-profile antenna that included an integrating artificial magnetic conducting ground plane via fused deposition modeling and extrusion-based direct ink write of conductive materials [70]. The creation of these antennas proves AM structural and electrical integration to be a viable option for the rapid prototyping of high performing antennas. A photo of each of these antennas is shown in Figure 2.20 [68-71].

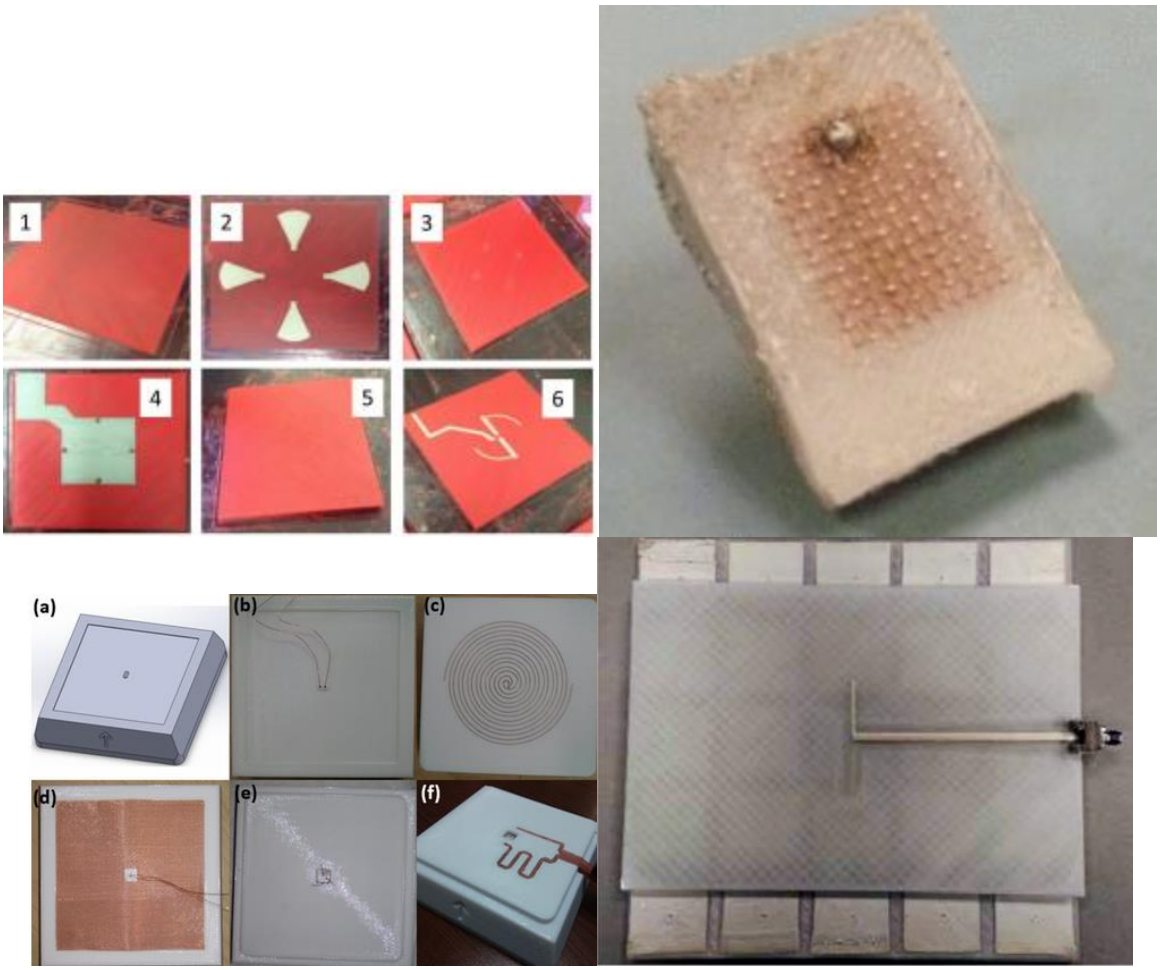

Figure 2.20: Examples of embedded electronics: seven layer phased array antenna with vias (top left) [68], patch antenna with ultrasonically embedded copper wire (top right) [69], Archimedean spiral antenna with ultrasonically embedded copper wire (bottom left) [71], and a low profile antenna with direct written conductive elements [70].

Multifunctional AM also has the potential to create complex electronics for sensor applications as reported by multiple authors [72] [73] [74]. Muth and coauthors produced a 3D printed embedded strain sensors using a photocurable elastomer as a structural reservoir while extruding conductive carbon grease ink into the uncured reservoir, as illustrated in Figure 2.21. After curing, the ink remained a fluid while the elastomer solidified, proving that 3D soft sensors can be created using AM structural and electrical methods [72]. In 2015, Shemalya and coauthors were able to utilize AM techniques to print embedded capacitive sensors using FFF and wire embedding [59]. These sensors were able to distinguish separate metallic materials as well as salt water from distilled, a fully embedded

demonstration model is shown in Figure 2.22 [73]. As a final example, Wu and coauthors utilized FFF and DIW extrusion to print passive wireless sensors and integrated circuitry. These researchers printed hollow structures for conductive paths and then injected the structures with conductive ink to form 3D conductive paths that cured at room temperature. This approach yielded functional resistors, inductors, capacitors, and an inductor-capacitor-resonant passive sensor circuit (Figure 2.23) [74].

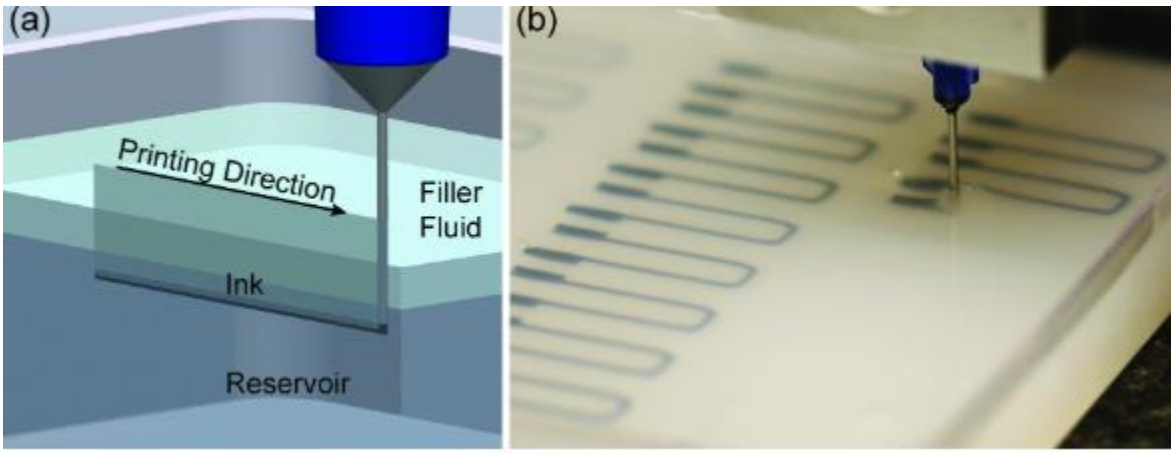

Figure 2.21: Elastic strain sensors created through the injection of conductive carbon crease into an uncured photocurable elastomer resin [72].

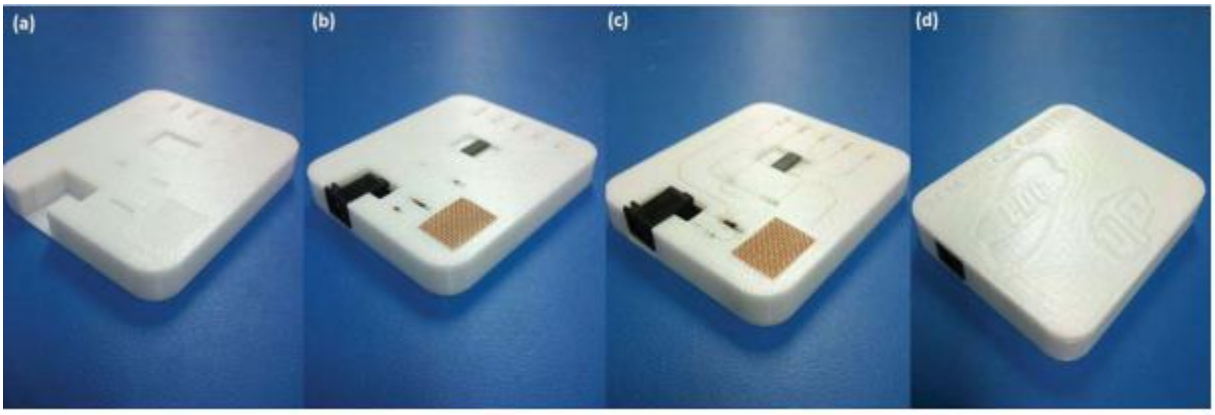

Figure 2.22: Embedded capacitive sensor created through ultrasonic wire embedding in an FDM structure [73].

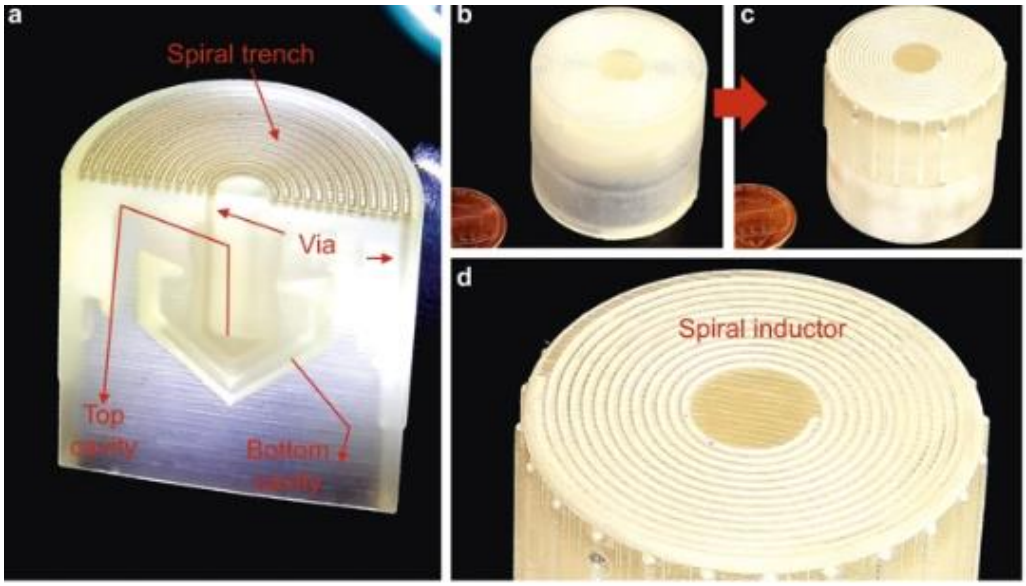

Figure 2.23: Capacitor-resonant passive sensor circuit created through the injection of conductive material into a hollow FDM structure [74].

Another application of multifunctional AM to produce electrical structures is the fabrication of 3D printed batteries as documented by a multitude of researchers [75] [76] [77]. In particular, lithium ion batteries have been emphasized in this approach. In 2013, Sun and coauthors used DIW extrusion to print the anode and cathode of lithium ion batteries exhibiting high power densities [75]. Later on, in 2018, Saleh and coauthors reported printing highly complex 3D silver lattice electrodes via aerosol jet 3D printing resulting in significantly higher battery performance compared to typical thin solid silver electrodes [76]. An illustration of these two reports is shown in Figure 2.24. In a 2020 review of the additive manufacturing of batteries, Pang and coauthors state that with continuous advancement 3D printed batteries with high durability, safety, and energy will eventually be used throughout many fields [77].

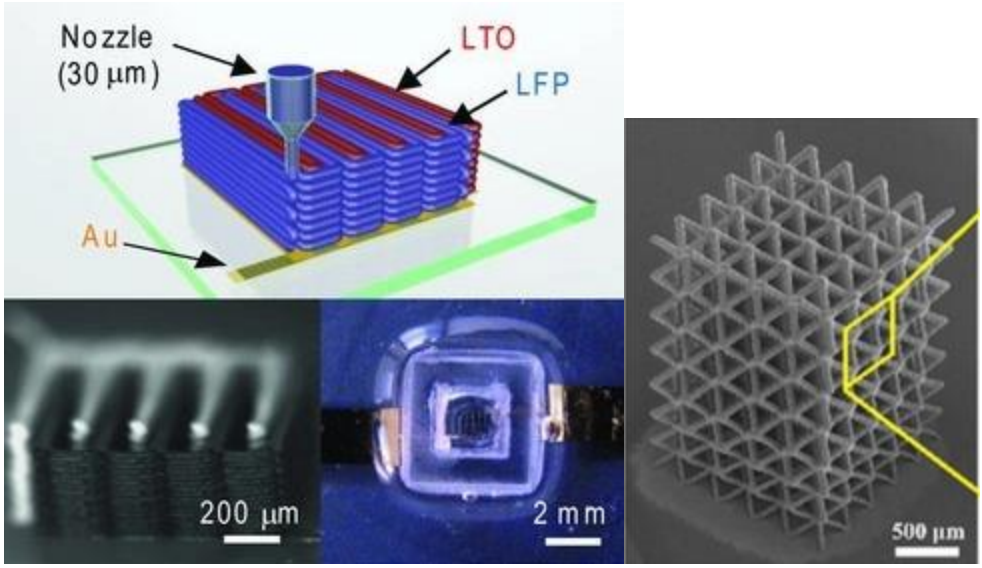

Figure 2.24: DIW extrusion printed anode and cathode of lithium ion batteries (left) [75] and printed highly complex 3D silver lattice electrodes via aerosol jet 3D printing (right) [76].

In 2015 researchers demonstrated their use of additive manufacturing to print a small satellite (a Cubesat) propulsion system. The team successfully embedded a micro pulsed plasma thruster and heated copper wires into an FFF structure, using the same approach documented earlier [59], as shown in the CAD rendering in Figure 2.25. This approach significantly contributed to the investigation of utilizing AM structural and electrical integration to bring multifunctional 3D printed parts to space [78].

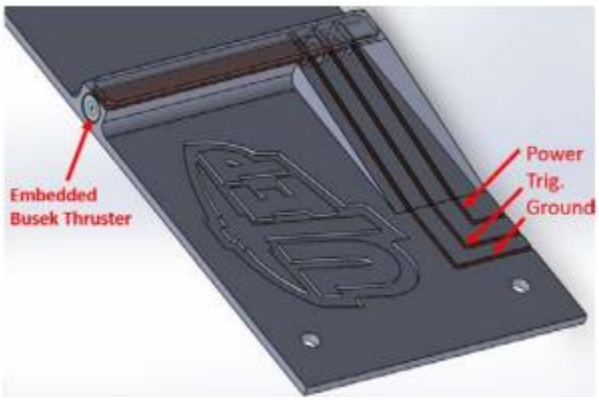

Figure 2.25: Micro pulsed plasma thruster created using ultrasonic wire embedding into a FDM structure [78].

2.3.3 Surface Electronics

Although embedded electronics offer a layered and spatially efficient approach for integrating structural and electronic to create complex electrical devices, surface-based electronics require less processing complexity. In this review, 'surface electronics' are associated with printed conductive traces on surface of AM-produced structures. This includes but is not limited to sensors, interconnects, and antennas.

In 2012, Paulsen and coauthors demonstrated utilizing aerosol jet printing to print conformal electronics on 3D structures. The researchers demonstrated printing a phased array antenna on a curved surface, as shown earlier in Figure 2.8, as well as LED and propeller power lines along with an antenna directly printed on an fused deposition modeling printed UAV structure shown in Figure 2.26.

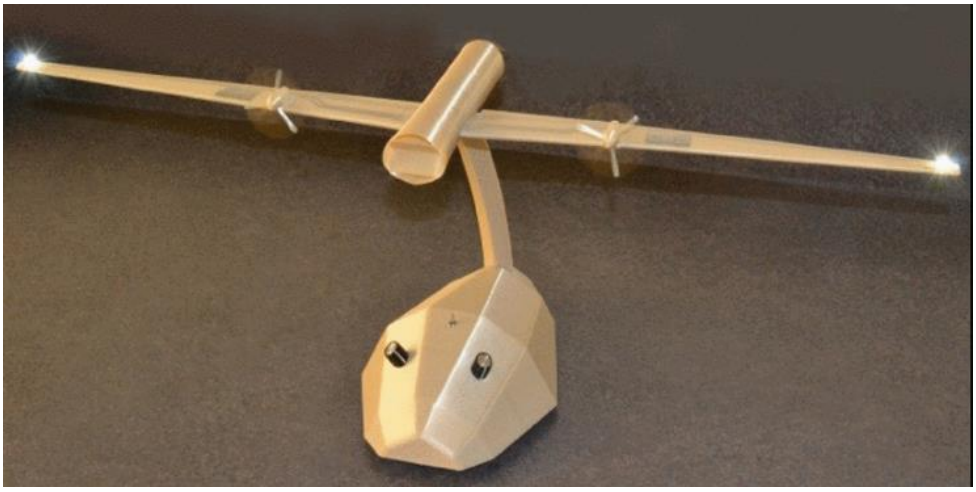

Figure 2.26: AM produced UAV with aerosol jetted antenna and electrical connections printed on its surface [56].

There has been a prominent interest in the application of DW conductive ink for microwave circuitry. Cai and coauthors used aerosol jet technology to print 3D dielectric polyimide structures which were then used as the substrate for aerosol jet silver nanoparticle deposition [79]. These conductive lines were utilized as transmission lines and characterized up to 50 GHz; Figure 2.27 shows an example of the printed transmission lines on the aerosol jetted polyimide substrate. Researchers were able to

print a 65 μm layer of polyimide with a resolution of 0.65 μm per layer along with line widths of approximately 80 μm. After 30 layers of printed polyimide, the thickness of the substrate did not increase linearly due to the increased sample thickness trapping solvent, requiring the need for a post-processing 'sintering' step. After printing the polyimide substrate, silver nanoparticle transmission lines were printed, processed, and characterized up to 50 GHz. This work represents the first aerosol jetted printed polyimide dielectric substrate. However, since the polyimide was printed with only 65 μm thick layers, more work must be completed before it can be deemed an appropriate option for hybridizing 3D AM structures with DW conductive traces.

In another example of printed transmission lines, Deffenbaugh and coauthors printed and characterized silver-based transmission lines on both VP and FFF AM substrates. Both of these substrates featured temperature processing limitations including 111 °C for the VP substrate and a 90 °C heated build plate for the FFF substrate. These temperature processing limitations led to larger losses when compared to the same substrates with bulk copper silver lines [80]. Furthermore, in 2017, Qayyum and coauthors demonstrated printing ultrawideband 3D interconnects using aerosol jet deposition of silver nanoparticles [81]. These interconnects were printed conformally on a 3D inkjet printed polymer substrate, shown in Figure 2.28 [81]. These examples serve as previously studied integration of AM structures with DW transmission lines and provide a starting point for Research Question #4 in this thesis.

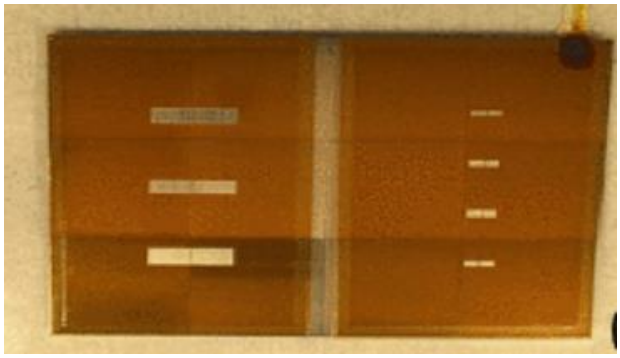

Figure 2.27: Aerosol jetted 3D dielectric polyimide substrate used for aerosol jet silver nanoparticle deposition of transmission lines [79].

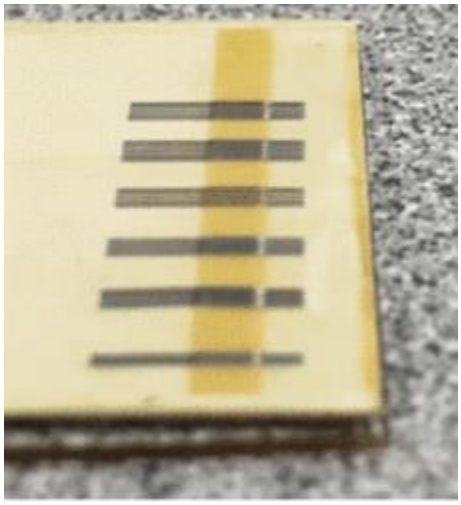

Figure 2.28: Aerosol jet printed ultrawideband interconnects conformally printed on a 3D inkjet printed polymer substrate [81].

As a final example of surface electronics printed on AM 3D substrates, the work of MacDonald and coauthors on the rapid prototyping of 3D structural electronics is presented. In this work, an investigation into the 3D printing of electronics was presented along with the fabrication of a 3D printed electrical gaming die, shown in Figure 2.29 [82]. After multiple design iterations, researcher's VP printed die-shaped structure with channels filled with micro-dispensed silver-based ink interconnects for a final product featuring a microprocessor, accelerometer, and LEDs. These researchers also conducted a study to compare their AM-based rapid prototyping approach to traditional electronics prototyping methods and found a dramatic decrease in functional prototyping design cycle. This work demonstrates the feasibility of using the integration AM structural and electrical processes for the rapid prototyping of multifunctional complex electrical devices.

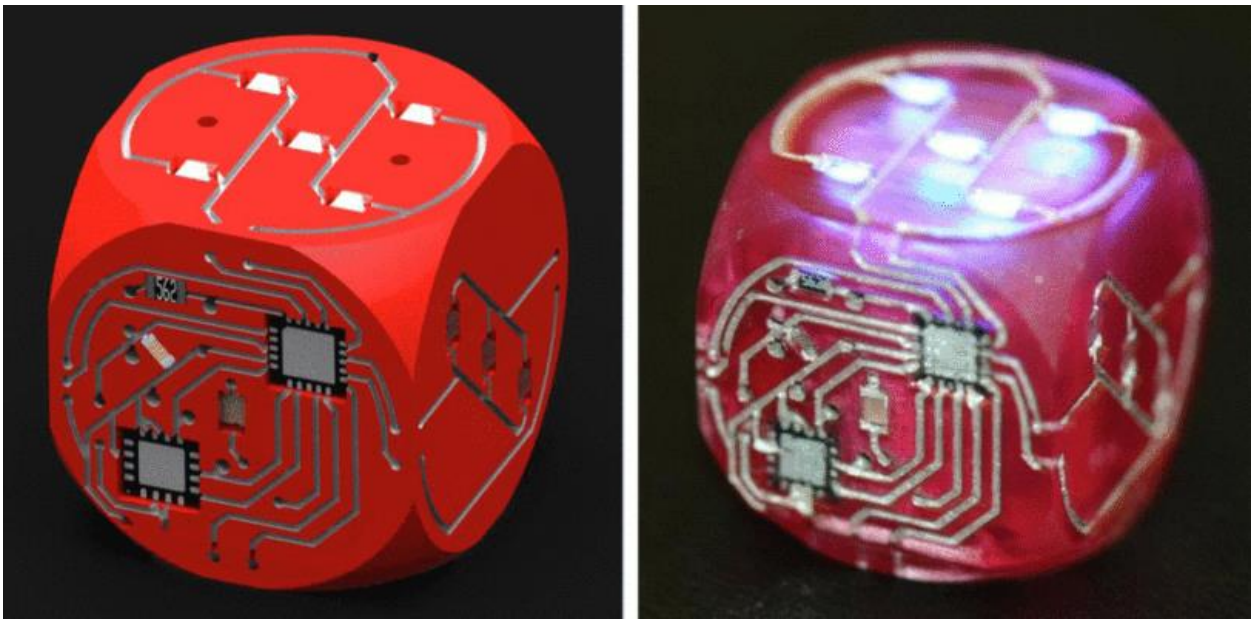

Figure 2.29: 3D printed die-shaped structure with DIW printed conductive interconnects along with an accelerometer, microprocessor, and LEDS [82].

2.4Limitations Integrating DW Electronics and AM

While Section 2.3 highlighted using multiple additive manufacturing methods to create multifunctional 3D complex electronic structures, the feasibility and performance of these structures is not without limitations. This is due to a variety of factors including temperature processing limitations of AM substrate structures, as well as adhesion and placement of conductive inks on AM substrates.

2.4.1 High Temperature Processing

With the research discussed in Section 2.3, it is clear that hybridizing AM technologies to create complex AM electronics is not only a possibility, but a reality with seemingly endless applications and abilities. However, due to temperature processing limitations of AM substrates, the overall performance of the electronics is limited. Although material science continues to progress and produce higher conductivity inks, printed metal inks still suffer from high resistivity in relation to their traditionally manufactured interconnects featured in printed circuit boards. These high resistivities result in a

reduction in overall electrical performance due to higher voltage drops and overall power loss though the circuit [59].

Metal loaded inks capable of reaching higher conductivities rely on the ability for metallic nanoparticles to show a reduced melting temperature compared to their respective bulk material; this trend for various metals is shown in Figure 2.30**Error! Reference source not found.** [83] [84]. This melting of nanoparticles together is known as sintering and occurs mainly due the nanoparticles' large surface to volume ratio leading to a reduction in surface energy. This sintering process forming large metal particles from smaller particles in known as Oswald ripening, and it halts at the point where the larger particles obtained are approximately 50% larger than their original size. This halt in sintering leaves behind a porous structure resulting in an overall conductivity lower than the bulk material [85] [86]. However, these inks require organic materials to stabilize the nanoparticles and maintain a dispersed solution which require higher temperatures, outside of the usability range of most AM materials, to burn off and allow the particles to sinter [85]. In an attempt to make conductive inks AM substrate compatible, many metallic DW inks rely on high surface area metallic flakes which come closer together and form conductive contact paths as their polymer solvents cure and evaporate at lower temperatures such as 120°C or even room temperature. However, since the flakes are too large for actual sintering to occur, these inks feature higher resistivity than their nanoparticle-based counter parts [87]. An example SEM image of a silver flake ink is shown in Figure 2.31. Illustrated by Perez and coauthors, these various metallic ink processing effects are shown Figure 2.32, with (a) featuring particles without post-processing surrounded by their solvent, (b) showing solvent evaporation and particle contact resulting in ink conductivity, (c) showing low temperature sintering courtesy of Oswald ripening discussed earlier, and (d) showing a fully melted bulk metal [1].

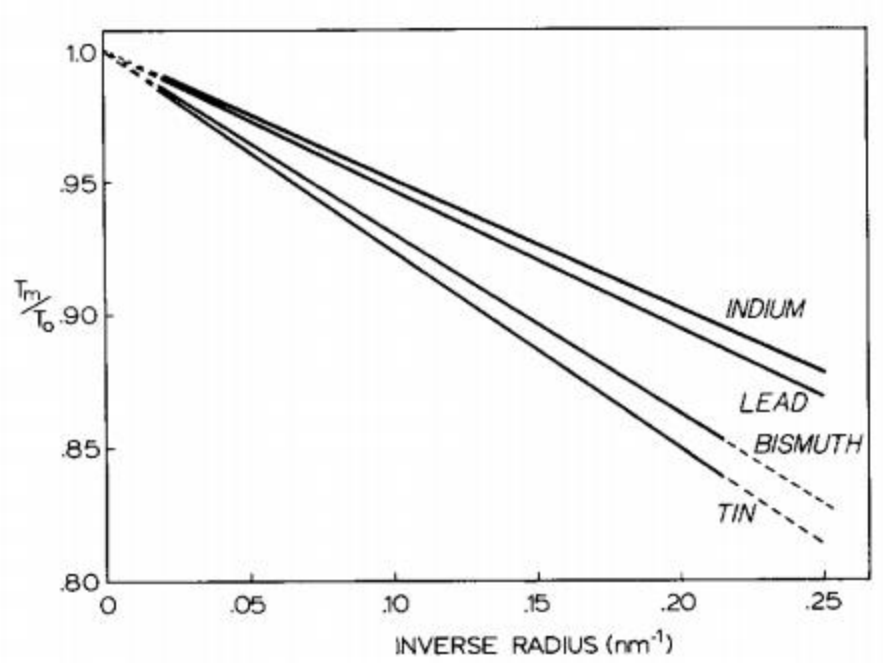

Figure 2.30: Trend showing the decrease in melting temperature of various metals as their particle radius decreases [84].

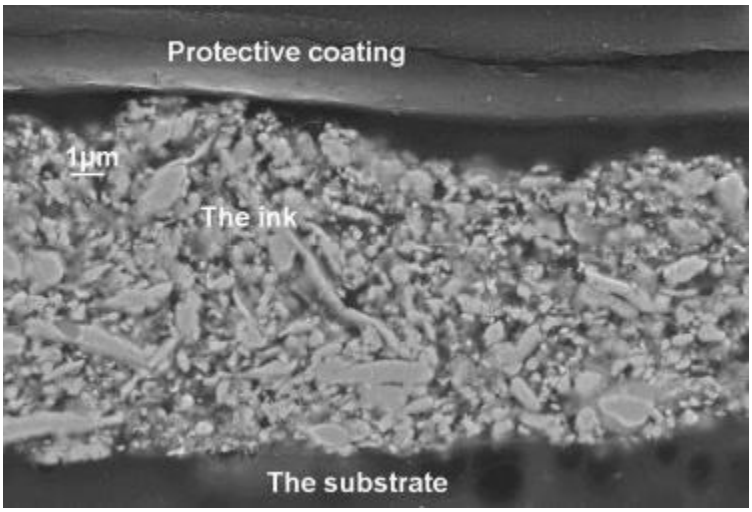

Figure 2.31: SEM image of conductive ink featuring high surface area silver flakes dispersed in a polymer binder [87].

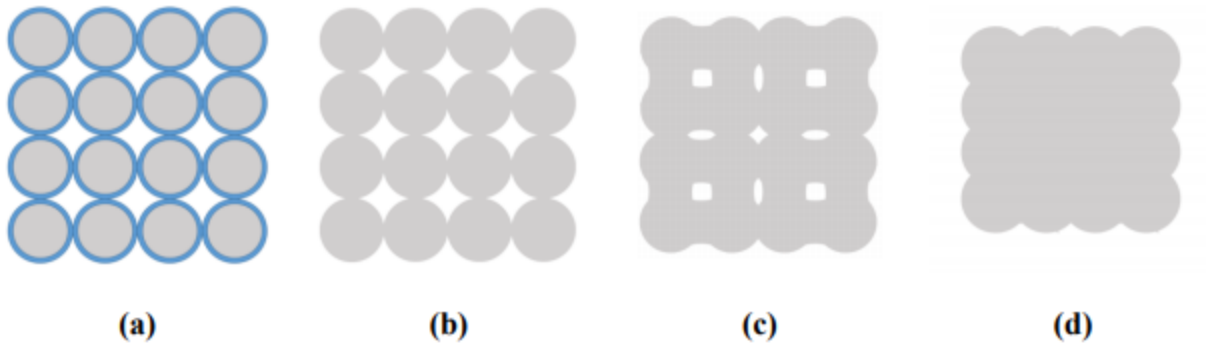

Figure 2.32: The process of sintering and fully melting metallic nanoparticles [1].

One of the main reasons for deposited inks being unable to achieve high conductivity on AM surfaces is the low temperature processability of various AM polymer dielectric substrates. A significant property of the AM polymer substrates with relation to temperature processability is their glass transition temperature or Tg – the temperature at which a polymer becomes 'soft' and susceptible to deflection and deformation. As stated by Perez and coauthors, most metal-based DW inks need to be post-print processed at temperatures of at least 100°C to become conductive [1]. Unfortunately, not all AM substrate materials can withstand this temperature without degrading or reaching their Tg. For example, the FDM and POLYJET materials made by Stratasys advertised for their "high temperature" applications are listed in Table 2.1 with the highest Tg being ULTEM 1010 with 215 °C. Although ULTEM 1010 has the highest Tg, it is characterized as being 'brittle' by Stratasys. Furthermore, ULTEM and other FFF materials feature poor surface finish, discussed further in Section 2.4.2. After going through a selection process, Espalin and coauthors chose Accura PEAK as the most viable vat photopolymerization material for AM electrical applications. However, the PEAK required a UV and thermal post cure in order to reach a glass transition temperature of 110 °C [3]. The highest performing conductive trace in Section 2.3 had a reported conductivity of 40% bulk silver after sintering aerosol jet silver nanoparticles at 200C for 1 hour [81]. However, this sintering temperature was well beyond its substrate's glass transition temperature (Tg). Of the other papers reviewed in Section 2.3, the highest reported ink conductivities

post-processing were equal to 4.16% and 2.06% of bulk silver without degrading their AM substrate [68] [70].

Table 2.1: Properties of AM materials and processes most compatible with the printing of electronics [3].

Material	AM Process	Glass Transition/Heat Deflection Temperature (°C)
ULTEM 9085	FFF	186
ULTEM 1010	FFF	215
Antero 800NA	FFF	149
RGD525*	PolyJet	80

*Via Stratasys Material Selection Guide for Factory Floors & PolyJet Materials Data Sheet

In an effort to circumnavigate this AM substrate temperature processing limit, researchers at The University of Texas at El Paso have chosen a novel approach of thermally embedding copper wires with bulk resistivity into FFF substrates – coined the Multi3D system, as discussed in Section 2.3.1 [59]. However, when only considering DW inks, the m4 3D printer from Roach and colleagues discussed in Section 2.3.1 was only able to achieve a resistivity of 200 * 10^-6 Ω·m from its silver ink using photonic curing from a xenon flash lamp, far higher than bulk silver with a resistivity of 1.59 *10^-8 Ω·m [63]. The printer was used to DW conductive traces alongside extrusion DIW soft elastomer resin, inkjetted acrylate-based polymer, and FFF printed ABS. With the photonic curing method, the printer was able to achieve lines with consistent resistivity without further oven post-processing. This method also provides a method for avoiding complications caused by the relatively low temperature limit for oven post-processing. Lopes and coauthors also used an alternative sintering approach with selective laser sintering; however, they found that attempting to cure the side profiles of the DIW ink using the laser resulted in sample substrate degradation, as shown in Figure 2.33 [58].

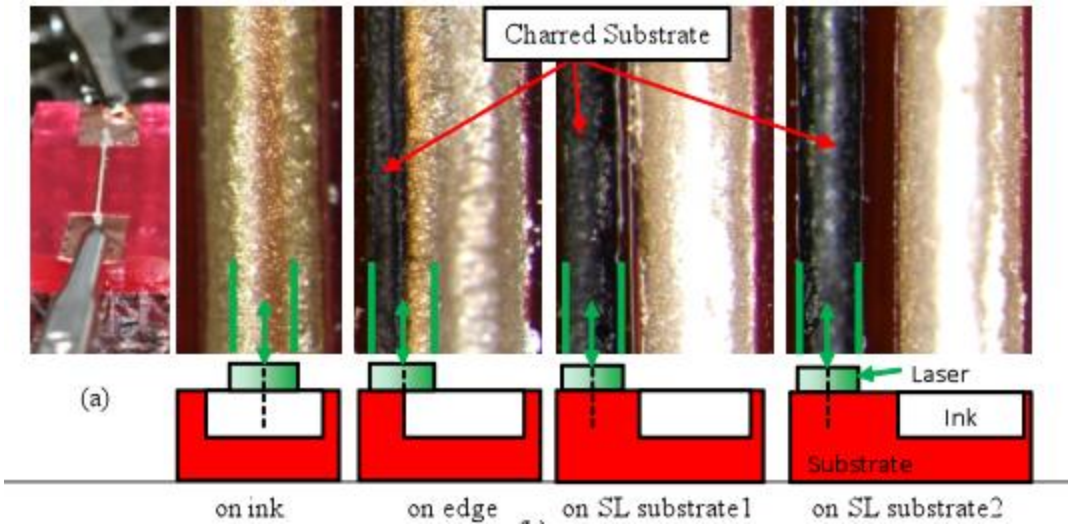

Figure 2.33: Substrate degradation resulting from laser sintering of a metal-based conductive ink [58].

As discussed by Jang and coauthors, other sintering techniques such as microwave sintering, electrical sintering, plasma sintering, and laser sintering have may drawbacks including the requiring complex instruments and a narrow operation range to achieve particle sintering. Jang and coauthors proposed that intense pulsed light sintering (IPL), another name for the photonic curing used by the m4 3D printer previously discussed, is capable of quickly heating and sintering particles without damage to low temperature capable substrates. This effect is due to localized heating occurring on metal nanoparticles as a result of surface plasmon resonance caused by IPL irradiation [88]. Although IPL shows very promising capabilities and advantages, sintering results can dramatically change with different trace widths and pattern intervals under the same IPL conditions. This can lead to non-uniform resistance in applications requiring varying traces and patterns [89].

In an attempt to offer an alternate solution to high conductivity printed inks, Mireles and coauthors attempted to create an FFF system for various low temperature solder alloys. Although these alloys were able to provide higher conductivity, successful deposition with constant parameters remained an issue [90]. Laser direct structuring (LDS) offers another alternative capable of obtaining robust and highly conductive traces with almost any thermoplastic substrate. However, this LDS process requires the part to first be given a chemical alkaline bath, adding another step to the build process [91].

2.4.2 Poor Adhesion/Interaction with AM Substrate

In their characterization of materials to be compatible with AM electronic parts, Espalin and coauthors highlighted “high spatial resolution” and “superior surface finish with minimal porosity’, stating that VP holds an advantage over FDM [3]. A substrate with high porosity will result in uncured flowing ink forming shorts between lines (shown in Figure 2.34); this is especially an issue in substrates printed with strands of material such as FFF. For example, when Optomec and Stratasys partnered to print conformal circuits delivering power and antennas on a FFF modeled UAV structure, as shown earlier in Figure 2.26, the wing surface had to be grid blasted and applied with a dielectric undercoat to smooth the FDM surface and fill holes between material strands [56].

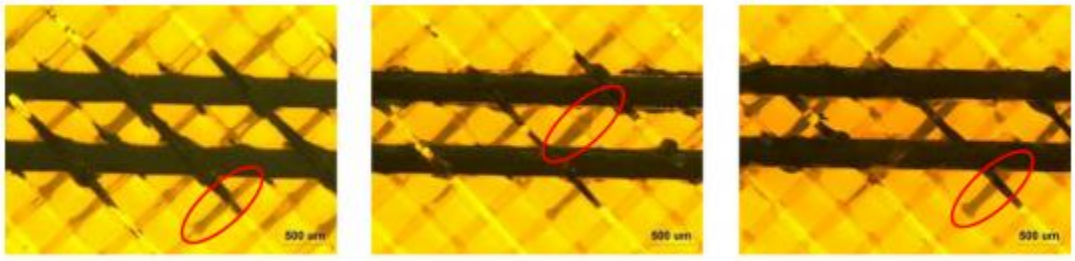

Figure 2.34: Shorts in uncured conductive ink electrical connections printed on an FDM substrate [3].

Direct write printed ink adhesion to its AM substrate is especially important as poorly adhered inks will cause open circuits and possibly damage to a device. Although traces printed on the surface of a part can be repaired, embedded traces with poor adhesion would be impossible to repair, rendering a functional AM product useless [92]. Adhesion remains an issue with AM electronics as printed traces are exposed to a variety of environments including different coefficients of thermal expansion compared to their substrate, high humidity, loading/unloading, and stretching. These conditions can cause ink traces to undergo delamination from their substrate resulting in poor substrate adhesion and eventually full removal [93].

Expanding on the topic of differing coefficients of thermal expansion between AM conductive traces and AM substrates, Roach and coauthors stated that, when printing a range of materials in

combination, a mismatch in shrinkage causes strain developed from defects such as warping and bending [63]. In an effort to increase adhesion between substrates, some authors have turned to various forms of surface treatment to enhance adhesion between metallic inks and polymer substrates. For example, in an attempt to enhance adhesion between copper ink and a polyimide substrate, Jeon and coauthors turned to oxygen plasma treatment and a two-step IPL sintering method [94].

2.5 High Performance Dielectric AM Substrates

Kapton film already widely used in many industries including those involved in aerospace, microelectronics, and biomedicine due to its highly desirable balance of electrical, chemical, and mechanical properties over a wide range of temperatures [95] [96]. Kapton has been used in applications with temperatures ranging from -269C to 400C and boasts excellent chemical resistance [97]. Because of these excellent properties exhibited by Kapton, it has been chosen to operate in environments as harsh as outer space [98]. Much like Kapton film, printed UV-DIW all-aromatic polyimide features a temperature limit greater than 400 °C before a loss in mechanical properties occurs.

UV-DIW printed all-aromatic polyimide is not the only high-performance polymer printed for research or commercial purposes. As stated by Rau and coauthors, high performance polymers such as PEEK, PEI, PPS, and PEKK have been additively manufactured and characterized. These referenced polymers are capable of maintaining mechanical stability over a higher range of temperatures compared to typical AM polymers including 143 °C (PEEK), 181 °C (PEI), 85 °C (PPS), and 162 °C (PEKK) [99] [100] [101]. However, this range of temperatures at which these materials lose mechanical properties is still far below the 400 °C limit of UV-DIW all-aromatic polyimide. The UV-DIW AM process of the all-aromatic polyimide used in this thesis make it a unique AM polymer for electronics as it features high thermal stability; this allows for the processing of metal loaded inks at higher temperatures while also being

printed with a UV-DIW system that allows for multimaterial printing such as integrated electronics and superior surface finish, unlike the FFF process used for PEI, PPS, and PEKK.

With PEI, also known commercially as ULTEM, having the highest Tg of the mentioned high-performance AM materials, its properties as a dielectric should be compared to the UV-DIW polyimide. The dielectric constant of printed all-aromatic polyimide had not been tested prior to this thesis; however, the manufacturers of Dupont Kapton HN film report a dielectric constant of 3.4-3.5 at 1 kHz, higher than 3.2-3.0 possessed by ULTEM-9085 [96].

Figure 2.35 shows the dielectric constant of FFF materials (PC, ULTEM 9085, ABS-M30, and PC-ABS), Kapton, and FR-4, the substate typically used for printed circuit boards, reported by Espalin and coauthors [3]. Kapton has a slightly higher dielectric constant than the FFF materials listed; however, it is still notably lower than the material used for printed circuit boards, FR-4, proving its viability as an electronics substate. Kapton also features a much higher dielectric strength, the maximum voltage required to cause a dielectric breakdown in a material, than all other mentioned materials [102].

In this thesis, the dielectric constant and dissipation factor of the all-aromatic polyimide, will be determined and compared to Kapton film and ULTEM-9085. The dielectric constant along with the dissipation factor, or loss factor, are considered to be among the most important and relevant substrate material values affecting the performance of a circuit (discussed further in Section 3.1) [103] [104]. If the measured dielectric properties of the UV-DIW all-aromatic polyimide are able to match or come close to that of Kapton, it would be reasonable to state that UV-DIW polyimide is a high performing dielectric substrate along with its high temperature processing limitations and superior surface finish.

	Volume resistivity (ASTM D257) (Ω cm)	Dielectric constant (ASTM D150)	Dissipation factor (ASTM D150)	Dielectric strength (ASTM D149) (V/mm)
PC[a]	2.0E+14–6.0E+13	3.0–2.8	0.0006–0.0005	360–80
ULTEM 9085[a]	1.0E+14–6.0E+13	3.2–3.0	0.0027–0.0026	290–110
ABS-M30[a]	4.0E+14–5.0E+13	2.9–2.7	0.0052–0.0049	370–71
PC-ABS[a]	2.0E+14–4.4E+13	2.9–2.7	0.0035–0.0032	340–90
Kapton[b]	1.0E+17	3.5	0.0026	154,000
FR-4[c]	5.0E+12	4.6	0.015	–

Figure 2.35: Dielectric properties of various AM and non-AM materials used in electrical applications [3].

2.6 Literature Review Summary

After reviewing direct write technologies, printed electronics, and the integration and limitation of combining additive manufacturing with direct write electronics, this section summarizes the major findings and current voids in research. Of the many direct write technologies available today, those best suited for printed conductive inks for electronics include aerosol jetting, material extrusion, and inkjetting. These technologies are able to print conductive inks with very high precision and resolution for the purpose of creating complex electronics. However, they each come with their own unique advantages and disadvantages with respect to printing electronics.

Aerosol jetting is a non-contact direct write technology able to conformally print any ink capable of being aerosolized, making it ideal for printing conductive metal nanoparticle inks. One feature of aerosol jetting that can be both helpful and harmful to research is its high customizability with respect to printing parameters. With over five different alterable printing parameters that alter printed trace properties, the traces are highly customizable but sometimes require trial and error or statistical design of experiments to obtain a desirable trace. The aerosol jetting process also yields a relatively low output of material with respect to extrusion and inkjet direct write.

Extrusion-based direct ink write is perhaps the easiest to implement of all DW methods. With its main printing mechanism relying of physical force of an ink through a nozzle, it allows for the largest

variety of inks with different properties – notably viscous metal inks with high solids loading leading to higher conductivity conductive traces. Depending on the driving technology, extrusion is also highly precise allowing for the printing of complex electrical devices.

Inkjet direct write relies depositing droplets of ink from a set height onto a substrate below. This technology is highly precise and maneuverable, allowing for the printing of complex geometries including those used in complex electronics. The main drawback of ink jetting electronics is its limited material choice due to its limited viscosity range. Highly loaded highly conductive metal loaded inks can often not be printed due to nozzle clogging issues.

Of the various conductive inks discussed. including carbon-based inks and metal loaded inks (e.g., gold, silver, and copper), silver loaded inks provide the most feasible option for printing conductive traces. Metal loaded inks feature higher conductivities than carbon-based inks; however, copper inks are subject to lower conductivity due to oxidation over time and gold inks are more expensive and less available. Because of these reasons, silver loaded inks are the preferred choice for the direct write printing of conductive traces in this thesis.

Various applications of the direct write of conductive inks were discussed including integrating the direct write processes into other AM structural printing methods to create complex 3D electronics. After reviewing the various previous and current integration of AM structures with DW conductive inks some clear limitations stood out:

- Typical AM substrates lose mechanical and/or chemical stability at relatively low temperatures, which limits the post-process curing temperature, and thus final conductivity, of the printed DW conductive inks. Ultimately, the low Tg of printed AM substrates this leads to poor performance in electronics applications.
- The AM substrates capable of the highest processing temperatures, and subsequently the highest conductivity processed inks, are produced through FFF. However, FFF produces parts

with a poor surface finish, which can lead to poor ink adhesion and electrical shorts between conductive traces.

- The dielectric constant and dissipation factor are considered the most important and relevant substrate material values that affect the performance of a circuit [103] [104]. In order for an AM material to be electronics compatible, it must feature a dielectric constant and dissipation factor comparable with well-established electronics substrates, such as ULTEM 9085, ULTEM 1010, and Kapton film.

In this thesis, an attempt at using a novel polymer material, UV-DIW all-aromatic polyimide, as the AM substrate for direct write electronics will be explored as a potential remedy to these limitations. Unlike currently available AM processable polymers, this material has high temperature stability (400 °C), which could allow for higher conductivity traces after post-processing the metal loaded inks at higher temperatures. This polymer is also printed through UV-DIW printing, allowing for a very smooth surface finish. UV-DIW also has the potential to be integrated with in-situ multimaterial electronics printing.

3. Results and analysis of the investigation into the conductivity and adhesion performance of aerosol jetted and extruded silver inks onto all-aromatic polyimide substrate

To gain a better understanding into the conductivity and adhesion performance of aerosol jetted and extruded silver inks onto all-aromatic polyimide substrate, the first two research questions are investigated:

- **Research Question 1:** How does increasing the processing temperature of silver-loaded inks printed onto Dupont Kapton affect conductivity and adhesion?
- **Research Question 2:** How does the silver-loaded conductive trace conductivity and adhesion performance compare when printed on AM all-aromatic polyimide versus commercial Dupont Kapton?

3.1 Introduction to Research Question #1 and #2

As discussed in Section 2.4, one of the limitations regarding the integration of DW Electronics and AM structures is the relatively low-temperature processing capabilities of substrate AM materials. This low temperature processing capability restricts the curing/sintering temperatures of conductive inks, which in turn limits their conductivity and leads to poorer application performance and limited scopes of feasible electronic applications. As discussed in Chapter 1 and Section 2.5, the additively manufactured all-aromatic polyimide material used in this thesis is chemically very similar to commercial Dupont Kapton, allowing it to reach temperatures more than 200C above the leading commercial available AM materials such as ULTEM (Table 2.1).

Another limitation regarding the integration of DW electronics and AM structures (discussed in Section 2.4) is the poor adhesion and interaction of DW inks with AM surfaces. This limitation mainly applies to materials produced through FFF such as ULTEM due to their inherent rough surface finish; VP produced parts feature a higher surface resolution resulting in smooth surfaces that allow for better DW ink adhesion. Given that adhesion is key for overall function of DW conductive traces in electronics, the adhesion between DW conductive inks and the polyimide must be investigated. Processing inks at higher temperatures could also cause shrinkage and delamination, as discussed in Section 2.4, giving another reason to investigate the adhesion of the inks after processing at varying temperatures.

Due to limited material availability and a desire to compare the performance of the AM all-aromatic polyimide as an DW electronics substrate to commercial Kapton, the effect of sintering at higher temperatures on ink adhesion and conductivity will first be investigated with commercial Kapton film as the substrate (this will answer Research Question 1). Using Kapton film as the substrate also provides an opportunity to determine the optimum post-processing temperature range that results in the best balance of conductivity and adhesion for the chosen DW inks before printing on the AM polyimide. Using these experimentally determined optimum ink processing temperatures, the resistivity and adhesion of AJ and DW conductive traces will be tested again on imidized all-aromatic polyimide film to answer Research Question 2, discussed in Section 3.3.2.

In order to determine the possible difference in interfacial adhesion between the DIW ink on a Kapton substrate and an imidized all-aromatic polyimide substrate, the material wetting will also be assessed. Wetting of the ink is important to achieving good adhesion between the silver-based liquid ink and the substrate [105] [106]. Better adhesion between the ink and substrate is typically observed as the contact angle decreases closer to 0°; a representation of this contact angle is shown in Figure 3.1 [107]. The aerosol jetted traces printed in this thesis will not be measured for contact angle due to the

deposition process involving accelerated nanoparticles striking the substate surface rather than a liquid ink.

$$\gamma_{sv} = \gamma_{sl} + \gamma_{lv} \cos\theta$$

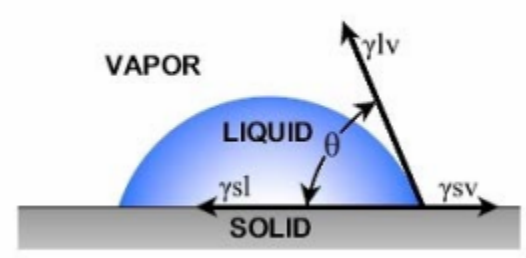

θ = Contact Angle

γ_{lv} = liquid-surface free energy

γ_{sl} = solid-surface free energy

γ_{sv} = solid-liquid free energy

Figure 3.1: Representation of contact angle formed by material wetting between a liquid ink and solid substrate [107].

3.2 Experimental Method for Answering Research Question #1 and #2

3.2.1 Materials

In order to investigate the effect of increasing sintering temperature on the resistivity and adhesion of DW inks on the polyimide substrates, commercially available DW inks must be chosen. For reasons discussed in Section 2.1 and Section 2.2, DIW extrusion and aerosol jetting are the chosen means for depositing conductive traces in this work. Due to each of their common use in the literature discussed in Chapter 2, Dupont CB028 was chosen as the ink to be used for DIW extrusion and Clariant Prelect TPS G2 was used for aerosol jetting. These inks also advertised a preferable shelf life and conductivity curing at 160 °C and 200 °C, respectively. Table 3.1 shows the advertised properties of Dupont CB028 and Table 3.2 shows the advertised properties of Clariant Prelect TPS G2. Due to its recommendation by Dupont as the choice for applications that require an 'excellent balance of properties over a wide range of temperatures', Kapton HN was used as the commercial Kapton film substrate in this set of experiments. The properties of this film can be seen on the datasheet found on Dupont's website [96]. In order to obtain a solid all-aromatic polyimide film substrate upon which DIW and AJ silver samples could be deposited, UV-DIW formulation 50k molecular weight polyamic acid, the

precursor to polyimides, with 2.5 wt% photoinitiator TPO was bladed over a standard glass slide and imidized up to 425 °C in a vacuum to obtain a flat all-aromatic polyimide film adhered to the glass slide upon which the inks could be printed. A photo of these glass slides is shown in Figure 3.2.

Table 3.1: Aerosol Jet Clariant Silver Nanoparticle Ink Advertised Properties.

Item	*Value*	*Unit*
Viscosity at 20 °C	50 ± 20	mPA*s
Solids Content	50	Wt-%
Density	1.8 ± 0.2	g/cm^3
Shelf life	6	months
Volume Resistivity	2	[x times bulk silver] on glass at ideal sintering
Sheet Resistance	0.03	[Ohm/sq] on glass at 'ideal sintering'
Recommended/Typical Cure	200°C 1hr	

Table 3.2: Extrusion Direct Ink Write Dupont CB028 Silver Microparticle Ink Advertised Properties

Sheet Resistivity	7 - 10	mΩ/sq/mil
Viscosity @ 25C	15 - 30	Pa. S
Recommended/Typical Cure	160° 1 hr	

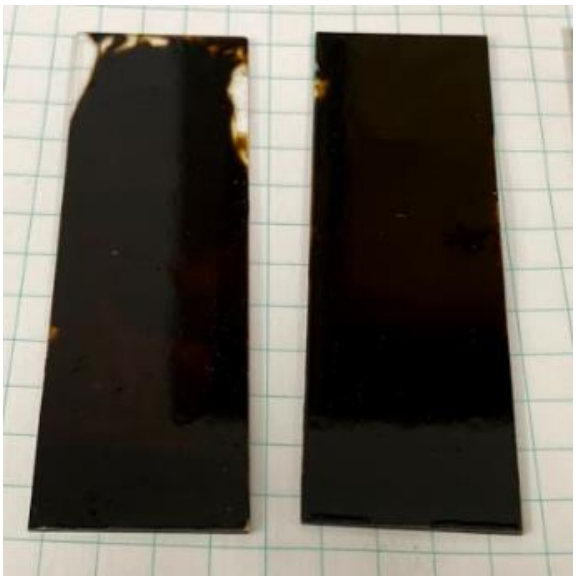

Figure 3.2: All-aromatic polyimide adhered to standard glass slides.

3.2.2 Printing and Processing

In order to determine how increasing the post-processing temperature affected the resistivity and adhesion of the printed silver inks, multiple samples were processed at varying temperatures ranging from the manufacturer's recommended values up to 400 °C - the temperature at which Dupont

states Kapton HN film is used and the approximate temperature at which the printed imidized all-aromatic polyimide starts to breakdown in mechanical properties [5]. The extrusion DIW samples were printed with a Nordson EFD pneumatic fluid dispensing system while the AJ samples were printed with an Optomec M3D system. After being processed through this range of temperatures, the extrusion DIW and AJ traces' resistivity and adhesion characteristics were measured.

In order to obtain a measurement of the volume resistivity of a trace of the silver inks used in this thesis, the following equation was used:

$$\rho = \frac{RA}{L} \qquad 1$$

Equation 1 equates the resistivity, ρ, of a printed trace to a function of the trace resistance, R, trace cross-sectional area, A, and trace length, L. Aside from the length term, which is predetermined when creating the AJ or DIW print path, the trace resistance and trace cross-sectional area each require precise measurement tools to get an accurate measurement of their values. Trace resistance cannot simply be measured using a typical two probe multimeter, since this measurement includes a resistance of the cables and the contact resistance between the probes and the trace of interest. Rather, a four probe method must be used, which eliminates the effect of the cable and contact resistance and is able to obtain accurate resistance measurements [108]. This method consists of passing a known current though a sample and then measuring the voltage potential across two points a known distance apart. Using Ohm's law, the measured voltage and known current can be used to determine the resistance term used in Equation 1. An image representation of this concept is shown in Figure 3.3 and Figure 3.4. This four point probe approach to determine conductive trace volume resistivity has been widely used in past research [18] [22].

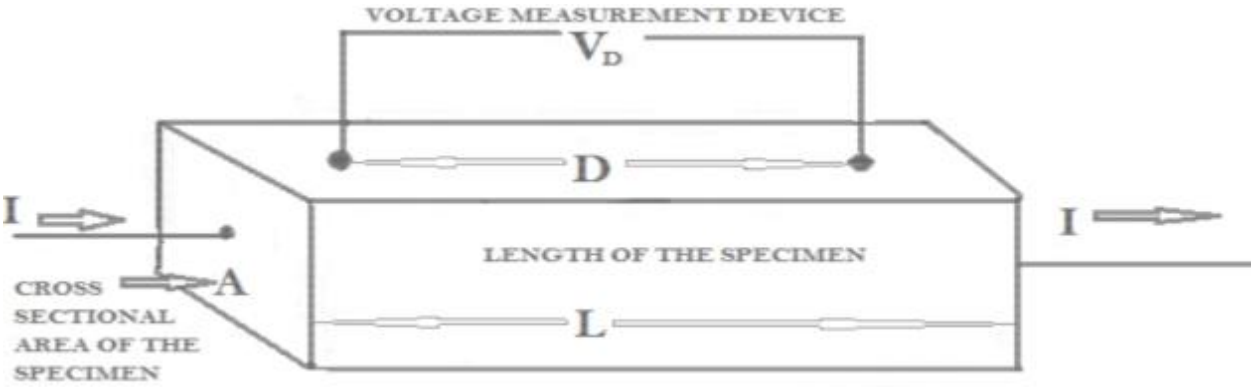

Figure 3.3: Representation of the four point probe measurement of resistance from current input, I, and voltage measurement, V_D [108]

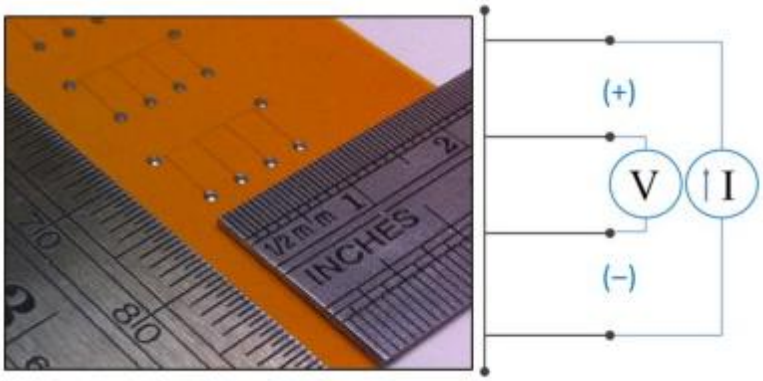

Figure 3.4: Aerosol jetted silver ink printed in four point probe resistance test arrangement with the current source (I) and the measured voltage (V) [51].

After determining how resistivity could be measured using the four-point probe and stylus profilometer approach, the extrusion DIW and AJ inks could be printed and processed. Originally, the extrusion DIW samples were printed on 0.001'' thick Kapton HN film. To adhere to the four-point method of testing resistivity, the first iteration of extrusion DIW samples were printed as shown in Figure 3.5. In this arrangement, the current would be applied through probes contacting the end of the rightmost and leftmost points of the horizontal trace and the voltage would be measured through probes contacting the bottom of the two vertical traces. However, after speaking with Virginia Tech ECE professor Dr. Arthur Ball, it was determined that the vertical voltage measuring areas of the

arrangement should be shortened to reduce any potential contact resistance error. This recommendation led to the second iteration of extrusion DIW samples, shown in Figure 3.6.

Figure 3.5: First iteration of resistivity and adhesion test samples printed with extrusion DIW of CB028 silver-based conductive ink.

Figure 3.6: Second iteration of resistivity and adhesion test samples printed with extrusion DIW of CB028 silver-based conductive ink.

Extrusion DIW Printing

After attempting to obtain a 2D cross-sectional profile of the trace shown in Figure 3.6, it was found that the Dupont Kapton film was too warped to obtain accurate profiles. This warpage was deduced to come from the ink shrinkage after drying and oven curing. In an attempt to combat this warpage, it was decided that a smaller nozzle should dispense the CB028 ink on a thicker Kapton Substrate. Therefore, the ink gauge was reduced from 30 GA, with an inner diameter of 0.15 mm, to 32 GA, with an inner diameter of 0.10mm; the 0.001'' thick Kapton HN film was replaced with 0.005''

Kapton film. It was also believed that allowing a longer time for the ink to spread before hardening could lead to more shrinkage-induced warping of the film. For all these reasons, a small study was conducted aimed at determining the optimum method to reduce film warpage. This study took place with the same arrangement shown in Figure 3.6 and printed with the new 32 GA nozzle on the new 0.005'' thick film four separate times for four separate samples. One of these samples was printed on a 90°C heated surface for immediate hardening, another was printed and immediately placed in an oven at 160 °C for 10 minutes, another was printed and immediately placed in an oven at 160 °C for 20 minutes, and the final sample was left to spread for 1 hour before they were all placed in an oven and heated at 350 °C for one hour.

After placing these samples in an oven at 350 °C for one hour, they were removed and visually inspected for film warpage; the post-processed samples are shown in Figure 3.7. It was determined that there was no obvious visual difference between the various samples and all of them were free from warping with the new smaller nozzle and thicker film. However, the 10-minute immediate cure method was used in an attempt to possibly minimize spreading and therefore avoid shrinkage related delamination at higher processing temperatures. The final extrusion DIW printing parameters are shown in Table 3.3. These parameters were used for DIW printing on both commercial Dupont Kapton and bladed imidized UV-DIW all-aromatic polyimide material. Due to limited material availability of polyimide adhered to glass slides, three resistivity arrangements were printed per polyimide film. For DIW of conductive ink, this simply meant repeating the same printing pattern spaced out to fit three resistivity patterns on the same slide.

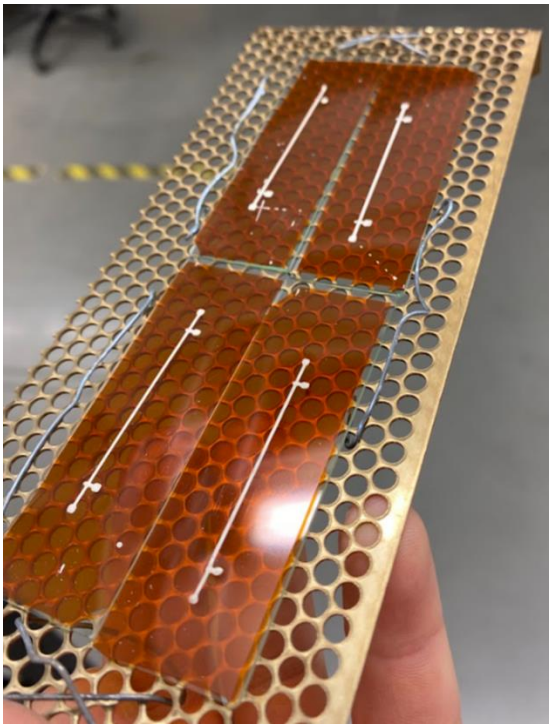

Figure 3.7: The four printed extrusion DIW samples after being placed in an oven at 350°C for one hour created to determine the best method for minimizing film warpage.

Table 3.3: Extrusion DIW parameters used to print Dupont CB028 silver ink.

Nozzle Inner Diameter	0.10 mm (32 GA)
Pneumatic Pressure	90 PSI
Deposition Head Offset	0.1 mm
Print Speed	3.0 mm/s

Aerosol Jet Printing

Moving onto the process for printing the aerosol jetted resistivity arrangements. Based on the Optomec Aerosol Jet M3D user manual, as well as previously cited literature, the ultrasonic atomizer was used for ink atomization, mainly stemming from its advertised viscosity. In using the ultrasonic atomizer, a wide array of printing parameters can be altered including atomizer gas flow rate, sheath gas flow rate, ultrasonic atomizer current, tube temperature, platen temperature, and deposition speed. A process diagram highlighting these various factors is shown in Figure 3.8. Due to the wide variability possible from combining these factors, previous literature using Clariant silver nanoparticle ink

published by Smith and coauthors [18] as well as Zhang and coauthors [51] was studied in order to obtain good starting point.

The main goal in obtaining an acceptable aerosol jetted silver trace was to print continuous uniform lines with the most material and least overspray possible in order to obtain a higher degree of accuracy when measuring the cross-sectional area of the lines. This resulted in some unforeseen challenges as parameters initially chosen for thick lines worked for the first 30 minutes of printing but quickly dropped in quality as the system started depositing the ink while it was too 'wet', which resulted in splatter and overspray. This event of aerosol jetted lines changing in quality and geometry over time with constant printing parameters was also found by Smith and coauthors [18]. The line quality in printing a 2mmx2mm square arrangement before and after printing for 30 minutes is shown in Figure 3.9.

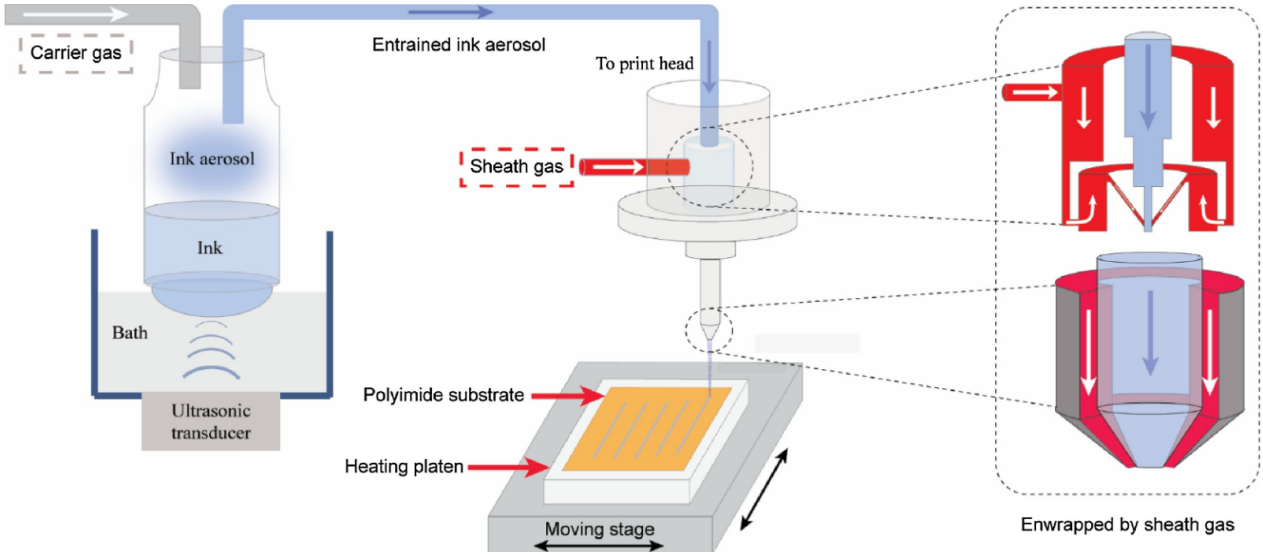

Figure 3.8: The process diagram for aerosol jetting using the ultrasonic atomization process [51].

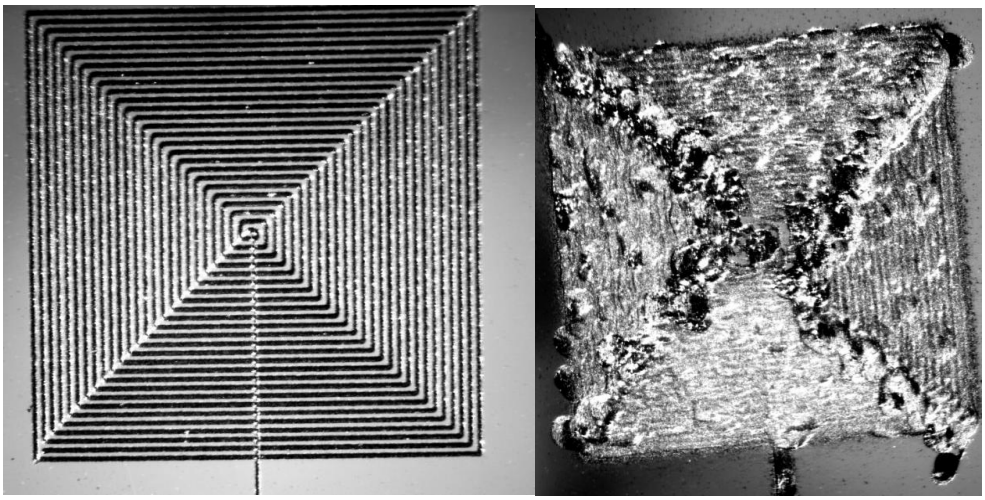

Figure 3.9: Result of aerosol jetting a 2mmX2mm square of silver nanoparticle ink before (left) and after (right) 30 minutes of printing.

After discovering that the initial printing parameters inspired by literature did not result in acceptable silver traces, a trial and error approach was adopted. With prior knowledge of the limitations of the Optomec system used in this thesis, ultrasonic atomizer power was kept current at its upper threshold. Smith and coauthors found that a platen temperature of 60 °C resulted in the highest quality lines, so that factor was kept constant as well [18]. Therefore, the deposition speed, sheath gas, and carrier gas printing characteristics were altered until a constant line with minimal overspray was observed and held visually constant after 1 hour of continuous printing. The progression of line quality after varying these parameters is shown in Figure 3.10, with the final parameters being shown in Table 3.4. The final line quality was achieved through steadily decreasing the carrier gas to limit the amount of material traveling and increasing the sheath gas to achieve a tighter spread of particles.

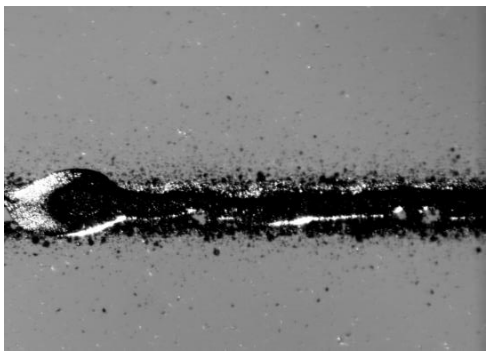

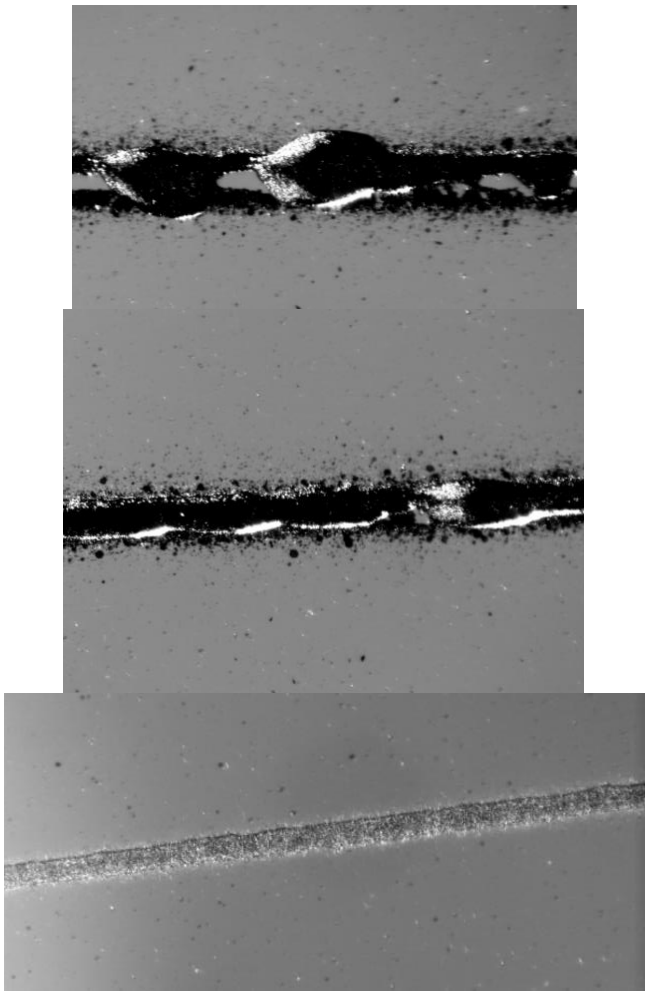

Figure 3.10: Progression, top to bottom, of printed silver nanoparticles after varying printing parameters used for visual inspection of line quality (trace widths range from approximately 45 μm to 100 μm).

Table 3.4: Final printing parameters chosen for aerosol jetting silver nanoparticles after trial and error approach to achieving acceptable line quality.

Sheath gas flow rate	65 sccm
Carrier gas flow rate	24 sccm
Platen temperature	60 C
Deposition Speed	2.0 mm/s
Tube temperature	Not used
Platen vacuum	ON
Atomizer current	FULL
Nozzle Tip Diameter	150 μm

In order to match the aerosol jetted resistivity arrangements printed for the extrusion DIW,

Optomec VMTools AutoCAD widget was used. The shape infill was optimized to have a consistent ink fill

in on 2mm x 2mm probe contact pads. The final AutoCAD shape used for printing on commercial Dupont Kapton film is shown in Figure 3.11 and features a 35 mm trace length in the center portion used for the final resistivity testing – identical to the length used in the extrusion DIW arrangement. For printing on bladed imidized UV-DIW all-aromatic polyimide material, the same resistivity pattern made was multiplied in AutoCAD to fit three patterns on one slide (Figure 3.12).

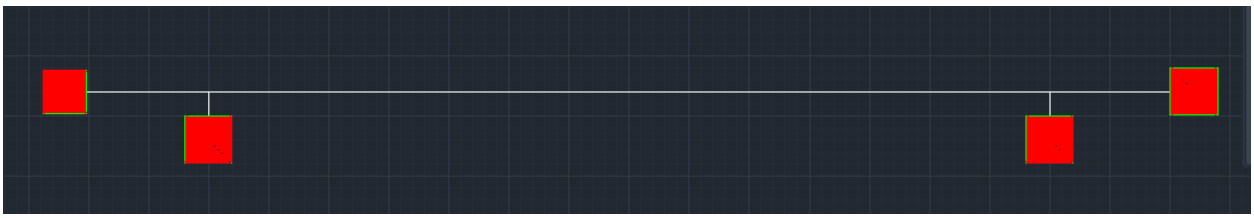

Figure 3.11: AutoCAD VMTools drawing used for printing resistivity testing arrangements with the Optomec Aerosol Jet on commercial Dupont Kapton film.

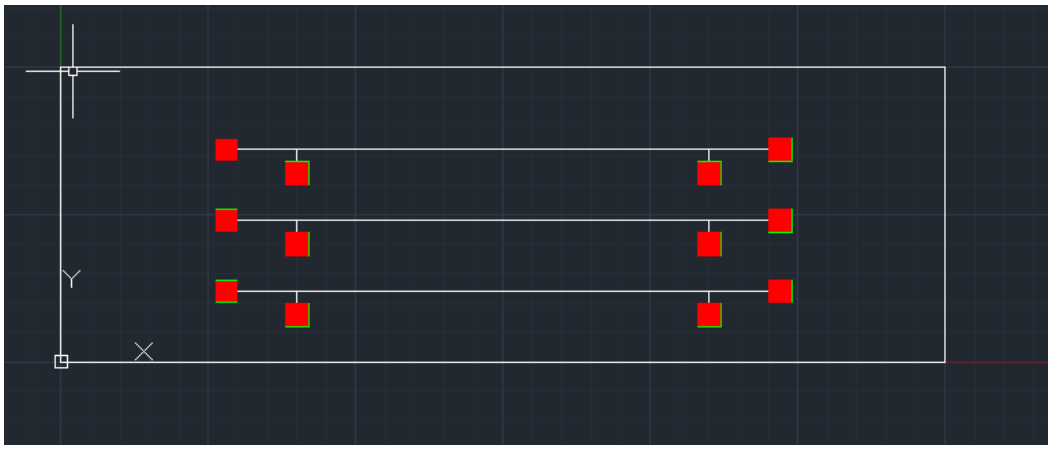

Figure 3.12: AutoCAD file used to output a toolpath including three resistivity arrangements for the Optomec Aerosol Jet on bladed imidized UV-DIW polyimide.

3.2.3 Sample Oven Post Processing

After successfully eliminating warpage from the DIW on Dupont Kapton samples and achieving desirable line quality from the aerosol jetting of silver nanoparticle ink, three separate samples were printed of each DW process for each processing temperature. For the extrusion DIW of CB028 on Dupont Kapton, samples were treated at 160 °C, 200 °C, 250 °C, 300 °C, 350 °C, and 400 °C (a total of 18 total samples). For the aerosol jetting of Clariant Prelect TPS G2 silver nanoparticle ink, samples were treated at 200 °C, 250 °C, 300 °C, 350 °C, and 400 °C (a total of 15 total samples). The samples treated at

160 °C, 200 °C, and 250 °C were placed in an open-vent ambient Fisher Scientific Vacuum Oven Model 282A for one hour at their specified temperature. Due to limitations with the Fisher oven, the samples treated at 300 °C, 350 °C, and 400 °C were placed in a KJ Group GSL 1600X Tube Furnace with ambient airflow for one hour along with a 30 minute ramp-up time as required to avoid damaging temperature overshoot as specified by the user manual.

After printing the triple resistivity arrangements on four separate bladed imidized UV-DIW polyimide film slides for DIW and another four slides for AJ, the slides were processed using the same methods as the commercial Dupont Kapton substrate slides. The four DIW slides were processed for one hour at 300 °C, 325 °C, 350 °C, and 375 °C in a KJ Group GSL 1600X Tube Furnace with ambient airflow including a 30 minute ramp-up time as required to avoid damaging temperature overshoot. Three of the AJ samples were sintered at 300 °C, 325 °C, and 350 °C in the same KJ Group GSL 1600X Tube Furnace and the one remaining slide was processed at 275 °C in an open-vent ambient Fisher Scientific Vacuum Oven Model 282A for one hour. The reasoning for these temperature processing ranges is discussed in Section 3.3.1 and Section 3.3.2. A photo of printed and processed DIW and AJ samples on bladed imidized UV-DIW all-aromatic polyimide film is shown in Figure 3.13 and Figure 3.14.

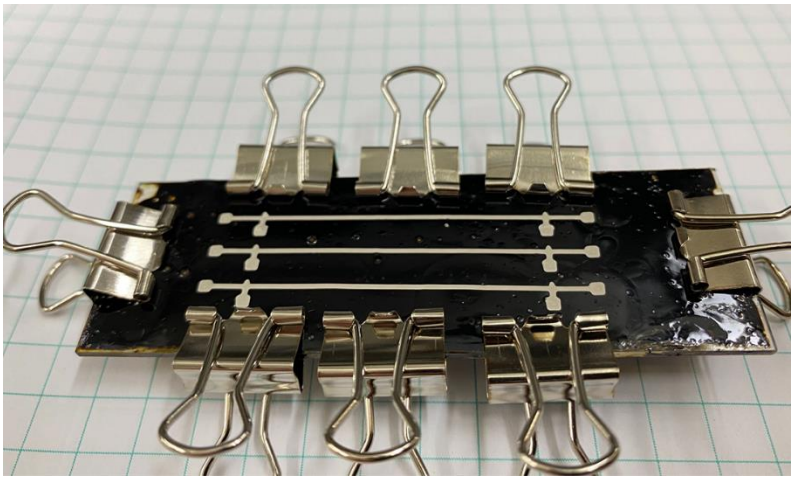

Figure 3.13: Three DIW resistivity arrangements printed on a bladed all-aromatic polyimide substrate.

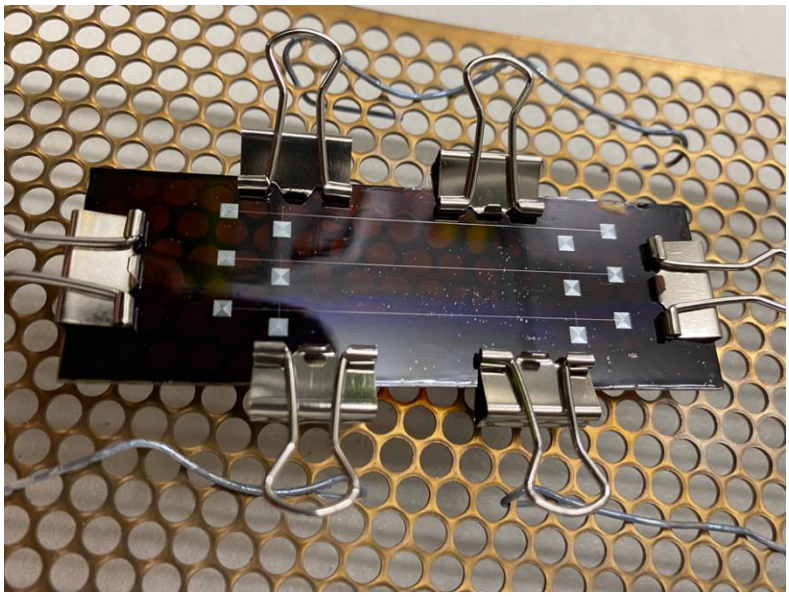

Figure 3.14: Three AJ resistivity arrangements printed on a bladed all-aromatic polyimide substrate.

3.2.4 Resistivity Testing

Rather than using separate devices to pass a known current and then measure the voltage for resistance, a Hewlett Packard 34401A Digital Multimeter with four-point probe resistance measurement capabilities and a resolution of 100 μΩ was used (Figure 3.15). To obtain 2D cross-sections to measure the cross-sectional area of the conductive traces printed in this thesis, a DektakXT stylus profilometer with 4 angstrom repeatability was used. A photo of thesis profilometer with an aerosol jetted sample beneath its stylus is shown in Figure 3.16.

Figure 3.15: Hewlett Packard 34401A Digital Multimeter used in this thesis for resistance measurements.

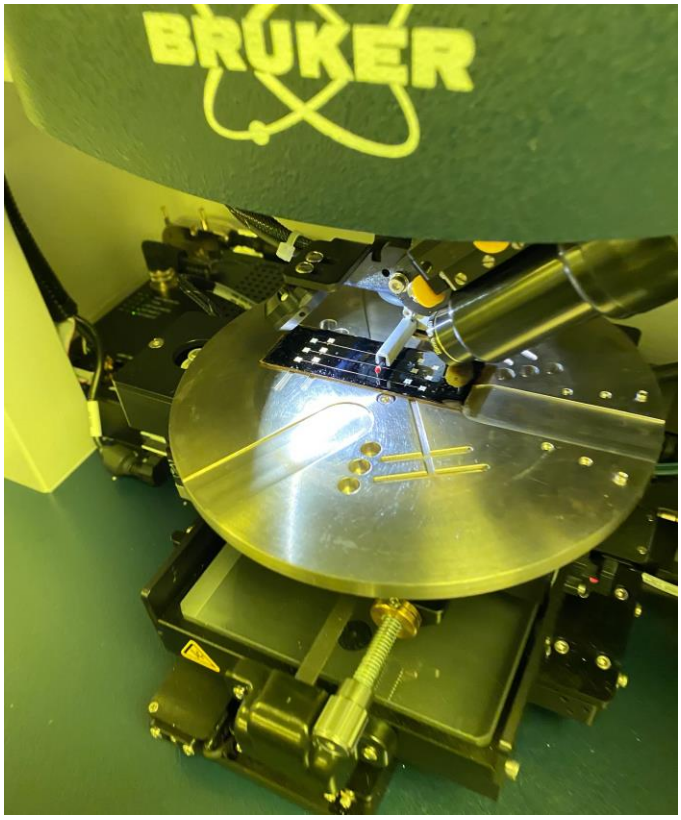

Figure 3.16 DektakXT Stylus Profilometer used to determine 2D trace cross-sections.

These samples were tested for resistivity using the four-probe resistance measurement with the HP 34401A digital multimeter and Bruker DektakXT stylus profilometer. The DektakXT was used to take measurements at 25%, 50%, and 75% along the length of the center 35mm portion to achieve a more accurate average cross-sectional area for each line. Each Kapton film substrate was also adhered to a standard glass slide with double sided tape to aid in getting more accurate profilometry scans. A photo of the DIW and AJ traces being measured for resistance using the four point probe method is shown in Figure 3.17 and Figure 3.18, respectively.

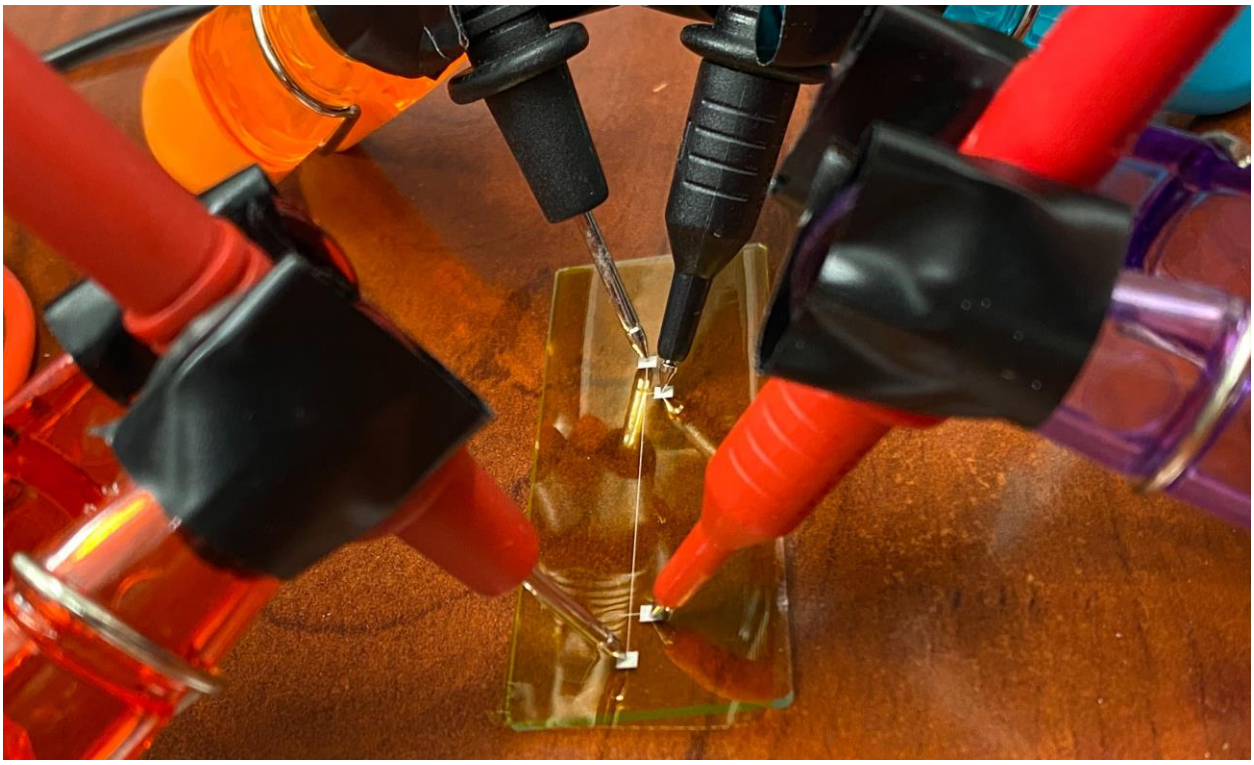

Figure 3.17: Aerosol jetted silver nanoparticle ink on Dupont Kapton film being tested four resistance using the four point probe test method.

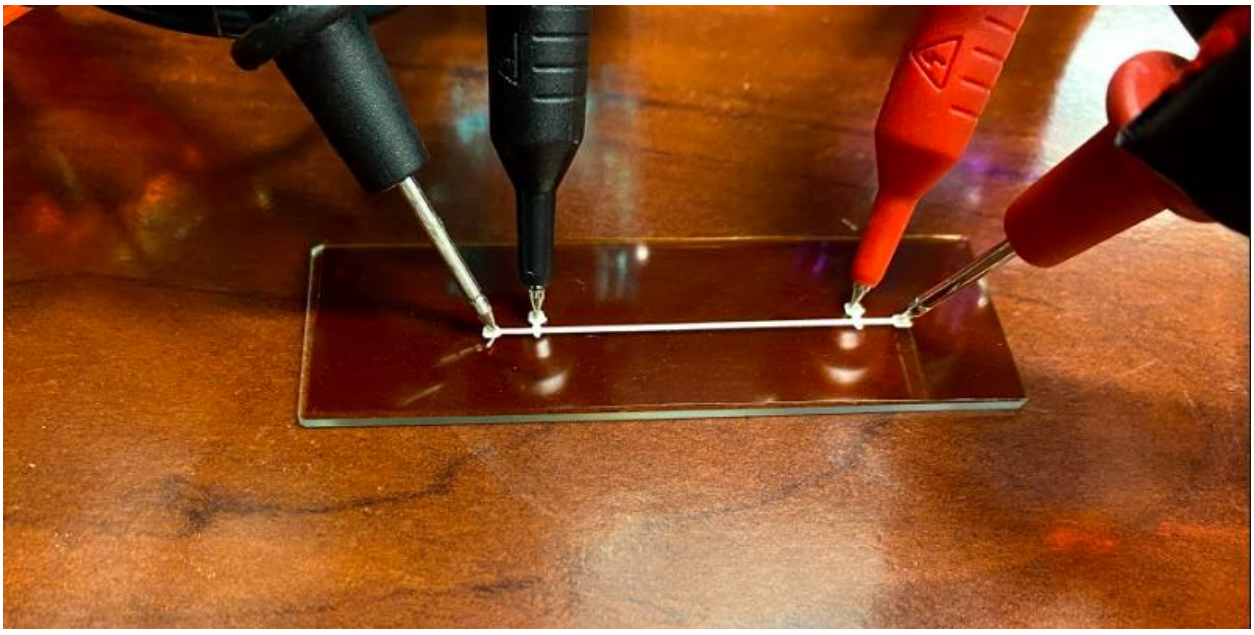

Figure 3.18: Extrusion direct ink write printed silver ink on Dupont Kapton being tested for resistance using the four point probe test method.

3.2.5 Adhesion and Material Wetting Testing

In order to test adhesion of the of the DIW and AJ traces, a standard scotch tape test was used. This method simply involves placing a stretch of standard 3M Scotch tape along the length of the trace, pressing down on the tape to assure good adhesion to the trace, and tearing the tape off in a brisk and steady motion at an angle of 180 degrees. This method is seen in literature and is commonly used as a qualitative test of ink adhesion to a substrate [57] [109]. A photo of an DIW and AJ sample with scotch tape applied is shown in Figure 3.19 and Figure 3.20, respectively. Since this test is qualitative rather than quantitative, a sample pass (if no part of the silver was removed) and fail (if any of the silver was visually removed) test was conducted. Each of the samples were inspected with a microscope before and after testing in order to assure that any trace removal was found.

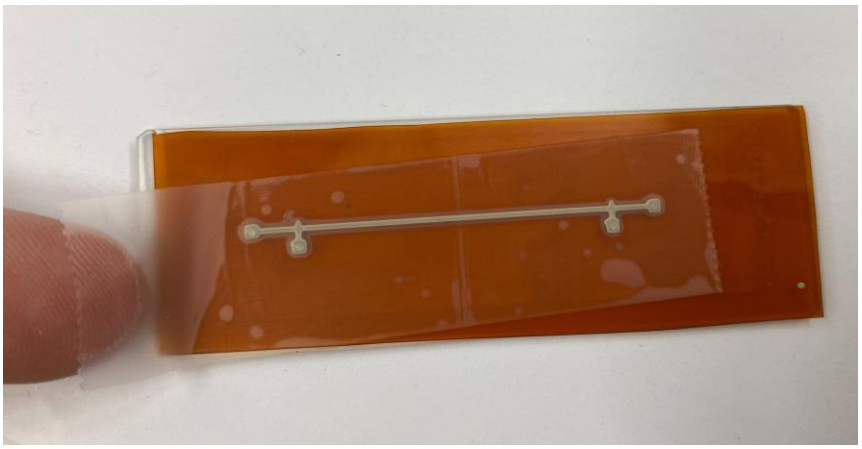

Figure 3.19: Scotch tape applied over a DIW sample with heat treated silver ink.

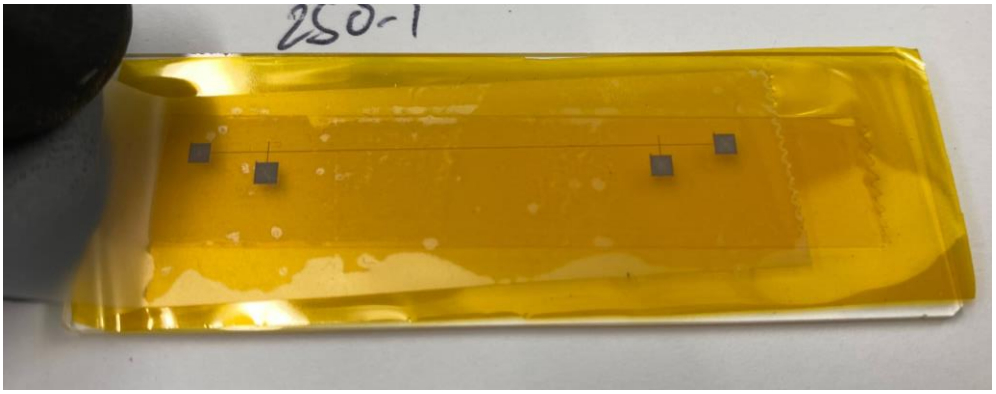

Figure 3.20: Scotch tape applied over an AJ sample with heat treated silver ink.

In order to investigate the DIW CB028 ink material wetting on Kapton HN films and all-aromatic polyimide films, ten separate droplets of DIW ink were deposited on a piece of 0.005'' thick Kapton HN film and then also on bladed all-aromatic polyimide film. The droplets were dispensed from a 15GA nozzle with 0.5 second periods of pneumatic pressure extrusion using the same DIW system previously discussed, an example of these droplets on all-aromatic polyimide film is shown in Figure 3.21. These droplets were imaged using a microscope camera and backlight and then processed in ImageJ image measurement software to determine the approximate contact angle for each droplet. Figure 3.22 and Figure 3.23 show the image capture setup diagram and an example measurement made in ImageJ. The contact angle was measured 1 minute and 5 minutes after the ink was dispensed to allow it time to spread if needed.

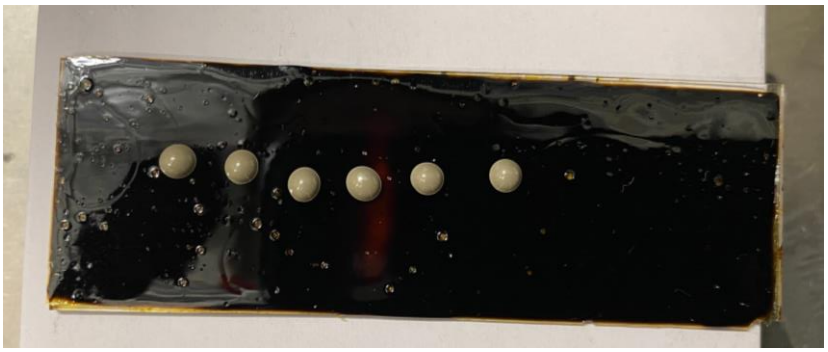

Figure 3.21: All-aromatic polyimide film with silver CB028 silver ink droplets used for contact angle measurements.

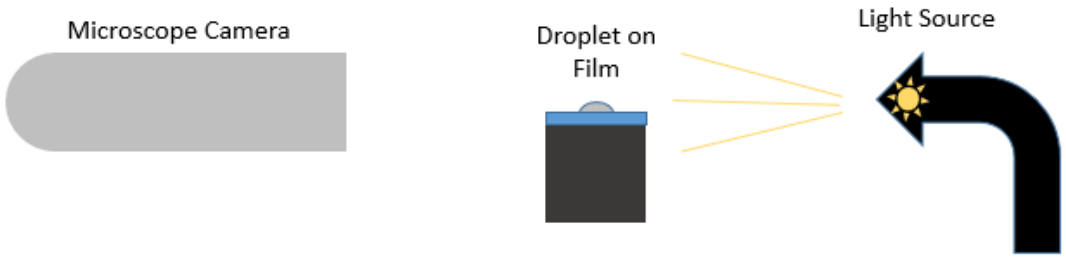

Figure 3.22: Experimental setup diagram for obtaining contact angle photos of CB028 silver ink droplets.

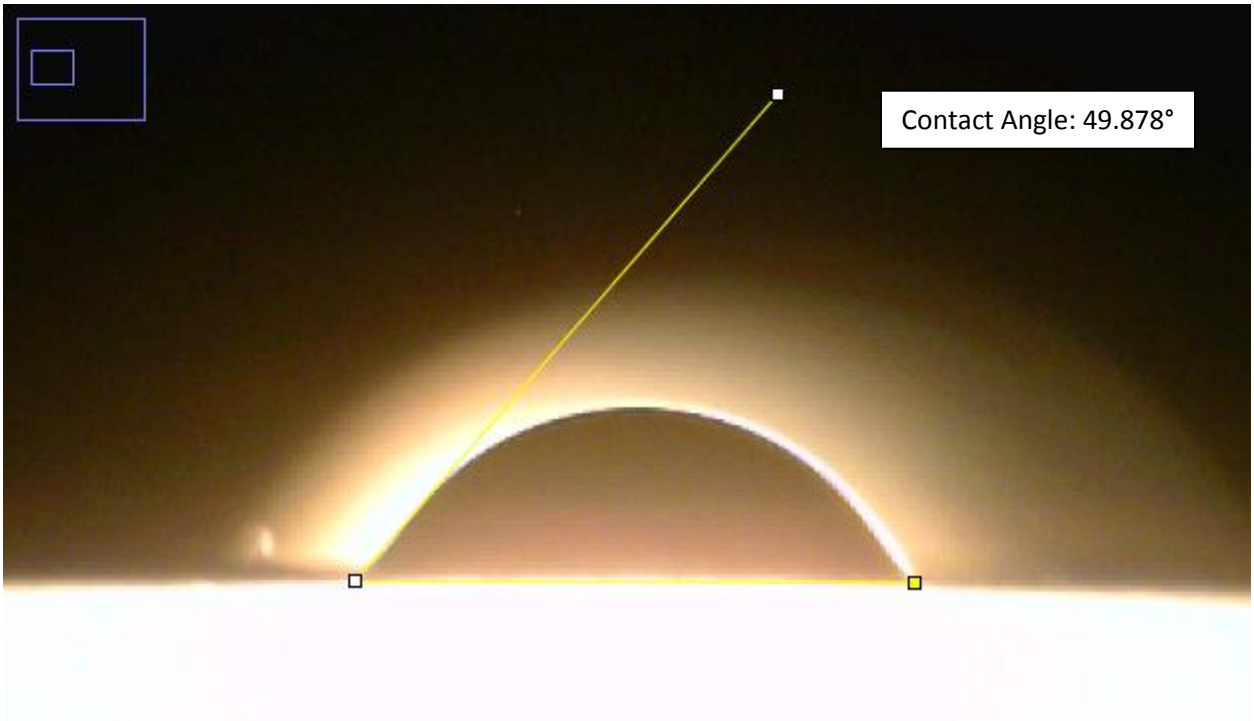

Figure 3.23: Example measurement of CB028 silver ink droplet contact angle on bladed polyimide film 1 minute after extrusion, completed in ImageJ software.

3.3 Results and Discussion

3.3.1 Research Question #1

Research Question #1: How does increasing the processing temperature of silver-loaded inks printed onto Dupont Kapton affect conductivity and adhesion?

Results

After printing and post-processing thermal treatments as described in Section 3.2.2 and Section 3.2.3, the samples were tested for resistance, cross-sectional area, and scotch tape adhesion performance. As shown in Figure 3.24 and Figure 3.25, the resistivity of the DIW and AJ samples were determined through the testing of the resistance and cross-sectional area using methods discussed in Section 3.2. The actual values shown in Figure 3.24 and Figure 3.25 are included in Table A.1 and Table A.2 (located in Appendix A), respectively. This includes the original tested resistance and cross-sectional area values as well as the resistivity in relation to the resistivity of bulk silver.

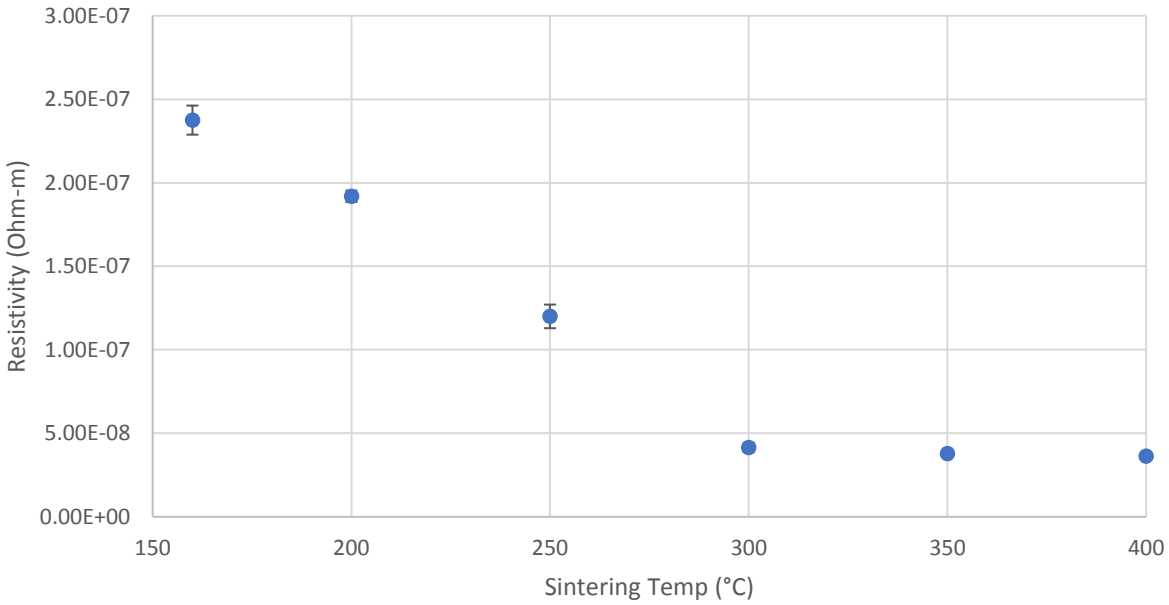

Figure 3.24: Resistivity of the DIW traces after being treated at varying temperatures for 1 hour.

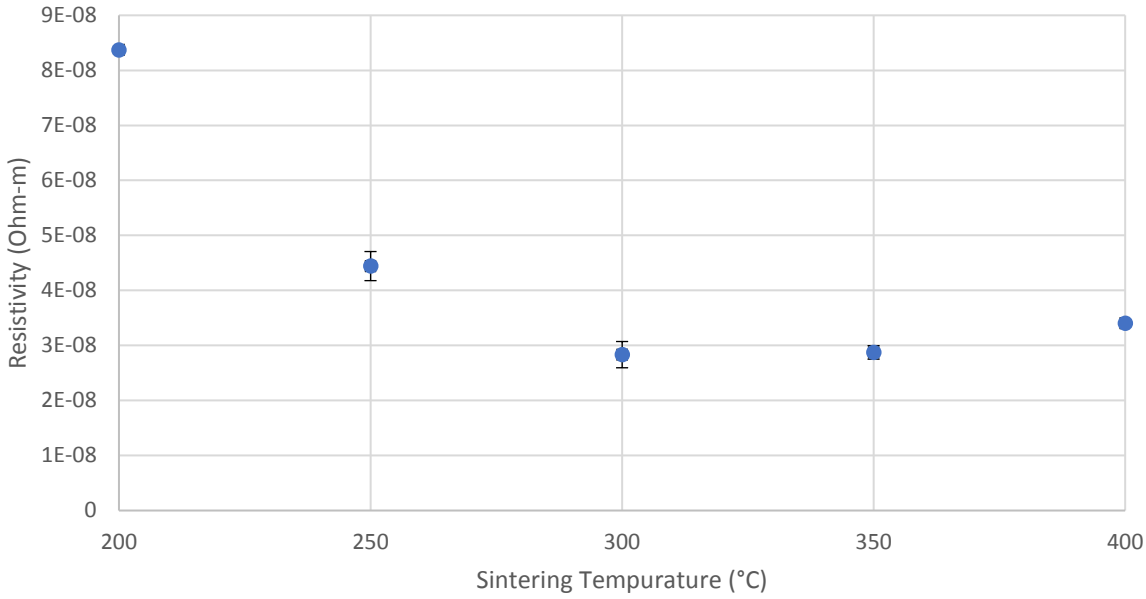

Figure 3.25: Resistivity of the AJ traces after being treated at varying temperatures for 1 hour.

Following the procedure discussed in Section 3.2.5, each sample was inspected before and after scotch tape was applied/removed to determine if any amount of trace was removed. Table 3.5 present the results of the scotch tape trace adhesion test. An example of an aerosol jetted sample processed at 200 °C before and after failing a scotch tape adhesion test is shown in Figure 3.26.

Table 3.5: Scotch tape adhesion test results of DIW and AJ samples.

Processing Temperature (°C)	DIW Samples Passed	AJ Samples Passed
160	3/3	N/A
200	3/3	1/3
250	3/3	1/3
300	3/3	2/3
350	3/3	2/3
400	3/3	2/3

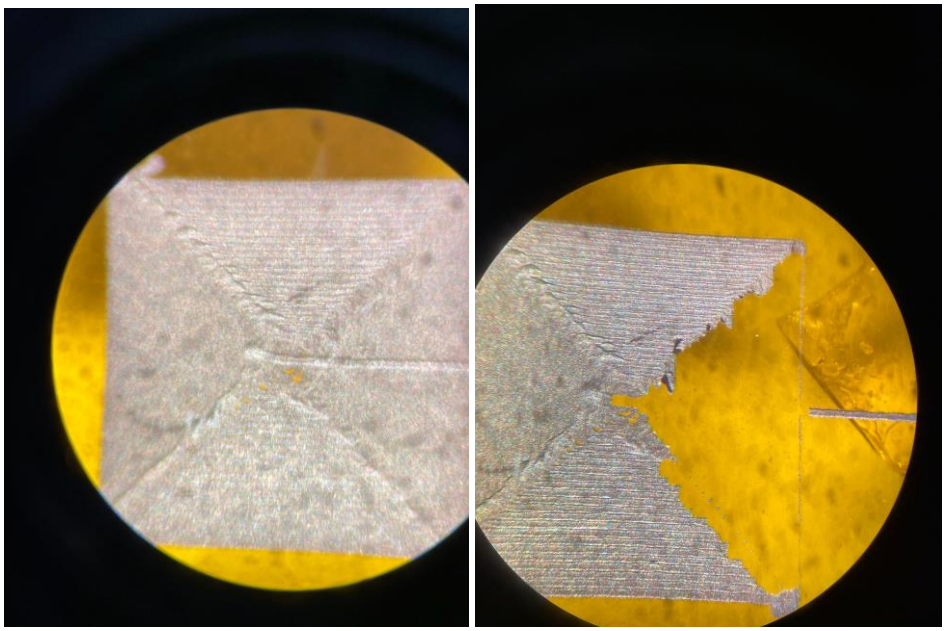

Figure 3.26: Aerosol jet sample processed at 200 °C filled in 2mm x 2mm square before and after failing a scotch tape adhesion test.

Discussion

Figure 3.24, Figure 3.25, and Table 3.5 show that increasing the processing temperature of Dupont CB028 past its manufacturer-specified value of 160 °C up to 400°C has notable effects on the resistivity of the printed traces. The traces' resistivity decreased from around 14.94±0.55 times the value of bulk silver at 160 °C to 2.29±0.028 times bulk silver – a decrease of around 83% at 400 °C. This result is enhanced by the fact that all of the samples, regardless of processing temperatures, passed the scotch tape adhesion tests achieving no removal of their trace. This indicates that electronics printed on an additive manufactured part capable of processing temperatures above 300°C (such as printed all-aromatic polyimide) would be able to perform better than the same electronics printed on a additively manufactured part capable of processing temperatures around 200 °C (such as ULTEM 1010).

The decrease in resistivity is likely partially due to burn off of non-metal ink additives as processing temperatures increased. This concept is illustrated by Figure 3.27 showing some decrease in average cross-sectional area of each DIW trace as the applied processing temperature increased. A two-tailed t-test between the sample cross-sectional areas of 250 °C and 300 °C revealed a p value of

0.01232, indicating that the difference between the two sets of areas is significant. It is worth noting that the Kapton substate used with the DIW traces experienced a color darkening after being processed at 400 °C. This indicates a chemical change in the Kapton and a possible decrease in mechanical properties; Figure 3.28 shows the color difference between a Kapton substrate processed at 300 °C and 400 °C.

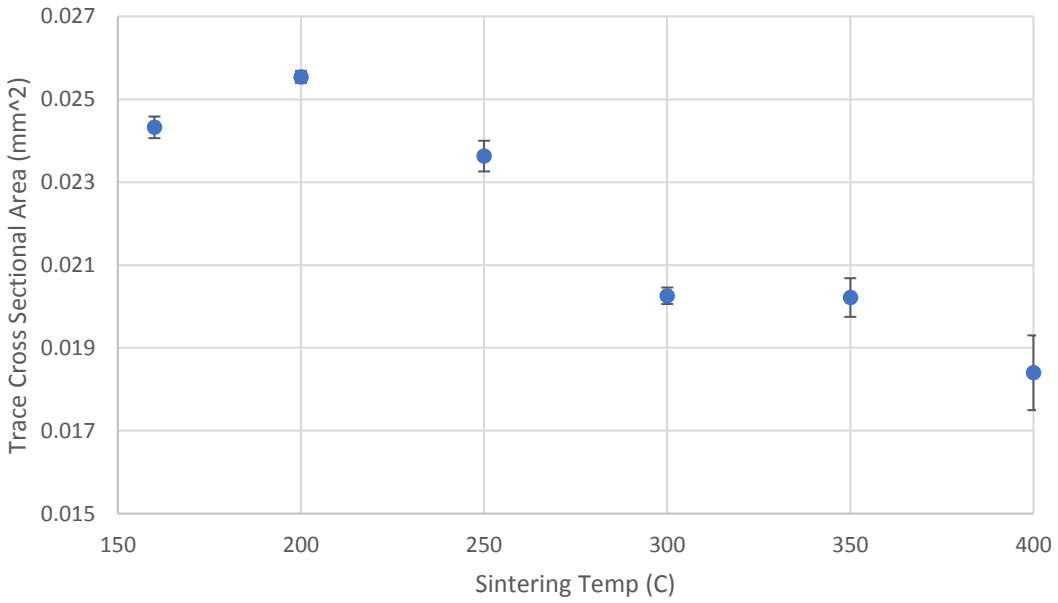

Figure 3.27: Average cross-sectional area of each DIW silver trace at varying processing temperatures.

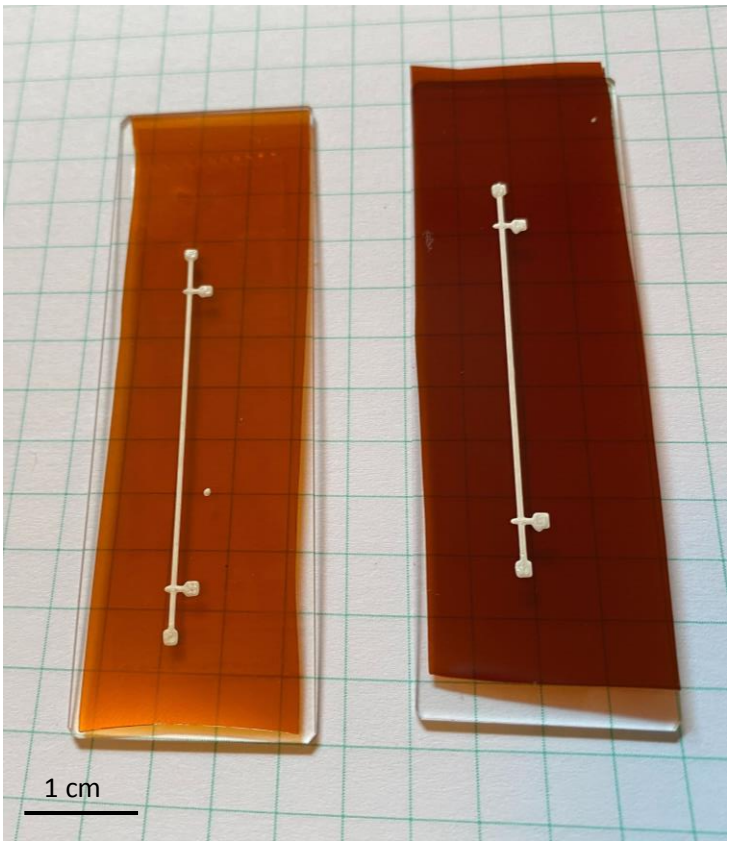

Figure 3.28: The substrate color difference between a DIW resistivity sample processed at 300 °C (left) and 400 °C (right).

From Figure 3.25 and Table A.2, it is clear that, like the DIW traces, the AJ traces experience a significant decrease in resistivity ($p=0.0005$) after increasing the processing temperature from 200 °C up to 400°C. This decrease is highlighted by the fact that the resistivity of the silver traces have an average of 5.27±0.013 times the resistivity of bulk silver after 200°C processing and an average of 1.78±0.15 times the resistivity of bulk silver at a processing temperature of 300 °C. The resistivity of the AJ traces then steadily increases to an average resistivity of 1.81 times bulk silver after 350 °C processing and 2.14 times the resistivity of bulk silver after 400 °C processing. This rise in resistivity above a processing temperature of 300°C indicates that 300°C is the optimum processing temperature of the aerosol jetted silver nanoparticles. This finding is corroborated in past in literature where Rahman and coauthors investigated the high temperature stability of aerosol jetted silver nanoparticles and found that impedance of silver nanoparticle traces increased at processing temperatures greater than 300 °C which

was attributed to increased grain growth of sintered metal nanoparticles at increased temperatures [110].

As seen in Table A.1, the DIW silver samples all passed the scotch tape adhesion testing at all temperatures ranging from 160 °C to 400 °C. This indicates that the increasing processing temperature did not have a significant effect on the adhesion of the ink to the Kapton substate. The aerosol jetted resistivity arrangements did not experience an overall consistent trend in passing/failing the scotch tape adhesion testing. Samples at both the high and low end of the temperature spectrum experience delamination and a failure to withstand the removal of scotch tape. It is worth noting that samples treated at 200 °C and 250 °C experienced a passing rate of only 33% while the samples treated at 300 °C, 350°C, and 400 °C experienced a passing rate of 66%. This could indicate that the increased coalescence of particles after processing at higher temperatures increased their adhesion to the substrate and cohesion to other particles. However, more studies are needed before this conclusion can be made.

One of the main findings sought after by the scotch tape adhesion testing of these silver traces was to determine if processing the traces at higher temperatures past the manufacturer specification of 200 °C had any negative impact on the traces adhesion to the substrate. From this adhesion test, it can be concluded that increasing the processing of the AJ traces to 400 °C, past the manufacturer specification of 200 °C, did not have any negative effect on the adhesion of the silver nanoparticle traces to the Kapton substrate.

3.3.2 Research Question #2

Research Question #2: How does the silver-loaded conductive trace conductivity and adhesion performance compare when printed on AM all-aromatic polyimide versus commercial Dupont Kapton?

Results

After printing four extrusion DIW samples of silver Dupont CB028 onto blade-casted all-aromatic polyimide and completing thermal post-processing, as described in Section 3.2, the samples were tested

for resistance, cross-sectional area, and scotch tape adhesion. The tests were also completed for the four other blade casted all-aromatic polyimide films with three resistivity arrangements per slide printed on with aerosol jetted Clariant Prelect TPS G2 silver nanoparticle ink. The results of the DIW and AJ resistivity measurements are shown on Figure 3.29 and Figure 3.30, respectively, along with the previous results from Kapton for comparison. The full resistivity data for the DIW and AJ traces printed on the all-aromatic film are shown in Table A.3 and Table A.4 (Appendix A), respectively.

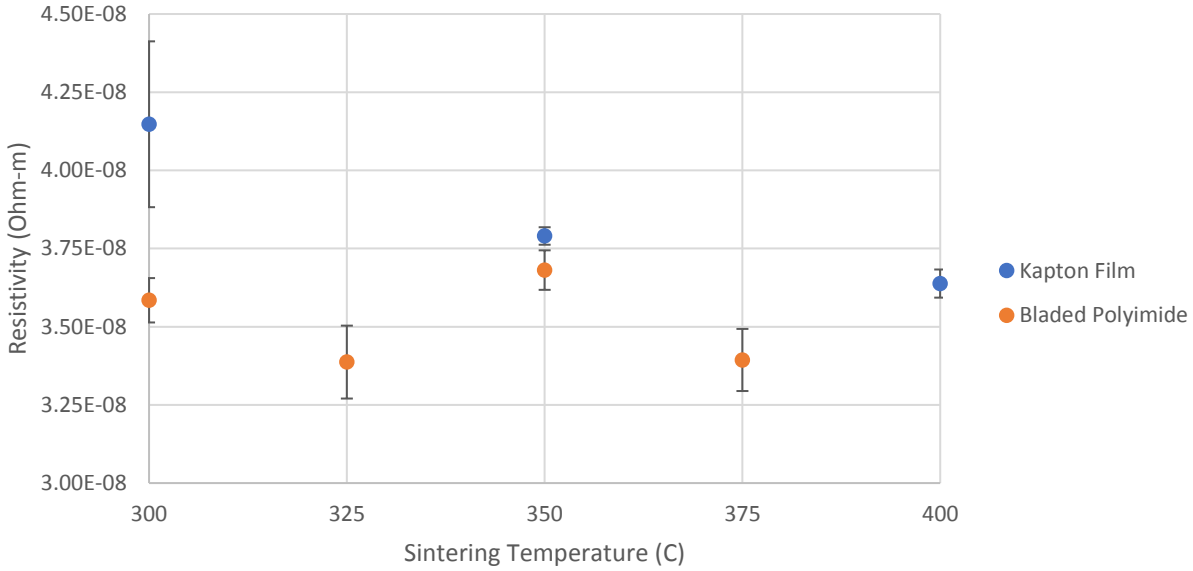

Figure 3.29: Measured resistivity of DIW traces on commercial Kapton film and lab-made all-aromatic polyimide film.

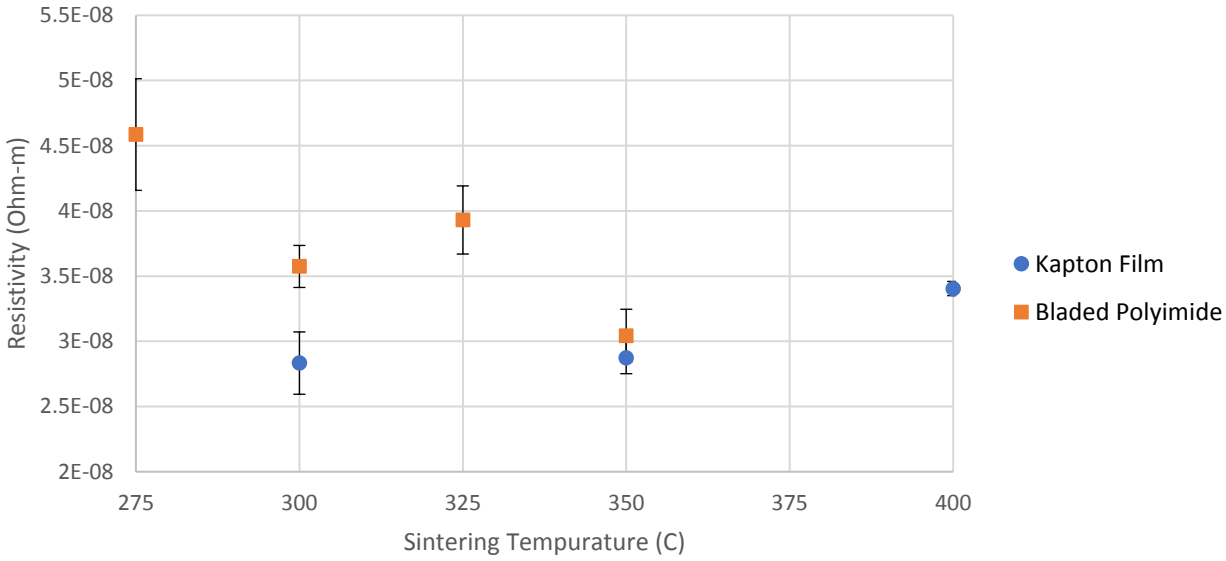

Figure 3.30: Measured resistivity of AJ traces on commercial Kapton film and lab-made all-aromatic polyimide film.

After performing a scotch tape adhesion test on all silver traces on all-aromatic polyimide substrate, the results were collected and are shown in Table 3.6. All DIW passed the test and experienced no trace delamination; however, some AJ samples did not pass the test and experienced some silver delamination.

Table 3.6: Scotch tape adhesion test results of DIW and AJ traces on all-aromatic polyimide film.

Processing Temperature (°C)	DIW Samples Passed	AJ Samples Passed
275	N/A	2/3
300	3/3	2/3
325	3/3	1/3
350	3/3	3/3
375	3/3	N/A

Table 3.7 shows the average results of the 10 angle measurements per film after sitting for 1 minute and 5 minutes; full measurement data is shown in Table A.5. In order to determine if the two substrates statistically differ in contact angle 1 and 5 minutes after droplet deposition, a two-tailed t-test was conducted. This t-test resulted in a p value of 0.2974 after 1 minute and 0.9016 after 5 minutes,

indicating that there is insufficient evidence to infer that there is a difference in the measured ink contact angle of the two films.

Table 3.7: Contact angle average and standard deviation of CB028 silver ink on Dupont Kapton film and polyimide film.

Droplet #	Kapton Film After 1 Minute	Polyimide Film After 1 Minute	Kapton Film After 5 Minutes	Polyimide Film After 5 Minutes
Average	54.54	52.81	52.01	52.15
Std. Dev.	4.21	2.21	1.26	2.94

Discussion

Figure 3.29 and Table A.3 shows that Dupont CB028 ink printed on all-aromatic polyimide film experiences the similar resistivity at processing temperatures equal to or greater than 300°C when compared with traces printed on commercial Kapton and processed at similar traces. In terms of direct comparison at 300 °C and 350°C, DIW traces experienced very similar values of trace resistivity. Being exact, traces processed at 300 °C experienced an average resistivity of 2.25±0.04 times the resistivity of bulk silver when printed on all-aromatic polyimide compared to 2.61±0.17 times the resistivity of bulk silver when printed on commercial Kapton film. Furthermore, traces processed at 350 °C experienced an average resistivity of 2.32±0.04 times bulk silver when printed on all-aromatic polyimide compared to 2.38±0.02 times the resistivity of bulk silver when printed on commercial Kapton film. A two-tailed t-test revealed that the resistivity differences from traces on both films at 300 °C and 350 °C are not significant with p values of 0.1411 and 0.1967. Therefore, it can be said that trace resistivity of DIW CB028 performs similarly when printed on all-aromatic polyimide compared to Kapton film.

Figure 3.30 and Table A.4 shows that Clariant Prelect TPS G2 silver nanoparticle ink aerosol jetted on all-aromatic polyimide film experiences similar resistivity at processing temperatures equal to or greater than 250 °C when compared to traces printed on commercial Kapton and processed at similar values. In terms of direct comparison at 300 °C and 350°C, AJ traces experienced very similar values of

trace resistivity. More specifically, traces processed at 300 °C experienced an average resistivity of 2.25 ±0.10 the resistivity of bulk silver when printed on all-aromatic polyimide film compared to an average resistivity of 1.78±0.15 times the resistivity of bulk silver when printed on Kapton film. This difference and better performance on Kapton film is considered significant with a two-tailed t-test p value of 0.03815. This trend is continued at a processing temperature of 350 °C, traces printed on all-aromatic polyimide experienced an average resistivity of 1.95±0.09 times the resistivity of bulk silver – higher than the average resistivity of traces printed on Kapton and processed at the same temperature which experienced an average resistivity of 1.81±0.08 times the resistivity of bulk silver. This difference in resistivity between the two films processed at 350 °C is not considered significant with a two-tailed t-test p value of 0.5392. It is unclear whether the significant difference between the 300 °C samples is due to differing interaction between the silver nanoparticles and the two substrates. It is possible that the ink being close to the end of or past its shelf life during printing on all-aromatic polyimide contributed to the higher resistivity of the printed traces. This is due to, because of COVID-19 related closures, the Clariant ink was printed on all-aromatic polyimide almost 4 months after being printed on Kapton film.

Like those DIW traces printed on Kapton film, all DIW traces printed on all-aromatic polyimide and processed at temperatures from 300 °C to 375°C passed the scotch tape adhesion test. Furthermore, aerosol jetted traces on all-aromatic polyimide featured a 66% pass rate at sintering temperatures greater than 250 °C; the exact same passing rate was found with traces printed on commercial Kapton film and processed in the same temperature window. These findings indicate that overall material adhesion between the inks and the two substrates is similar and both are capable of reliably performing as an electronics substate for DIW silver ink – additional investigation is needed before the same can be said about AJ silver ink due to the 33% failure rate with both substates after processing at temperatures greater than 250 °C. This conclusion is further supported by the

investigation into material wetting, which determined that the contact angle of CB028 silver ink on both commercial Kapton polyimide and the all-aromatic polyimide was statistically the same. This indicates that good adhesion and similar line widths from DIW ink can be expected on both substrates. Examples of measured cross-sectional trace profiles of both AJ and extrusion DW samples showing similar spreading on each substrate after processing at 350 °C is shown in Figure 3.31. The AJ profile sample shape showing an accumulation of particles at the edges of the trace is called the 'coffee ring effect' and is commonly seen in literature [22].

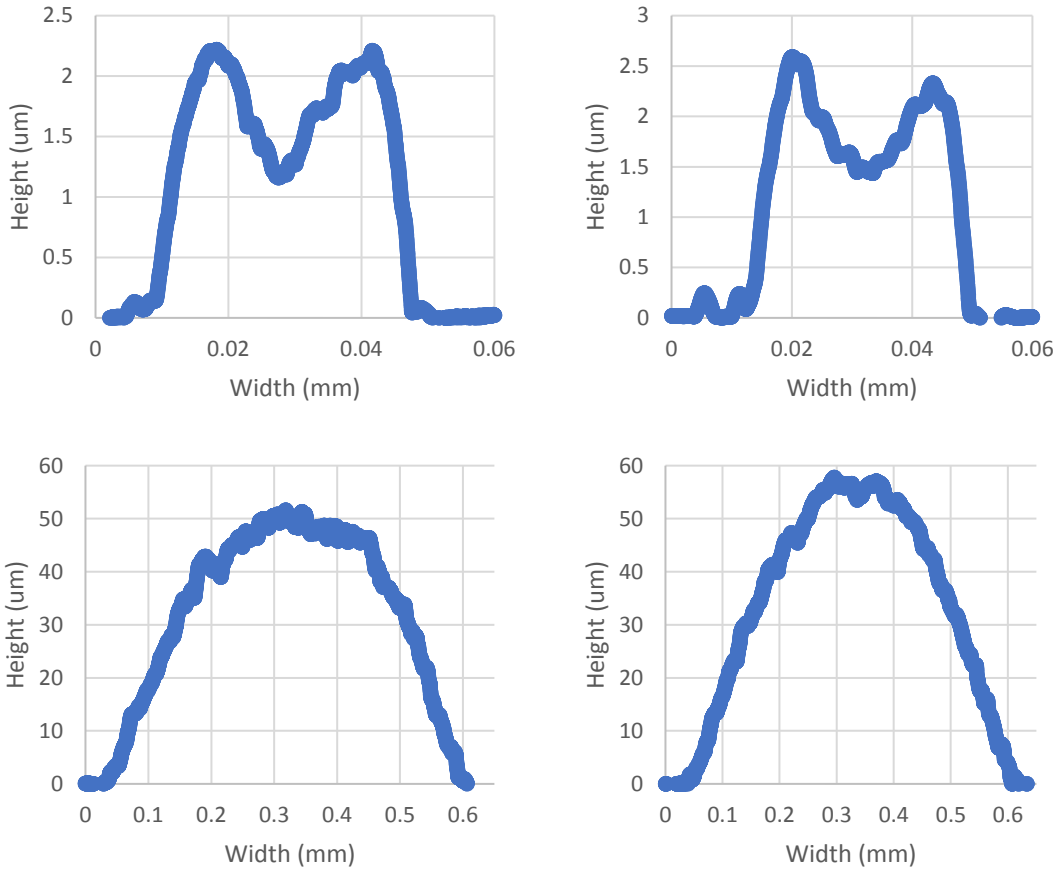

Figure 3.31: Examples of 350 °C processed extrusion DW (lower half) and AJ (upper half) profiles on bladed polyimide (left half) and commercial Kapton (right half) measured with the DektakXT stylus profilometer.

Data from the tables and figures previously discussed can also be used to estimate an optimum processing temperate for future research involving printing DIW or AJ silver traces on 3D printed all-

aromatic polyimide. The results in Section 3.3.2 indicate that the lowest resistivity DIW silver ink occurs at 325 °C and 375 °C and at 350 °C for AJ silver ink. However, due to the possible AJ silver ink material expiration affecting printed traces, as well as previous literature suggesting an optimum processing temperature of 300 °C, more investigation may be needed before a claim can be made that a 350 °C processing temperature will result in better performance than a 300 °C processing temperature.

3.4 Possible Applications of 3D Printed Complex Structure All-Aromatic Polyimide

Section 3.3.2 shows that the additive manufacturable all-aromatic polyimide has adhesion and temperature processing capabilities very similar to commercial Dupont Kapton. The main advantage of the all-aromatic polyimide is its ability to be printed into complex structures through either UV-DIW or VP. This enables the creation of complex electronics created with all-aromatic polyimide structure along with AM deposited conductive traces with processes such as extrusion direct ink write, aerosol jetting, and ink jetting.

An interesting finding when evaluating the possible electronic applications with all-aromatic polyimide as the substrate was the solderability increase of the CB028 ink after processing at higher temperatures. It was found that the CB028 could not be soldered after being processed at temperatures lower than 300 °C. Figure 3.32 shows soldering attempts on DIW resistivity samples processed at 400 °C (left) and 250 °C (right). The sample processed at 400 °C was able to be soldered easily versus the 250 °C, was not able to be soldered at all. The solderability of the higher temperature processed DIW ink indicates that complex structures and conductive traces could be printed with all-aromatic polyimide and silver inks to form a complex AM printed electronic parts integrated with separately produced electronic components such as IC chips and capacitors.

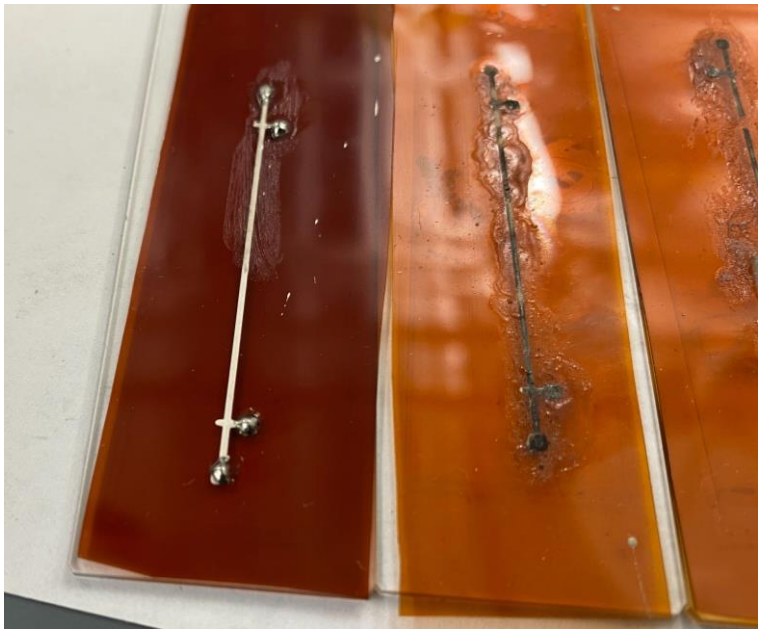

Figure 3.32: DIW CB028 resistivity samples processed at 400 °C (left) and 250 °C (right) showing the inability for the 250 °C sample ink to be soldered.

To test this concept, a DIW silver Dupont CB028 ink was applied to a printed complex all-aromatic polyimide lattice structure to form a circuit to which an LED could be soldered onto. This structure was then processed at 350 °C indicating that the resistivity of the DIW silver would be about 2.15 times bulk silver, as shown in Table A.3. An LED was then soldered onto the conductive ink and connected to a current source using wires, as shown in Figure 3.33.

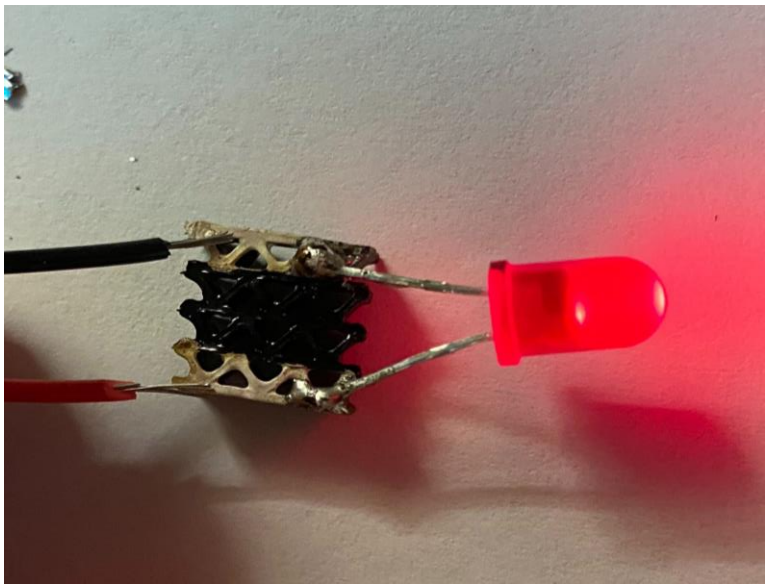

Figure 3.33: 3D printed all-aromatic polyimide lattice with conductive ink and a soldered-on LED.

Although this LED soldered onto a 3D printed all-aromatic polyimide truss structure is simple, it demonstrates a much larger space of capabilities and possibilities. This material is capable of being printed into complex structures and then processed at temperatures up to 400 °C which enables the soldering of separately manufactured electronic components. This opens possibilities for complex shapes with soldered-on complex electronics experiencing lower loss due to lower resistivity ink lines. Not only would the conductive ink traces feature solderability and lower resistivity, unlike ULTEM which would experience difficulty in soldering along with higher resistivity connections, the overall structure would be stable at higher temperatures than typical AM materials, which would allow for it to be deployed in harsher and more demanding environments.

4. Results and analysis of the investigation into the dielectric performance of UV-DIW printed all-aromatic polyimide

To gain a better understanding of the dielectric performance of UV-DIW all-aromatic polyimide, the following research questions is investigated in this section:

- **Research Question 3**: How does the dielectric performance of additively manufactured all-aromatic polyimide compare to commercial Dupont Kapton and similar high-performance AM polymer substrates?

4.1 Introduction to Research Question #3

In Section 2.5 the dielectric performance of various high-performance additive manufacturing polymers and standard printed circuit board material was discussed. The dielectric constant along with the dissipation factor, or loss factor, are considered to be among the most important and relevant substrate material values affecting the performance of a circuit [103] [104]. The measured dielectric constant of a material, also known as relative permittivity, is the AC frequency-dependent ratio of the capacitance of that material when placed between two plates with respect to the capacitance of a vacuum or air between the plates [111]. This relationship is shown in Equation 2 below:

$$\varepsilon_r = \frac{C}{C_0} \qquad 2$$

With respect to this thesis, insulating materials, such as the polymers discussed, are typically used as a substrate to insulate components of an electrical system. However, they can also be used as the dielectric material in a capacitor. Typically, a lower dielectric constant is better for high frequency AC circuit applications or to minimize electrical power loss in power applications [111]. Dissipation factor is the AC frequency-dependent ratio of the capacitive reactance of a material to its resistance indicating the electrical energy lost in an insulator. This loss, or power dissipation, is typically due to heat, and a

lower dissipation factor indicates that a material is a more efficient insulator of current. A perfect dielectric material features current that flows 90° out of phase with the voltage; however, most polymers are not perfect and feature a current that leads the voltage by some degree less than 90°. This imperfect dissipation loss angle is the tangent of the small angle between the perfect 90° current, known as capacitive current I_C, and the slightly less than 90° current, known as the resistive current, I_R [111].This concept is illustrated in Equation 3 and Figure 4.1.

$$Dissipation\ Factor = \tan(\delta) = \frac{I_C}{I_R} \quad 3$$

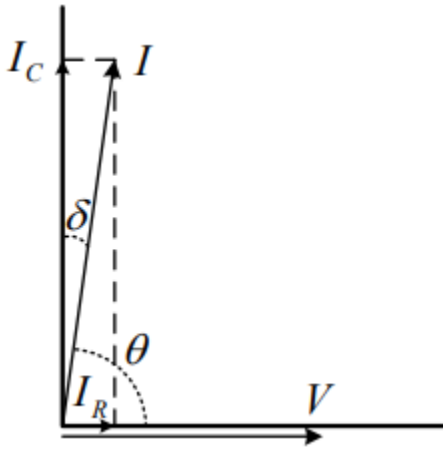

Figure 4.1: Dissipation loss angle, δ, that occurs when a current leads a voltage by some angle less than 90° [111].

Using an impedance analyzer in conjunction with a parallel plate capacitor-based sample test fixture provides an opportunity to determine the dielectric constant and dielectric loss tangent, another name for the dissipation factor, from analytical relationships. This is a achieved through a technique known as impedance spectroscopy, which is used to determine the resistance and capacitance of a material as a function of an applied AC sinusoidal voltage signal [112]. The impedance analyzer is able to measure the real and imaginary impedance of a capacitor material in the parallel plate test fixture as a function of its applied AC voltage signal frequency. The real and imaginary components of this material impedance, Z, are known as Z’ and Z’’ respectively; this relationship is shown in Equation 4. Equation 5

shows the formula for the capacitance of a parallel plate capacitor with a dielectric material between the plates in terms of the material dielectric constant, *k*, the constant permittivity of free space, $\in_0$, the flat area of the dielectric material, *A*, and the distance between the plates, *t*.

$$Z = Z' - jZ'' \quad (4)$$

$$C = \frac{k \ \in_0 \ A}{t} \quad (5)$$

From the real and imaginary impedance data measured with the impedance analyzer, the capacitance of the dielectric polyimide in the parallel plate set up can be calculated and used to find the dielectric constant, *k*, from Equation 5. As utilized in previous impedance and dielectric spectroscopy literature, the capacitance of the dielectric material is a function of the applied frequency its real and imaginary impedance – shown by Equation 6. Equation 5 and 6 can then be combined to reveal the overall formula to determine the dielectric constant of a material, ε', shown in Equation 7. The ε' term also represents the real part of the calculated permittivity of the material; when used in conjunction with the imaginary part of permittivity, ε'' shown in Equation 8, the terms can be used to calculate the loss tangent – also known as the dissipation factor of the material, as shown in Equation 9 [113] [114] [115].

$$C(\omega) = \frac{1}{\omega} \cdot \frac{Z''}{Z'^2 + Z''^2} \quad (6)$$

$$\varepsilon'(\omega) = \frac{t}{\omega A \varepsilon_0} \cdot \frac{Z''}{Z'^2 + Z''^2} \quad (7)$$

$$\varepsilon''(\omega) = \frac{t}{\omega A \varepsilon_0} \cdot \frac{Z'}{Z'^2 + Z''^2} \quad (8)$$

$$tan\delta(\omega) = \frac{\varepsilon''(\omega)}{\varepsilon'(\omega)} \quad (9)$$

Discussed in Section 2.5, it was found that Kapton has a slightly higher dielectric constant, with a value of 3.5, than some other additively manufactured materials such as polycarbonate, ULTEM 9085,

and ABS, which ranged from 2.7 to 3.2. However, its dissipation factor was relatively low and equal to ULTEM 9085 with a value of 0.0026 – lower than ABS. These values indicate that Dupont Kapton itself can perform at a high level as an electronics substrate, comparable with other high-performance AM polymers. One of the goals of this work is to characterize the dielectric performance of UV-DIW all-aromatic polyimide. Since the processed UV-DIW all-aromatic polyimide is chemically identical to commercial Kapton, it is expected that their dielectric properties will be very similar. However, given that the Kapton-imitation all-aromatic polyimide AM material investigated in this thesis is has never been electrically characterized and the fact that increased char yields of the AM all-aromatic polyimide introduces residual carbon (a known conductor of electricity) after processing [5], the dielectric constant and dissipation factor of the material must be determined. The next section will discuss the methods used to investigate and answer this research question.

4.2 Experimental Method for Answering Research Question #3

As discussed in the previous section, an impedance analyzer was used to collect data complex impedance data from running an AC sinusoidal voltage across the material in a parallel plate capacitor-based setup. This complex impedance data allowed for the calculation of the dielectric constant and dissipation factor of various printed polyimide disks, using Equations 6 through 9. The same method of data collection was also used to collect impedance data on a film of Dupont Kapton as a control to determine the overall accuracy of the method and provide a good source of comparison to a known value for the polyimide disks.

4.2.1 Materials

To begin the process for answering this research question, 50k molecular weight polyamic acid, the precursor to polyimides, with 2.5 wt% photoinitiator TPO was printed from a pneumatic syringe extrusion system. This particular PAA solution was previously determined to create the most desirable additively manufactured all-aromatic polyimide through the use of polyamic salts and use of this

solution was kept constant throughout this thesis. A more in depth view at the specific chemistry involved in this process is discussed by Rau and coauthors [5]. The syringe was equipped with a 25GA nozzle in a HPx High-Pressure Dispensing Tool and connected to a Nordson EFD pneumatic pressure controller set to 17.7 PSI, a number previously determined to work well for printing this particular PAA solution; the UV-DIW printing parameters are shown in Table 4.1.

Table 4.1: UV-DIW Polyimide dielectric testing disks printing parameters.

Nozzle Inner Diameter	0.10 mm (32 GA)
Pneumatic Pressure	17.7 PSI
Deposition Head Offset	0.2 mm
Print Speed	3.0 mm/s

With the final goal of testing 0.1mm-0.2mm thick disks with a diameter larger than 16mm (the size of the impedance analyzer test fixture electrodes), it was decided that a 1mm thick 25mm diameter disk should be printed. This was chosen with prior published and in-lab knowledge showing that printed polyimide structures laminated to glass experience 80-90% shrinkage in the Z direction. With respect to prior printing parameter knowledge from VT DREAMS Lab members, the printing system layer height was set to 0.2 mm and 5 layers of PAA solution were printed to create a 1mm thick 25mm diameter disk. Each layer was cured under Keynote Photonics LC4500 UV projector (405 nm, 10 mW/cm^2 intensity at the build plate) for five seconds following deposition. Five total disks were printed, and some select images of the printed unprocessed disks is shown in Figure 4.2.

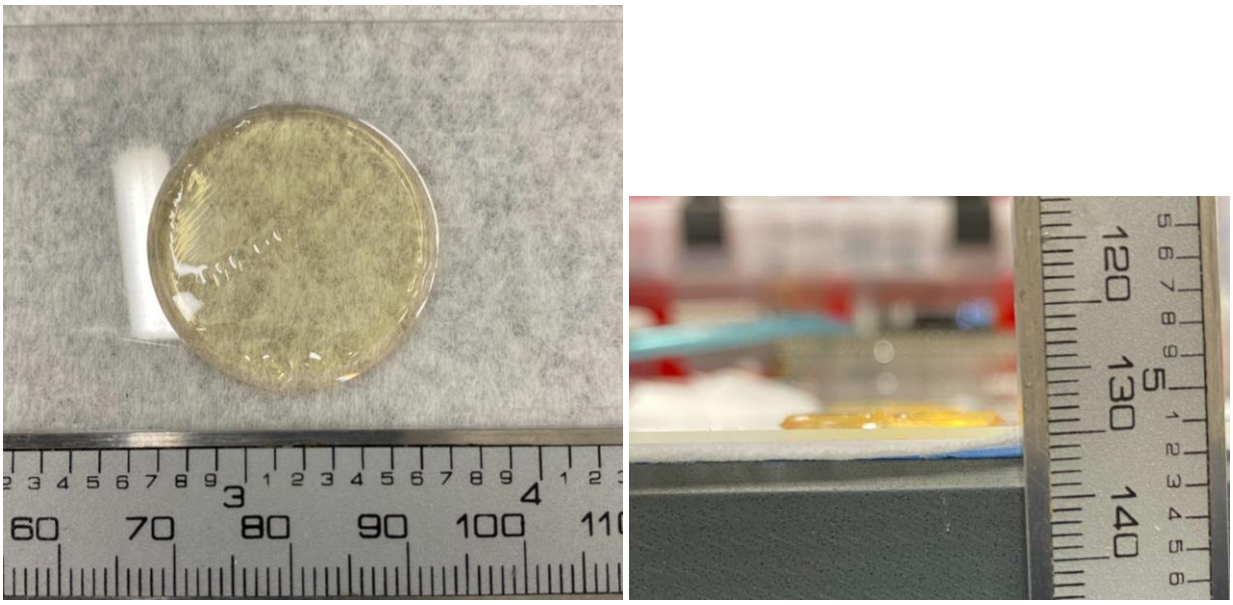

Figure 4.2 As-printed unprocessed five layer UV-cured polyimide precursor disk

In order to convert the printed 3D PAA precursor to all-aromatic polyimide, the structures had to be imidized at high temperatures. To avoid cracking and swelling from the printed precursor, the structures were given one full week to air dry to expel any trapped solvent, after which they were imidized in a vacuum up to 425 °C. Four of the five printed structures survived imidization without severe warping and one of them is shown in Figure 4.3.

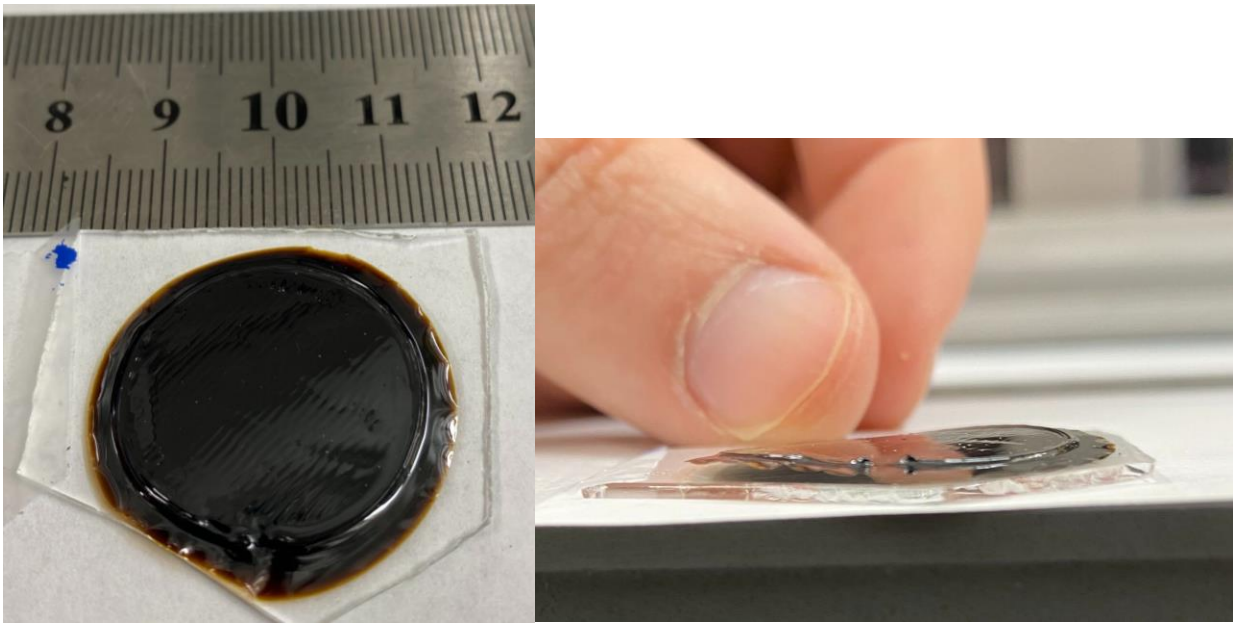

Figure 4.3: Imidized all-aromatic polyimide disk to be used for dielectric testing.

As mentioned earlier in this section, the overall goal was to print disks which could be placed between 16mm electrodes in a parallel plate set up. Since the polyimide disks printed featured a diameter of approximately 25 mm, this allowed for the precise custom cutting of the disks to closely match the electrode shape. Figure 4.4 shows the result of placing the 16mm diameter electrodes on top of the 25mm polyimide disks and cutting around the shape with a thin blade. This method was able to achieve polyimide disks that approximately matched or slightly exceeded size of the 16mm diameter electrodes.

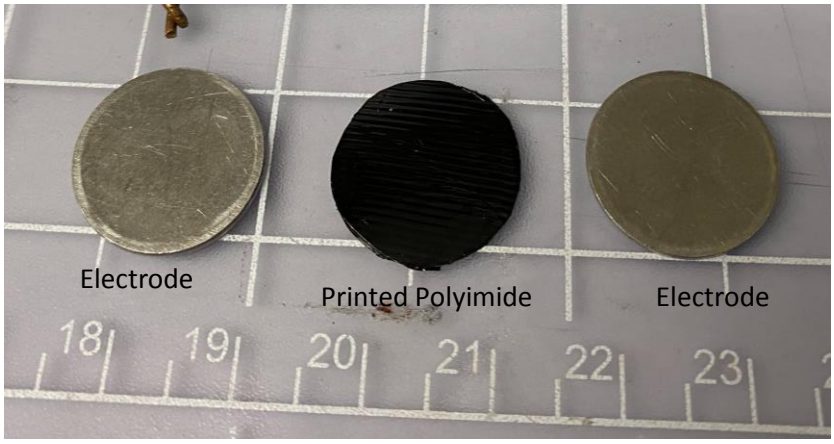

Figure 4.4: 16mm diameter electrodes used for impedance testing along with the 16mm imidized all-aromitic polyimide cut to match the electrode shape.

4.2.2 Methods

A Keysight E4990A 20Hz-30MHz impedance analyzer was used in conjunction with a custom parallel plate capacitor-based test fixture (shown in Figure 4.5). In measuring the dielectric constant and dissipation factor of its Kapton HN film, Dupont cites that its measurements are based on ASTM D150-92 [96]. This test method involves placing a sample between two metallic plates and taking a measurement of its capacitance to compare to the capacitance of a vacuum and determining the dielectric constant using Equation 2 discussed earlier. This same process was followed with the custom parallel plate fixture impedance data from 20Hz to 30MHz; Equations 6 through 9 were employed to determine the dielectric

constant and dissipation factor of the polyimide disks and Dupont Kapton. The three polyimide disks tested possessed thicknesses ranging from 0.19 mm to 0.11 mm, measured with digital calipers with resolution of 0.01 mm. Along with these disks, Dupont Kapton HN film with a known thickness of 0.127 mm was tested. Each disk was tested three separate times and its values were averaged.

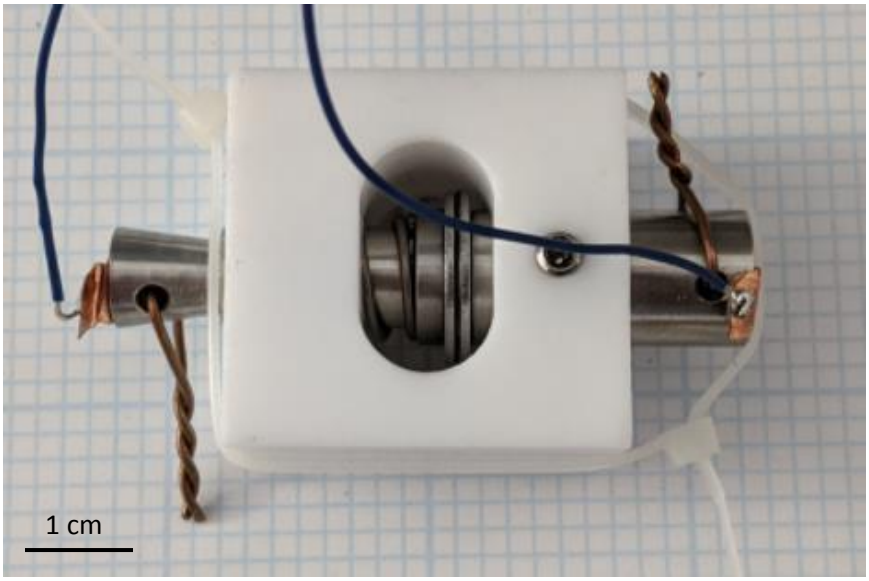

Figure 4.5: Parallel plate capacitor-based setup for measuring the impedance of printed polyimide and commercial Dupont Kapton.

4.3 Research Question #3 Results

As seen in these previously mentioned equations, the thickness and surface area of the disks are a determining factor of their dielectric constant and dissipation factor. Therefore, the disks were kept separate and measured to make sure that their calculated dielectric values were accurate. These geometric values are shown in Table 4.2. The area calculation was kept constant and equal to the surface area of the electrodes which was equal to 209.18 mm^2, calculated from its measured 16.32 mm diameter.

Table 4.2: Measured geometries of the impedance tested polyimide disks.

Disk	Thickness (mm)	Area (mm^2)
Printed Polyimide Disk #1	0.19	209.18
Printed Polyimide Disk #2	0.19	209.18
Printed Polyimide Disk #3	0.17	209.18

Printed Polyimide Disk #4	0.11	209.18
Dupont Kapton Disk	0.127	209.18

Using the imaginary and real impedance data measured by the impedance analyzer, along with the measured geometric values shown in Table 4.2, Equations 6 through 9 were used to calculate the dielectric constant and dissipation factor of the printed polyimide disks and commercial Dupont Kapton disk as a function of the applied frequency. For each of these disks, the final dielectric constant and dissipation factor was averaged from three separate trials at each applied frequency. Figure 4.6 and Figure 4.7 show the calculated average dielectric constant and dissipation factor for each disk at the measured frequencies. The data is noisy and includes a heavy variance at frequencies below 1 kHz and above 1Mhz; Figure 4.8 and Figure 4.9 show the dielectric constant and dissipation factor inside the frequency band of 1 kHz to 1 Mhz.

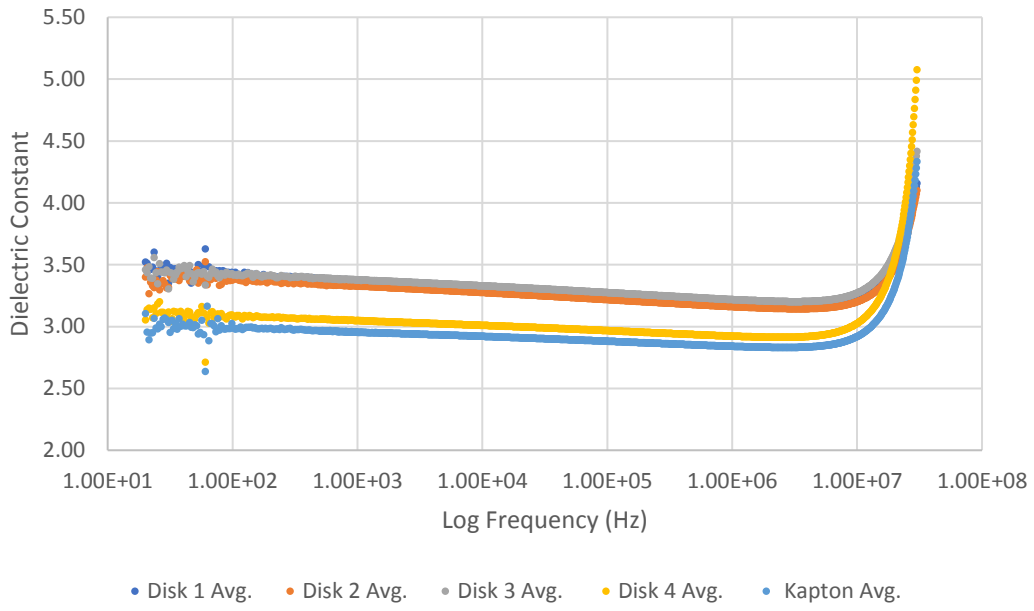

Figure 4.6: Calculated dielectric constant of the tested polyimide disks as a function of applied frequency.

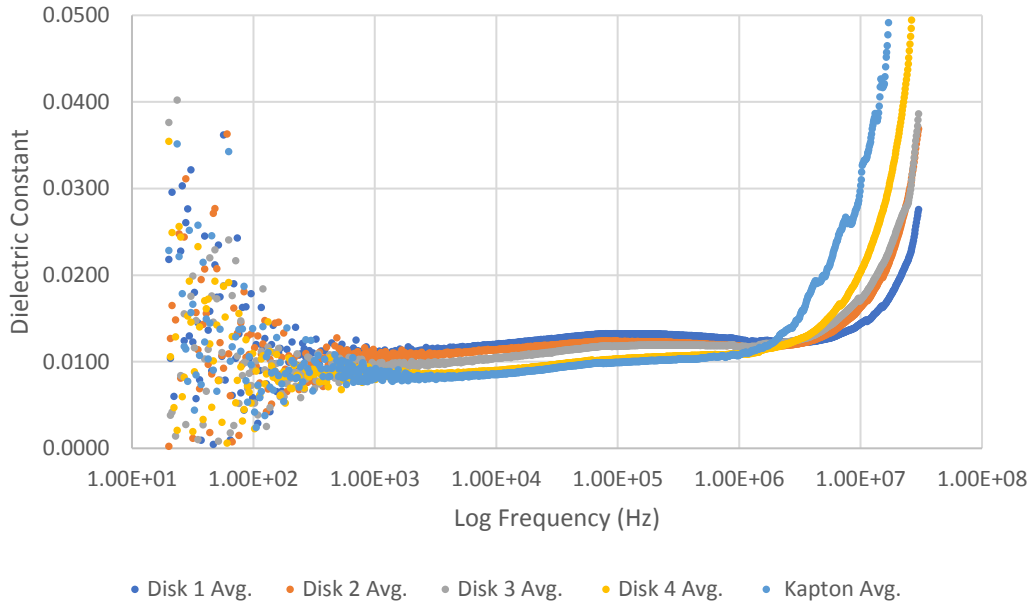

Figure 4.7: Calculated dissipation factor of the polyimide disks as a function of applied frequency.

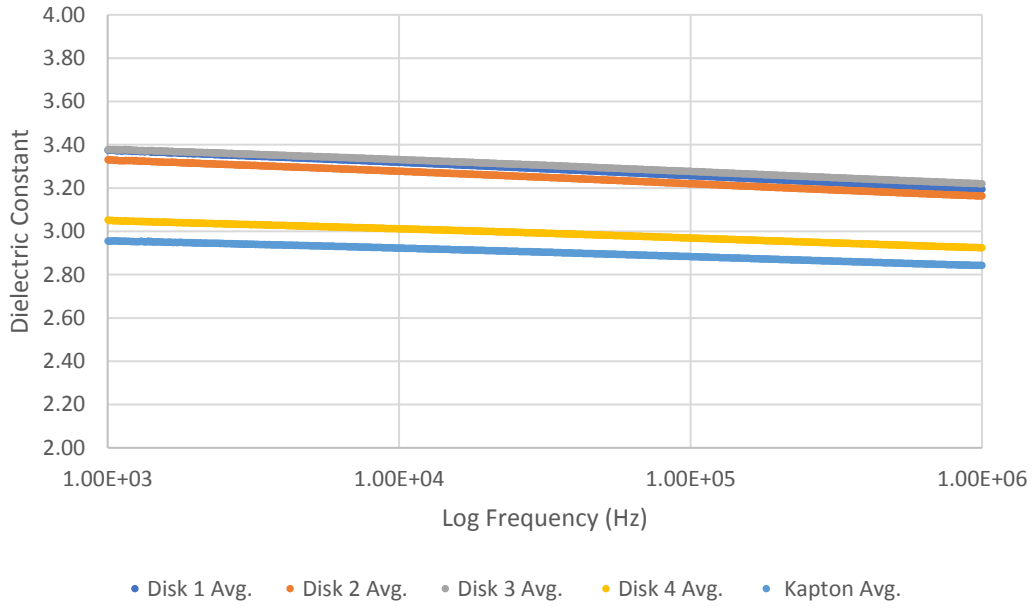

Figure 4.8: Narrow band calculated dielectric constant of the tested polyimide disks as a function of applied frequency.

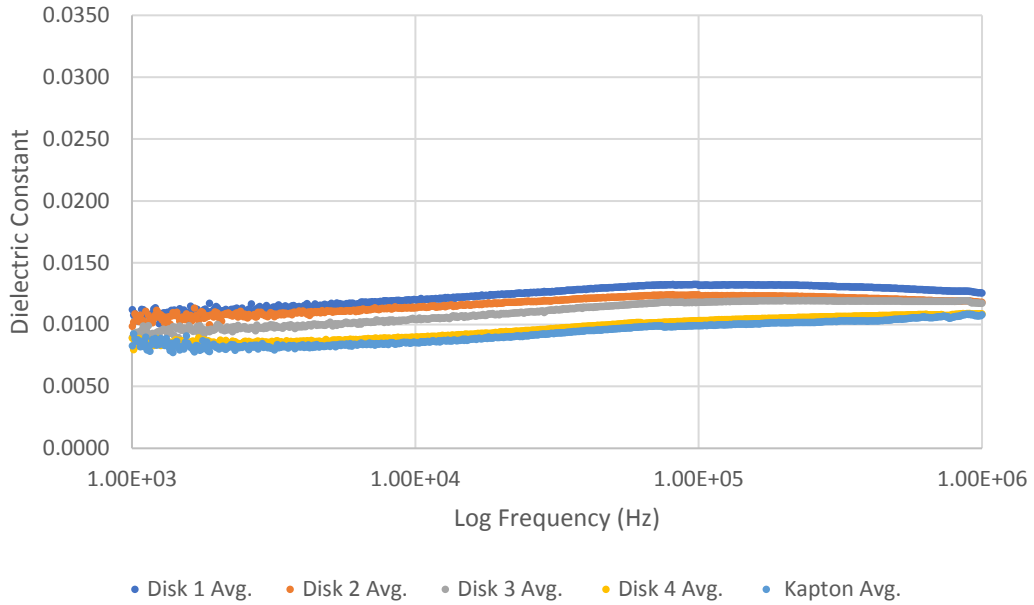

Figure 4.9: Calculated dissipation factor of the polyimide disks as a function of applied frequency.

4.4 Research Question #3 Discussion

As discussed in Section 2.5, specifically Figure 2.35, 0.005 inch thick Kapton HN film has a dielectric constant of 3.5 and a dissipation factor of 0.0026 at 1 kHz. Figure 4.8 and Figure 4.9 show that 0.005-inch-thick Kapton film has a dielectric constant of 2.955±0.003 and a dissipation factor of about 0.0083±0.00014 at 1 kHz. These measured values for Kapton film do seem to differ significantly from the manufacturer-stated values (by -0.55 for dielectric constant and +0.0057 for dissipation factor); however, it is worth considering that this test set up did not follow the exact standard used by Dupont in their testing and featured a custom made parallel test fixture. Therefore, one can consider the dielectric constant and dissipation factor calculated to be unique to the specific equipment used and the tested and calculated printed polyimide dielectric properties can be compared to the tested and calculated Dupont Kapton film properties.

Figure 4.8 showed that Disk 1, 2, and 3 seemingly overlapped in dielectric constant across all frequencies with Disk 4 being closer to the Kapton Disk. An explanation for this is that the decreased film thickness of Disk 4 and Kapton compared to Disk 1, 2, and 3 correlated with the dielectric constant of

the polyimide decreasing. This decrease in film thickness is shown in Table 4.2. However, the decreasing film thickness did not seem to influence the dissipation factor. These two trends were also seen by Oh and coauthors in their study on the dependence of dielectric properties on the thickness of thin dielectric films [116]. An explanation for these trends could be the decreasing of interfacial error with increasing thickness.

Figure 4.8 shows that the dielectric constant of commercial Dupont Kapton HN film is slightly lower than printed polyimide film, even with Disk 4 having a comparable thickness of 0.11mm to the Kapton's 0.127mm. The relative equality of the frequency dependent dielectric constant of disk 1 through 3, which featured similar thicknesses, shows that this test method was able to achieve consistent and accurate results for determining the dielectric constant of the thin polyimide films. These results show that the printed polyimide film features slightly higher dielectric constant than commercial Dupont Kapton HN film (3.05±0.005 versus 2.96±0.003 @1 kHz) despite having a similar thickness; this is likely due to the residual carbon in the UV-DIW polyimide disks. Furthermore, as seen in Figure 4.9, the dissipation factor of the printed polyimide featured a consistently higher dissipation factor than the Kapton HN film. Table 4.3 shows an estimate of each disks' dielectric constant and dissipation factor at set frequencies.

Table 4.3: Calculated dielectric constant and dissipation factor of the tested polyimide disks at varying applied frequencies.

		1 kHz		10 kHz		100 kHz		1 MHz	
Material	Thickness (mm)	Dielectric Constant	Dissipation Factor	Dielectric Constant	Dissipation Factor	Dielectric Constant	Dissipation Factor	Dielectric Constant	Dissipation Factor
Printed Polyimide Disk #1	0.19	3.38± 0.0039	0.0112± 0.00053	3.32± 0.0015	0.0120± 0.00009	3.26± 0.0013	0.0132± 0.00010	3.20± 0.0010	0.0126± 0.00005
Printed Polyimide Disk #2	0.19	3.33± 0.0035	0.0099± 0.00029	3.28± 0.0014	0.0114± 0.00011	3.22± 0.0013	0.0123± 0.00010	3.16± 0.0012	0.0118± 0.00021
Printed Polyimide Disk #3	0.17	3.38± 0.0026	0.0090± 0.00059	3.33± 0.0015	0.0104± 0.00003	3.28± 0.0013	0.0118± 0.00001	3.22± 0.0011	0.0117± 0.00001
Printed Polyimide Disk #4	0.11	3.05± 0.0050	0.0089± 0.00015	3.01± 0.0027	0.0090± 0.00005	2.97± 0.0021	0.0103± 0.00004	2.92± 0.0018	0.0109± 0.00004

Dupont Kapton HN Disk	0.127	2.96± 0.0003	0.0083± 0.00014	2.92 0.0001	0.0085± 0.00001	2.88± 0.0000	0.0099± 0.00008	2.84± 0.0001	0.0108± 0.00010

These findings should be considered when designing dielectric constant dependent circuits with this printed polyimide as the dielectric substrate. As stated earlier, the substrate dielectric constant along with the dissipation factor, or loss factor, are considered to be among the most important and relevant substrate material values affecting the performance of a circuit [103] [104], along with lower values of both properties leading to better circuit performance [105]. This experiment revealed that UV-DIW polyimide possessed similar but slightly higher values of both dielectric properties; therefore, under equal operating conditions and substrate geometries, UV-DIW is expected to perform with slightly higher loss and as a less efficient insulator of current when compared to commercial Kapton film. This is likely due to the residual carbon resulting in the AM structure from the formulation and post-processing of the UV-DIW polyimide parts.

5. Results and analysis of the investigation into the microwave application performance of UV-DIW printed all-aromatic polyimide

To gain a better understanding of the microwave application performance of UV-DIW all-aromatic polyimide, the following research questions is investigated in this section:

- **Research Question 4**: How does the dielectric performance and high temperature processing limit of the all-aromatic polyimide affect its RF performance and how does its performance compare to ULTEM 1010?

5.1 Introduction to Research Question #4

Disclaimer: This section of the thesis is coauthored with Dr. Bradley Davis. Dr. Davis provided the ideas and expertise for the introduction, background section, testing equipment, and the results analysis. Thomas Oja was responsible for the executing the methods, compiling the experimental results, and organizing the writing of this section.

In Section 2.3.3 various examples of extrusion DW conductive lines printed on AM substrates to produce transmission lines were discussed. Fully printed transmission lines open the possibility for rapid prototyping and deployment of structurally complex and high-performing RF and microwave components. Given the high degree of RF performance dependence on specific geometries, printing RF components such as transmission lines opens up the possibility for rapid iterative tuning and maximizing the potential of additively manufactured complex substrates [80].

As discussed in Section 2.5, Kapton film has a dielectric constant of 3.5 and a dissipation factor of 0.0026 at a frequency of 1 kHz [3]. Section 4.1 showed that the printed all-aromatic polyimide features dielectric properties very similar to those possessed by Kapton when tested at similar thicknesses with the same testing method. Using the same testing method that determined the cited dielectric property values for Kapton, ULTEM 1010 FFF material used in this section features a dielectric constant of 3.15 and a dissipation factor of 0.0013 [117]– both lower than Kapton and subsequently printed polyimide. The dielectric constant of ULTEM 1010 is similar to ULTEM 9085; however, ULTEM 9085 experiences a higher dissipation factor of 0.0026. ULTEM 1010 also has a glass transition temperature of 217 °C, higher than ULTEM 9085's value of 186 °C. As seen in Section 3.3, increasing the processing temperature from conductive inks results in dramatic decrease in resistivity. Therefore, the dielectric and temperature processing advantages of ULTEM 1010 over ULTEM 9085 indicate that ULTEM 1010 would perform better in RF applications.

Although ULTEM 1010 features a more favorable dielectric constant and dissipation factor over printed polyimide, ULTEM 1010 can only be processed with conductive inks at temperatures up 217 °C, far lower than the >400 °C range of printed polyimide. Given that RF application performance is dependent on substrate dielectric properties as well as line conductivity, this advantage in processing temperature experienced by the printed polyimide presents the possibility that the gap in dielectric

properties with the two AM materials could be closed by the decreased trace resistivity with the printed polyimide [80].

In this section, the microwave characteristics of the printed ULTEM 1010 and all-aromatic polyimide will be investigated and compared. In addition, the possible performance increase in an RF application from increasing the processing temperature of the RF structure with a printed conductive line from 200 °C (the upper threshold of ULTEM 1010) to 400 °C (the upper threshold of printed polyimide) will be investigated. This investigation will be completed through the printing of transmission lines with an ULTEM 1010 substrate and printed polyimide substrate. This investigation will include an ULTEM 1010 and printed polyimide transmission line substrate with conductive ink processed at 200 °C, as well as a printed polyimide transmission line substrate processed at 400 °C. This will allow for a comparison of the microwave performance of the two substrates with the same line resistivity as well as an investigation into the possible microwave performance increase of a printed polyimide substrate transmission line after being processed at 400° to decrease conductive trace resistivity.

To characterize the microwave performance of the two substrates, multiple methods could have been employed:

1. *Transmission line performance:* Planar transmission lines are the most basic microwave structure available to demonstrate printing, substrate manufacturing, and performance with a single measurement. There are several choices in the planar transmission line technologies that could have been instantiated: the microstrip transmission line, the coplanar waveguide and the stripline.
2. *Antenna performance*: an antenna range within an anechoic chamber was unavailable for this measurement. Additionally, the resolution of the printing method was insufficient to allow the construction of a suitable antenna at frequencies that are manageable in the available space. Finally, the thickness of the substrate must be carefully controlled to achieve the performance

necessary to evaluate the dielectric constant and conductive traces. Antenna construction is not a good method for evaluating material performance, particularly when resolution and accuracy are difficult to achieve.

3. *Other devices*: Other printed, two-dimensional devices such as circulators, resonators, couplers, and splitters are good choices for material characterization since they can be measured with precision and with external effects minimized. However, the basic building block for these devices is the often the planar transmission line (see 1.). Like the planar transmission line, these also require very high printer resolution, thickness control, and careful incorporation of connectors. These devices would also impart additional requirements on the ability to design, print and fashion properly controlled substrates. Consequently, these devices are more complex than the transmission line approach, so they were not chosen as a first-order evaluation test article.

Although more accurate testing methods could have been employed, these methods were unavailable due to the equipment (waveguide fixtures and cavities), infrastructure (anechoic chamber), and analysis software that would have been required. Therefore, the measurements were completed using microwave transmission lines. Although other techniques exist for characterizing the dielectric constant and conductivity of the materials more accurately, the construction of a microwave test article (transmission line) was expected to provide some valuable insight into the performance of both substrates under the various processing conditions for application in microwave devices. As a screening tool, the test method discussed will be useful in further refining the capabilities discussed in this thesis in adapting this printed all-aromatic polyimide material and its processes to microwave devices such as antennas, dividers, splitter and coupler in addition to transmission lines.

Of the various forms of transmission lines mentioned, microstrip transmission lines were chosen due to their simplicity and utility. The microstrip transmission line is widely used in printed circuit boards as a

means for transmitting microwave signals. Typically, being used in the microwave signal range, microstrip transmission lines consist of a strip conductor (silver DW ink), dielectric substrate (ULTEM 1010 and UV-DIW polyimide), and conductive ground plane (copper foil). A diagram of microstrip transmission lines is shown in Figure 5.1 [118]. The electromagnetic field generated by the microstrip is mostly confined to the dielectric material but is also present in the immediate surrounding air which makes it susceptible to interference by other fields. Since the field is primarily in the dielectric, microstrip lines are commonly used to evaluate the dielectric constant of substrate materials. Overall, their benefits include that they are small, low cost, allow simple connector mounting, easily controlled characteristic impedance, and their widespread usage has led to many analytical approximations to their performance being available.

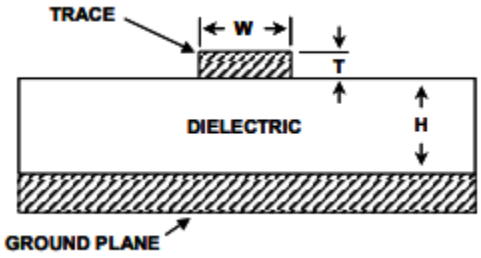

Figure 5.1: Microstrip transmission line featuring a trace, dielectric layer, and ground plane *[118]*.

5.2 Experimental Method for Answering Research Question #4

In order to fabricate transmission line substrates out of both ULTEM 1010 and printed polyimide, a substrate thickness had to be predetermined. Due to most commercially available coaxial end connectors matching typical printed circuit board thicknesses of 0.062 inches, a transmission line design thickness of 0.062 inches was chosen. Due to the coaxial end connectors featuring a width of 10 mm, the substrate also had to be wider than 10 mm. The substrate length requirement was not as restrictive; after consulting an RF expert at Virginia Tech, Dr. Bradley Davis, a minimum substrate length of 40 mm was determined to be acceptable.

Printing a 1.57 mm thick (0.062 inches) substate with a minimum length and width of 40 mm and 10 mm, respectively, with ULTEM 1010 was relatively trivial due to the material printing parameters being well established commercially and in research. However, printing a solid substrate with these dimensions using UV-DIW all-aromatic polyimide presented a challenge due to the solvent-laden polyimide precursor resin warping and shrinking in all directions during the drying and imidization stage. This required the substrate to be flattened while drying along with being printed wider, thicker, and longer than the final required dimensions to account for the shrinkage and warpage.

5.2.1 Materials

With the required substrate minimum length and width dimensions known, a 65 mm x 20 mm layer toolpath was made and printed with a 20 GA Nordson EFD nozzle and a HPx High-Pressure Dispensing Tool at 12.0 PSI; UV-DIW printing parameters are shown in *Table 5.1*. Each layer was photocured with a Keynote Photonics LC4500 UV projector (405 nm, 10 mW/cm^2). This layer was determined to be approximately 0.6 mm thick and it was found that 6-layer structures resulted in an acceptable final imidized transmission line substrate with an edge thickness of approximately 1.57 mm, width of 13.0 mm, and length of 55.0 mm. To keep the UV-DIW polyimide substrate flat during solvent removal, weighted glass slides in conjunction with cellulose sponges and Kim Wipes were used (Figure 5.2). This weighed arrangement was then placed in an ambient air oven at 60 °C for 24 hours, 80 °C for 24 hours, and 110 °C for 48 hours in order to slowly draw out solvent while keeping the part flat and free of cracking. The parts were then imidized in a vacuum up to 425 °C. Figure 5.3 shows the visual progression of the part after various stages of processing.

Table 5.1: UV-DIW Polyimide transmission line substrate printing parameters.

Nozzle Inner Diameter	0.10 mm (32 GA)
Pneumatic Pressure	17.7 PSI
Deposition Head Offset	0.2 mm
Print Speed	3.0 mm/s

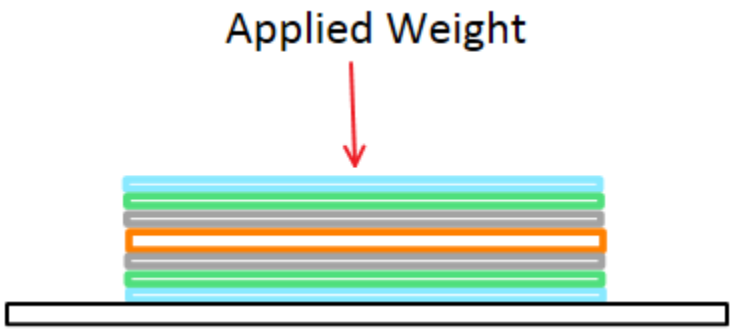

Figure 5.2: Weighted arrangement used to keep polyimide precursor flat during drying; includes glass sides (blue), cellulose sponge (green), Kimwipe (grey), and the printed part (orange).

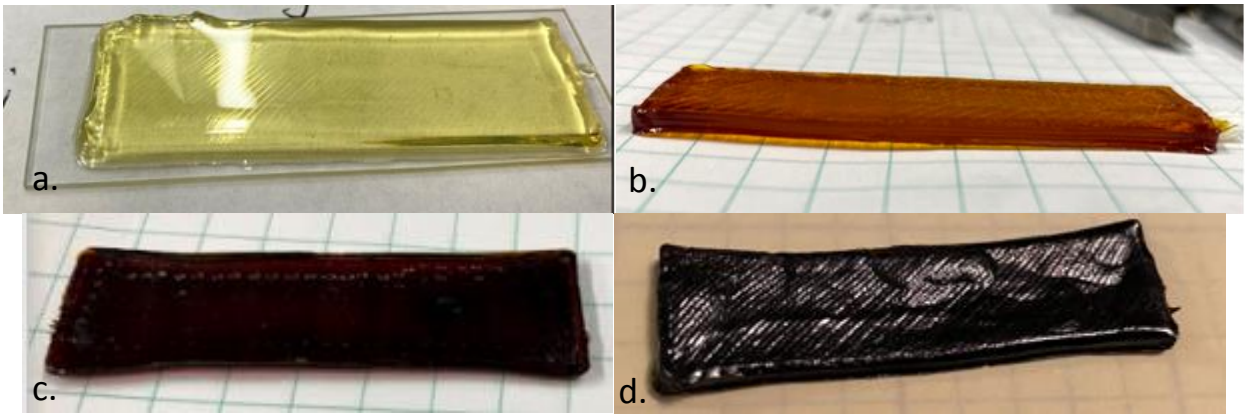

Figure 5.3: Various stages of UV-DIW polyimide transmission line substrate as printed (a), processed at 60 °C for 24 hours (b), processed at 110 °C for 48 hours (c), and imidized up to 400 °C.

After determining a viable method for obtaining repeatable polyimide transmission line substrates with an approximate thickness of 1.57mm, a minimum width of 10 mm, and a minimum length of 40 mm, two UV-DIW polyimide substrates were printed and processed. An ULTEM 1010 substrate of comparable dimensions was then printed; the dimensions of these substrates are shown in Table 5.2. For the UV-DIW polyimide substrates, the edge thickness slightly differed from the thickness in the center portion of the substrate, so both dimensions are reported.

Table 5.2: UV-DIW polyimide transmission line substrate dimensions.

Substrate #	Length (mm)	Width (mm)	Edge Thickness (mm)	Center thickness (mm)
UV-DIW Polyimide #1	45.57	11.81	1.65	1.50
UV-DIW Polyimide #2	46.05	12.24	1.63	1.50
ULTEM 1010 #1	50.05	15.03	1.70	1.70

After obtaining both the UV-DIW polyimide and ULTEM 1010 substrates, the conductive silver Dupont CB028 microstrip was deposited. Since the polyimide substrate was slightly curved, a more precise tip could not be used due to the required standoff distance being around 0.1 mm for higher gauge nozzles. Instead, the microstrip was deposited with a 15GA Nordson EFD syringe tip using 3.0 PSI of pneumatic pressure at 3mm/s at a standoff distance of approximately 10 mm above the substrate. This resulted in a constant volume of material being deposited per unit length over each substrate. The deposited silver ink was left to dry for 24 hours before each substrate was processed in the oven. The ULTEM 1010 substrate and the UV-DIW Polyimide #1 substrate were treated in a Fisher Scientific Vacuum Oven Model 282A for 1 hour at 200 °C. The UV-DIW Polyimide #2 substrate was treated at 400 °C for 1 hour in a KJ Group GSL 1600X Tube Furnace including a 30-minute ramp up time, as required by the user manual. The 400 °C processing temperature was chosen based on the extrusion DIW ink resistivity findings presented in Section 3.3.

To determine the average thickness and width of the microstrips, a DektakXT contact profilometer with resolution of 4 angstrom was used. Five separate, equally spaced out, profiles were recorded along the length of each trace. The average height and width of each line is presented in Table 5.3; the difference in the height and width of each trace can be attributed to slight variations in ink spreading due to different surface finishes and interfacial interaction properties between the substrates.

Table 5.3: Average profile height and width along the length of each substrate silver ink microstrip.

Substrate #	Height (μm)	Width (mm)
UV-DIW Polyimide #1	310.17	2.478
UV-DIW Polyimide #2	299.01	2.794
ULTEM 1010 #1	277.79	2.977

After processing the substates, copper foil tape with conductive adhesive was applied to the underside of the substrates to serve as the conductive ground plane. Lead solder was then used to solder the end connectors onto the copper foil (Figure 5.4). Since the CB028 silver ink was not solderable after being processed at 200 °C, the center pin of the coaxial connector was connected to the silver

microstrip using the same CB028 silver ink processed at 90°C for 4 hours to increase its conductivity. An example of this silver ink connection is shown on the ULTEM 1010 substrate in Figure 5.5.

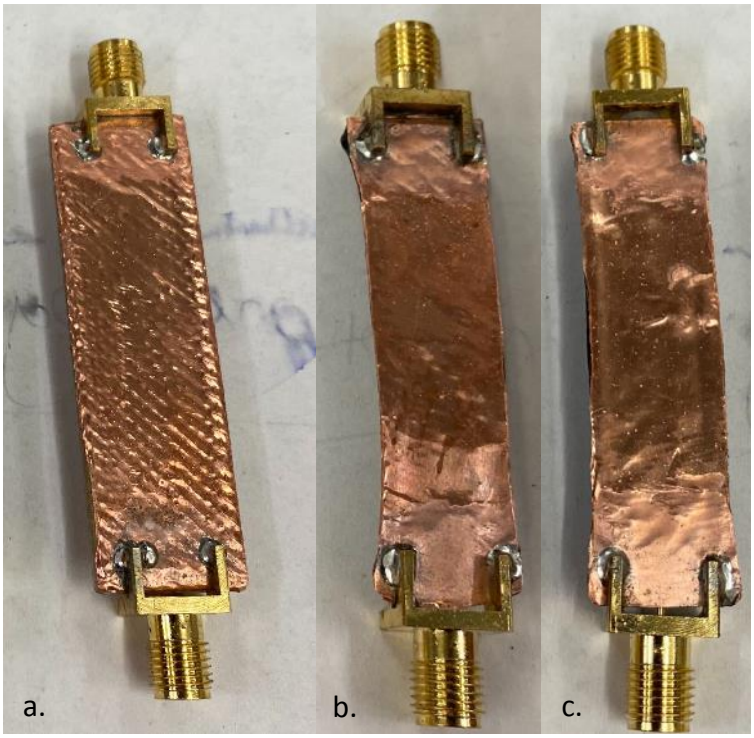

Figure 5.4: Photo of the copper foil ground plane and soldered coaxial end launch connectors on the ULTEM 1010 substrate (a), UV-DIW polyimide substrate treated at 200 °C (b), and the UV-DIW polyimide substrate treated at 400 °C (c).

Figure 5.5: Coaxial end launch connector on the ULTEM 1010 transmission line substrate showing the cured silver ink connection to the center pin.

5.2.2 Methods

To test the transmission line microstrips, a Keysight PNA Network Analyzer N5227B with a frequency range of 10 MHz to 67 GHz was used. A photo of the instrument along with its coaxial connection lines is shown in Figure 5.6. The transmission lines were tested for end-to-end transmission loss, S21, as well as signal reflection, S11 and S22, from 8 GHz to 12 GHz; this range was determined chosen based on the apparent peak signal strength when initially analyzing the data of each line (discussed in the next section) . A photo of each transmission line connected to the network analyzer is shown in Figure 5.7.

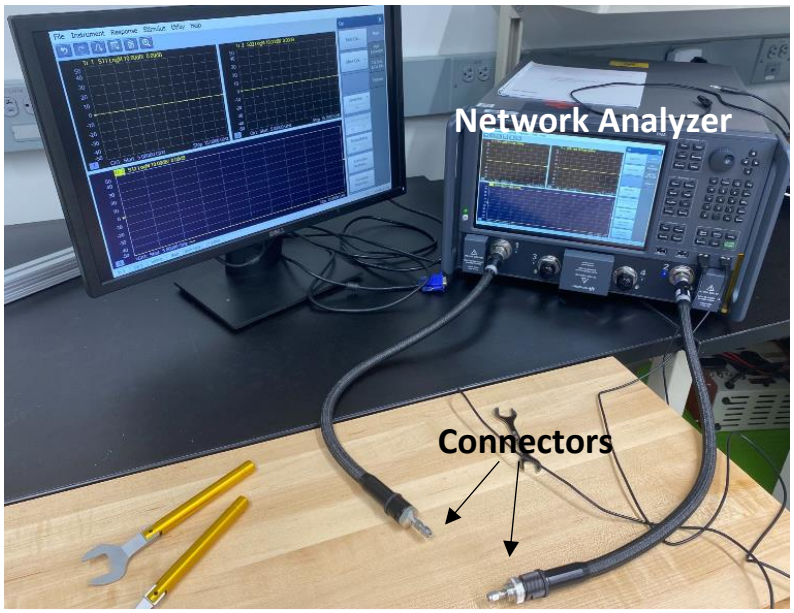

Figure 5.6: Transmission line experimental setup featuring the network analyzer and the coaxial connectors.

Figure 5.7: ULTEM 1010 (a), low temperature processed UV-DIW polyimide (b), and high temperature processed UV-DIW polyimide (c) transmission lines connected to the network analyzer (b. features a crack in the substrate that occurred after data collection).

In typical transmission line design for full scale functional parts, a PCB transmission line trace would be designed to match the impedance required by the circuit. This impedance (Z_O) can be estimated by a function of the transmission line microstrip width (*W)* and thickness (*T)* along with the relative permittivity of the dielectric layer (ε_r), and the distance (*H)* between the microstrip and the ground plane (the dielectric thickness). This relationship is shown in Equation 10 [118]; the microstrip thickness and width were approximated based on the profilometry width and height shown in Table 5.3. To complete this characteristic impedance calculation more accurately, Broadcom AppCAD was used; screenshots from the app calculations are shown Appendix B, along with the calculated values shown in Table 5.4. For these calculations the UV-DIW polyimide relative permittivity was estimated as 3.5, based on its dielectric property similarity to Kapton (Section 4.4). The ULTEM 1010 relative permittivity was assumed to be equal to 3.15 (Section 5.1). Originally, the microstrips were designed to have a characteristic impedance of 50 Ω which peaked in S21 signal transmission magnitude at 10 GHz. However, due to the warping previously discussed, this design could not be followed exactly with a

precise precision head. Instead the 10mm standoff 15GA nozzle was used to result in a characteristic impedance as close as possible to 50 Ω.

$$Z_O = \frac{87}{\sqrt{\varepsilon_r + 1.41}} ln\left[\frac{5.98H}{0.8W + T}\right] \quad (10)$$

Table 5.4: Calculated characteristic impedance of each transmission line microstrip.

Substrate	Characteristic Impedance (Ω)
UV-DIW Polyimide #1	58.87
UV-DIW Polyimide #2	55.24
ULTEM 1010 Substrate #1	60.16

5.3 Research Question #4 Results

Ultimately, the performance of the transmission line microstrips is best judged through a relative comparison of the S21 or S12 peak measurements. These measurements show the passband and the magnitude of the transmitted signal. The peak signal magnitude was for each line was determined to be within 9 GHz to 11 GHz during testing. Figure 5.8 shows the S21 measurement comparison of the three substrates in the wideband of 8 GHz to 12 GHz.

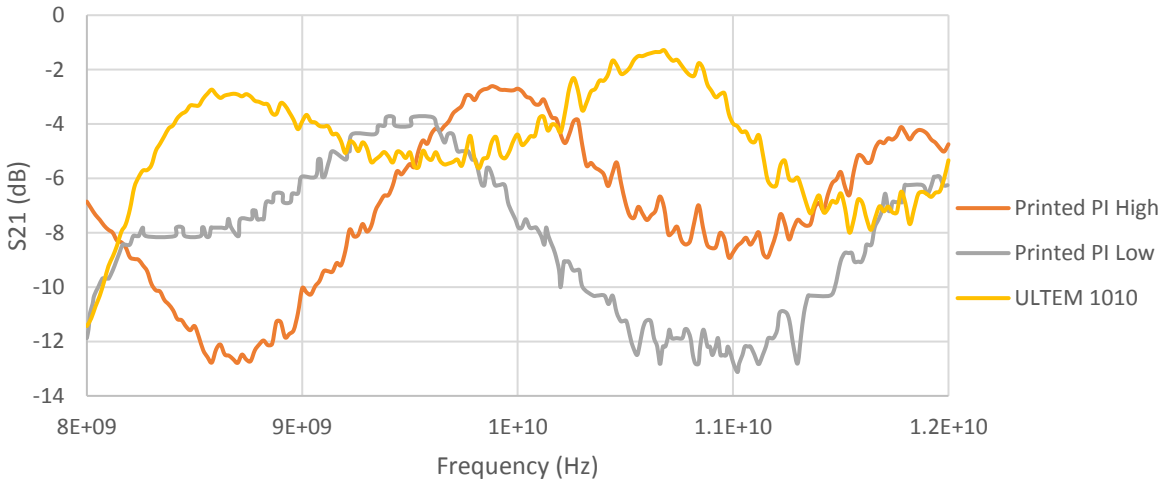

Figure 5.8: S21 data from each substrate from 8 GHz to 12 GHz.

5.3 Research Question #4 Discussion

As shown in Figure 5.8:, the S21 magnitude of the transmitted signal peaks occurred around 10 GHz for each signal, as designed. Ideally, with a more controlled substrate and microstrip printing process, the peaks would have exactly overlapped at 10 GHz, only differing in S21 magnitude rather than in frequency as well. However, a relative comparison of the peaks is still valid given their proximity.

With a closer S21 value to zero indicating better performance and lower loss, it is clear that the ULTEM 1010 substrate performed with the least loss. The ULTEM 1010 transmission line peaks at approximately 10.7 GHz with an S21 value of -1.29 dB. Whereas the 400 °C processed UV-DIW polyimide transmission line peaks at 9.88 GHz with an S21 value of -2.61 dB, and the 200 °C processed UV-DIW polyimide transmission line peaks at 9.51 GHz with an S21 value of -3.75 dB (Table 5.5).

Table 5.5: Peak S21 loss values for each printed microstrip transmission line substrate.

Substrate	S21 Peak (dB)	Frequency (GHz)
ULTEM 1010	-1.29	10.70
Printed PI High	-2.61	9.88
Printed PI Low	-3.75	9.51

Overall, these results show that the microstrip lines all function and that the warpage-free geometry of the ULTEM substrate helped it achieve the best performance. The 400 °C processed UV-DIW polyimide performed well despite a warped substrate and subsequent microstrip. Relative to the 200 °C-processed UV-DIW polyimide, these two transmission lines only differed in manufacturing by the post-processed oven treatment; it can be concluded that the better conductivity of the 400 °C processed transmission line helped its performance to minimize S21 loss to some degree. These results also indicate that the advantage in performance held by ULTEM 1010, given its favorable microwave dielectric properties, was minimized by the increased processing temperature capabilities of the UV-DIW polyimide. This is qualitatively evident when considering that, when processed at equal temperatures of 200 °C, the UV-DIW polyimide experienced a S21 peak performance gap with ULTEM

1010 of 2.46 dB – whereas the 400 °C processed UV-DIW polyimide experienced a peak S21 performance gap with ULTEM 1010 of only 1.32 dB.

There are some important shortcomings of the methods and testing that should be discussed. The microstrip transmission lines fabricated for this experiment are problematic in that there is a gap between the coaxial connector body and the silver microstrip. Within this gap, the center pin of the connector is essentially functioning as the microstrip line since it is above the ground plane on the other side of the dielectric substrate. Although this pin is still able to transmit the microwave signals effectively, its characteristic impedance will differ from that of the printed line. This difference introduces signal reflections at both connector ports and will raise the S11 and S22 values while lowering the S21 values; thus, negatively affecting the power of the transmitted signal between the two ports which is the primary measure in this experiment. Since the gap is slightly different between the samples, it introduces an error that is difficult to account for in the results. Therefore, it must be assumed that the error is consistent in order to compare the results. The gaps are most likely to narrow the band of operation around the design frequency due to multiple reflections and standing wave generation. In future research, the lines will be manufactured without this gap.

Other issues include that the lines were not well-controlled in width due to the stand-off dispensing technique that was necessary due to the UV-DIW polyimide warpage. This width inconsistency has the potential to create additional modes within the transmission line itself and can generate additional reflection issues. Additionally, the UV-DIW polyimide substrates are not completely flat or consistent in thickness, due to previously discussed warpage during post-processing. These printing inconsistencies create issues with microwave system design as the manufactured product performance will likely not be able to match the design analysis and simulation. The ULTEM 1010 substrate was the closest to a well-constructed line. The substrate was flat, and the line was relatively constant in width; however, the gaps between the line and connector body were still present. Furthermore, the ULTEM 1010 substrate

featured a rough surface finish (inherent in FFF parts) on the substrate side in which the copper tape ground plane was adhered which could have caused further inaccuracies due to air gaps.

Although the UV-DIW polyimide substrate experienced post-processing issues, which created a microstrip transmission line with inconsistent geometries, this set of experimentation was still able to demonstrate its high-temperature processing benefits. Increasing the processing temperature of the printed silver microstrip sample past the upper threshold of ULTEM 1010, 200°C, to 400°C closed a significant portion of the performance gap between the two substrates processed at the same temperature of 200 °C. This conclusion demonstrates that the printed silver ink conductivity increase resulting from increasing post-processing temperatures, past what AM substrates are typically capable of, resulted in a better performing microwave application.

In future experimentation, the transmission lines should be produced without the cap between the connector body and the microstrip to reduce any possible error in the results. The UV-DIW polyimide precursor should also be printed with the formulation that results in a significantly reduced amount of warpage. This formulation has been produced but was not available for this set of experimentation.

6. Conclusions and Future Work

6.1 Summary of Research

The primary goal of this research was to characterize the benefits, drawbacks, and possible applications of integrating additively manufactured all-aromatic polyimide with conductive silver direct write inks for electronics purposes. This goal was originally formulated since AM all-aromatic polyimide is mechanically and chemically stable at temperatures exceeding that of typical AM polymers used with direct write (DW) conductive inks. All-aromatic polyimide is also able to be printed through vat photopolymerization (VP) along with ultraviolet-assisted direct ink write (UV-DIW), giving it a superior surface finish when compared to fused filament fabrication (FFF) systems. The ability for the all-aromatic polyimide to be printed with a UV-DIW system also presents the opportunity for future integration with DW conductive ink systems for simultaneous AM of multimaterial hybrid electronic parts.

The primary goal of this thesis has been achieved through the characterizing the effect of the increased temperature stability of AM all-aromatic polyimide on the conductivity of DW silver inks, determining the most important dielectric properties of processed UV-DIW all-aromatic polyimide, and determining the achievable microwave application performance of UV-DIW polyimide relative to FFF ULTEM 1010. These tasks were completed through the formulation of the most relevant research questions stemming from a comprehensive literature review of current DW systems, DW systems used with conductive inks, the integration and application of the DW of conductive inks with AM structures, the limitations with this integration and application, and the currently available AM materials and systems most compatible with hybridization with the DW of conductive inks to create functional electronics. These research questions and their most important findings are presented below.

Research Question 1: How does increasing the processing temperature of silver-loaded inks printed onto Dupont Kapton affect conductivity and adhesion?

In order to characterize the effect of the increased temperature stability of AM all-aromatic polyimide on the conductivity of DW silver inks, a commercial Kapton film substrate was first used. This was done due determine an optimum conductivity temperature range for each conductive ink before testing on UV-DIW polyimide material due to limited UV-DIW polyimide material availability. It also provided the opportunity for a later comparison of the conductivity and adhesion performance of silver inks on Kapton compared to UV-DIW polyimide material. It was found that increasing the processing temperature of both AJ silver nanoparticle ink and extrusion DW silver ink past their initial manufacturer recommended processing temperature to the upper limits of UV-DIW polyimide material resulted in a dramatic decrease in resistivity from both traces. The resistivity of the AJ ink dropped 81% from 5.27±0.013 at 200 °C to 1.78±0.15 times the resistivity of bulk silver at 300 °C. This trend continued with the DW silver ink dropping 85% from 14.94±0.55 times bulk silver at 160 °C to 2.29±0.028 times bulk silver at 400°C. A scotch tape adhesion test was performed on all of the samples and while all the extrusion DW silver ink samples passed, only 1/3 of the AJ samples processed below 300 °C passed while 2/3 of the AJ samples processed above 300 °C passed.

Research Question 2: How does the silver-loaded conductive trace conductivity and adhesion performance compare when printed on AM all-aromatic polyimide versus commercial Dupont Kapton?

Research Question 1 provided an optimum temperature processing range for the AJ and extrusion DW inks on Kapton film. This range was used to determine the lowest resistivity of the conductive inks on film made from UV-DIW all-aromatic polyimide precursor material. It was found that the ink resistivity for both the AJ and extrusion DW performed similarly on both bladed UV-DIW all-aromatic polyimide material and commercial Kapton. The lowest resistivity measured from the AJ ink

was equal to 1.95±0.09 times bulk silver after processing at 350 °C while the lowest resistivity measured from the DIW ink was equal to 2.13±0.07 times bulk silver after processing at 325 °C and 2.16±0.03 after processing at 375 °C. The resistivity of the extrusion DW and AJ samples were directly compared between substrates at processing temperatures of 300 °C and 350 °C. A two-tailed t-test between these measurements found no significant difference between both sets of extrusion DW samples and the AJ samples processed at 350 °C. However, a t-test revealed a significant difference between the resistivity of the AJ samples processed on the two substrates at 300 °C.

The scotch tape adhesion testing revealed that AJ and extrusion DW ink printed on UV-DIW polyimide material performed similarly to commercial Kapton film with 2/3 of the AJ samples processed above 300°C passing and all extrusion DW ink samples passing. The ink wetting contact angle measurements from silver extrusion DW ink on Kapton film and UV-DIW polyimide material film revealed no statistical difference in the contact angle measurements indicating that the substrates have similar a similar surface energy and similar printed line widths and thicknesses can be expected on both substrates.

Research Question 3: How does the dielectric performance of additively manufactured all-aromatic polyimide compare to commercial Dupont Kapton and similar high-performance AM polymer substrates?

Determining the most important dielectric properties of UV-DIW all-aromatic polyimide was critical in determining its viability as an electronics substrate. Using an impedance analyzer and a parallel plate setup, the dielectric constant and dissipation factor UV-DIW disks was determined and compared to commercial Dupont Kapton film. It was found that at similar thicknesses, UV-DIW disks had slightly higher dielectric constant across all tested frequencies from 1 kHz to 1 MHz. At 1 MHz, the dielectric constant was equal to 2.92±0.0018 for UV-DIW polyimide and 2.84±0.0001 for commercial Kapton. The dissipation factor for each material was found to be relatively equal at similar thicknesses with a value of

0.0109±0.00004 for UV-DIW polyimide and 0.0108±0.00010 for Kapton. Although the measured dielectric property values are specific to the testing method and equipment utilized for this research question, it can be concluded that UV-DIW polyimide performs very similarly to commercial Kapton film as a dielectric substrate across a wide range of frequencies.

Research Question 4: How does the dielectric performance and high temperature processing limit of the all-aromatic polyimide affect its RF performance and how does its performance compare to ULTEM 1010?

Research Question 1 and 2 showed that utilizing UV-DIW all-aromatic polyimide's ability to maintain mechanical and chemical stability over a higher temperature range than typical AM materials resulted in dramatically decreased line resistivity. Additionally, Research Question 3 showed that the UV-DIW polyimide had similar dielectric properties to Kapton film. ULTEM 1010 is the only commercially available FFF material capable of maintaining mechanical stability up to 217°C. Since Kapton film has a higher dielectric constant than ULTEM 1010 (3.5 vs 3.15) as well as a higher dissipation factor (0.0026 vs 0.0013) when tested under the same conditions, it was hypothesized that microwave application performance gap between the ULTEM 1010 and UV-DIW polyimide could be closed with the decreased DW ink trace resistivity on UV-DIW polyimide processed at temperatures outside of ULTEM 1010's stability range.

This hypothesis was tested through a comparison of the relative performance of microstrip transmission lines made from ULTEM 1010 processed at 200 °C, UV-DIW polyimide processed at 200 °C, and UV-DIW polyimide processed at 400 °C. The peak S21 transmission strength was compared, with ULTEM 1010 processed at 200 °C equal to -1.21 dB, UV-DIW polyimide processed at 200 °C equal to -3.75 dB, and UV-DIW polyimide processed at 400 °C equal to -2.61. This finding confirms the hypothesis that, although ULTEM 1010 performed the best in this microwave application, the gap between the

performance of ULTEM 1010 and UV-DIW polyimide was reduced with UV-DIW polyimide's ability to be processed at a higher temperature range resulting in decreased microstrip resistivity.

6.2 Research Contributions

The summarized contributions of this research are:

- A comprehensive literature review directly pertaining to the future hybridization of DW conductive inks and AM dielectric structures for integrated layer by layer printing of multimodal electronic parts.

This literature review identified and discussed the DW systems most compatible with printing conductive inks on or in conjunction with AM structures and systems for the creation of fully additively manufactured multimodal electronic parts. Aerosol jetting and extrusion DIW were identified as the most compatible systems for this concept and various previous multimodal electronic parts printed with separate and hybridized systems were discussed. The most pressing and relevant limitations of integrating DW electronics and AM structures were discussed with the main limitations identified as low temperature processing limits typical of AM substrates along with poor adhesion and interaction of DW conductive inks with those AM substrates. Finally, the currently available highest performing AM substrates most utilized and compatible with the DW of conductive inks were identified and compared in processing temperature stability and dielectric properties.

- An evaluation of the conductivity and substrate adhesion effects from increasing the processing temperature of extrusion DW and AJ silver inks past the temperature threshold typically available from AM substrates

It was found that the tested extrusion DW and AJ inks experienced dramatic increases in conductivity when processed at temperatures above 200 °C up to 400 °C; the extrusion DW ink's adhesion characteristics were not negatively impacted and the AJ ink's adhesion improved after being processed at or above 300 °C. These results were first tested on Kapton film and then confirmed with UV-DIW all-

aromatic polyimide material film as the substrate. It was also found that this increased temperature range allowed for previously impossible soldering of Dupont CB028 ink, which affords the introduction of soldered electronic components. These results represent a major push forward in the possibility of creating a hybridized layer by layer system utilizing DW conductive inks and UV-DIW polyimide for the creation of high-performance electronics with high conductivity and well adhered conductive traces, previously unavailable with typical VP and FFF substrates.

- Characterization of the most relevant dielectric properties of UV-DIW all-aromatic polyimide along with commercial Kapton for a relative comparison

Using an impedance analyzer along with a parallel plate setup, the dielectric constant and dissipation factor, the dielectric substrate properties considered to be among the most important in circuit manufacturing [103] [104], of UV-DIW all-aromatic polyimide disks were determined. As a means of results confirmation and relative comparison, commercial Kapton film was tested as well. It was found that, at similar thicknesses, UV-DIW polyimide had a slightly higher but very similar dielectric constant and dissipation factor from 1 kHz to 1 MHz. Given that Kapton film has been widely used as an electronics dielectric substrate and insulator, this characterization confirmed that UV-DW polyimide can serve as a high performing dielectric substrate for conductive DW electronics.

- Analysis of the relative performance of UV-DIW all-aromatic polyimide and ULTEM 1010 as a microwave electronics substrate

It was found that the higher temperature processing capabilities of UV-DIW polyimide compared to the highest temperature capable FFF material, ULTEM 1010, was able to decrease the gap in microwave application performance caused by ULTEM 1010's superior dielectric properties. This was tested through the manufacturing of microstrip transmission lines made with extrusion DW silver inks and ULTEM 1010, processed around its upper temperature threshold of 200 °C, and UV-DIW all-aromatic polyimide, processed at 200 °C and its upper temperature threshold of 400 °C.

6.3 Limitations and future work

This work demonstrated that utilizing UV-DIW all-aromatic polyimide as an DW electronics substrate resulted in higher conductivity conductive traces along with a superior surface finish compared to FFF structures such as ULTEM 1010 (the current FFF substrate with stability at the highest temperatures). However, there are certain drawbacks that must be addressed. This work was completed with the DW of conducive inks on an already post-processed UV-DIW all-aromatic part. Given that the unprocessed photopolymer polyimide precursor to which the material is printed with is solvent laden during printing and post-processing, this poses the threat to the feasibility of integrating DW electronics with AM UV-DIW polyimide structures for multimodal parts. The solvent could alter silver ink traces, negatively impacting the final electronic performance. The UV-DIW polyimide precursor material used in this thesis also had the propensity to warp and shrink during post-processing which could also negatively impact final electronic performance.

Future work that could help circumvent these limitations includes, (i) designing and optimizing a UV-DIW process that would allow for simultaneous layer-by-layer printing of AM structure with DW conductive inks and (ii) developing a UV-DIW all-aromatic polyimide precursor formulation featuring less solvent and less post-processing warping.

(i) Designing and optimizing a UV-DIW process that would allow for simultaneous layer-by-layer printing of AM structures with DW conductive inks

In order to create fully embedded 3D multimodal electronic parts utilizing the UV-DIW polyimide along with DW conductive inks, a system must be designed allowing for the integration of these two processes. This could involve a single free form movement extrusion piece with the ability to dispense both polyimide precursor photopolymer and conductive inks. This could also involve two separate deposition heads or free form extrusion movement pieces. Creating a system capable of depositing these two materials with high resolution would allow for the creation of embedded conductive traces

along with vertical interconnects for the creation of complex multimodal fully additively manufactured parts. This would drastically reduce the prototyping time and financial requirements for government and corporate institutions looking to create complex structural electronics. This hypothetical system, along with the highly desirable properties of UV-DIW all-aromatic polyimide (discussed in Section 2.5), would be capable of manufacturing high-performance complex electronic systems capable of withstanding a variety of harsh and demanding environments, such as space systems.

(ii) Developing a UV-DIW all-aromatic polyimide precursor formulation featuring less solvent and less post-processing warping

Although the benefits of the post-processed UV-DIW all-aromatic polyimide are numerous, its solvent laden photopolymer precursor introduces issues that could negatively affect the feasibility and performance of the complex electronics discussed in (i). There currently exists a formulation of the all-aromatic polyimide precursor photopolymer material which is utilized in VP and features less solvent and warping. If the rheology of this formulation or a brand new reduced-solvent/warping formulation could be tuned for application in the UV-DIW process, many of the possible solvent and warping related issues could be solved. This would allow for seemingly seamless integration of DW conductive inks with UV-DIW all-all-aromatic polyimide for the creation of a hybridized system able to rapidly produce multimodal high-performance 3D electronics capable of being deployed in harsh environments such as space.

References

[1] Perez, K. B., and Williams, C. B., "Combining additive manufacturing and direct write for integrated electronics—a review," Proc. 24th International Solid Freeform Fabrication Symposium—An Additive Manufacturing Conference, SFF, pp. 962-979.
[2] Robinson, C. J., Stucker, B., Lopes, A. J., Wicker, R., and Palmer, J. A., 2006, "Integration of direct-write (DW) and ultrasonic consolidation (UC) technologies to create advanced structures with embedded electrical circuitry," Proc. 2006 International Solid Freeform Fabrication Symposium.
[3] Espalin, D., Muse, D. W., MacDonald, E., and Wicker, R. B., 2014, "3D Printing multifunctionality: structures with electronics," The International Journal of Advanced Manufacturing Technology, 72(5), pp. 963-978.
[4] Hegde, M., Meenakshisundaram, V., Chartrain, N., Sekhar, S., Tafti, D., Williams, C. B., and Long, T. E., 2017, "3D Printing All-Aromatic Polyimides using Mask-Projection Stereolithography: Processing the Nonprocessable," Advanced Materials, 29(31), p. 1701240.
[5] Rau, D. A., Herzberger, J., Long, T. E., and Williams, C. B., 2018, "Ultraviolet-Assisted Direct Ink Write to Additively Manufacture All-Aromatic Polyimides," ACS Applied Materials & Interfaces, 10(41), pp. 34828-34833.
[6] Palanivel, S., Sidhar, H., and Mishra, R. S., 2015, "Friction Stir Additive Manufacturing: Route to High Structural Performance," JOM, 67(3), pp. 616-621.
[7] Tumbleston, J. R., Shirvanyants, D., Ermoshkin, N., Janusziewicz, R., Johnson, A. R., Kelly, D., Chen, K., Pinschmidt, R., Rolland, J. P., Ermoshkin, A., Samulski, E. T., and DeSimone, J. M., 2015, "Continuous liquid interface production of 3D objects," Science, 347(6228), pp. 1349-1352.
[8] Gao, W., Zhang, Y., Ramanujan, D., Ramani, K., Chen, Y., Williams, C. B., Wang, C. C. L., Shin, Y. C., Zhang, S., and Zavattieri, P. D., 2015, "The status, challenges, and future of additive manufacturing in engineering," Computer-Aided Design, 69, pp. 65-89.
[9] Tie, A., 2018, "Researchers expand breakthroughs in 3D printing Kapton, the “ultimate” polymer," https://vtnews.vt.edu/articles/2018/11/mii-direct-ink-write-kapton.html.
[10] Williams, C. B., Mistree, F., and Rosen, D. W., 2011, "A Functional Classification Framework for the Conceptual Design of Additive Manufacturing Technologies," Journal of Mechanical Design, 133(12).
[11] Hon, K. K. B., Li, L., and Hutchings, I. M., 2008, "Direct writing technology—Advances and developments," CIRP Annals, 57(2), pp. 601-620.
[12] Hoey, J. M., Lutfurakhmanov, A., Schulz, D. L., and Akhatov, I. S., 2012, "A review on aerosol-based direct-write and its applications for microelectronics," Journal of Nanotechnology, 2012.
[13] Teh, K. S., 2017, "Additive direct-write microfabrication for MEMS: A review," Frontiers of Mechanical Engineering, 12(4), pp. 490-509.
[14] Renn, M. J., King, B. H., Giridharan, M. G., and Sheu, J.-C., 2010, "Direct write# system," U. S. P. a. T. Office, ed., Google Patents.
[15] Hoey, J. M., Akhatov, I. S., Swenson, O. F., and Schulz, D. L., 2009, "Convergent-divergent-convergent nozzle focusing of aerosol particles for micron-scale direct writing," U. S. P. a. T. Office, ed., Google Patents, U.S.A.
[16] Qi, L., McMurry, P. H., Norris, D. J., and Girshick, S. L., 2010, "Micropattern Deposition of Colloidal Semiconductor Nanocrystals by Aerodynamic Focusing," Aerosol Science and Technology, 44(1), pp. 55-60.
[17] Papyrin, A., Kosarev, V., Klinkov, S., Alkhimov, A., and Fomin, V. M., 2006, Cold spray technology, Elsevier.

[18] Smith, M., Choi, Y. S., Boughey, C., and Kar-Narayan, S., 2017, "Controlling and assessing the quality of aerosol jet printed features for large area and flexible electronics," Flexible and Printed Electronics, 2(1), p. 015004.
[19] Binder, S., Glatthaar, M., and Rädlein, E., 2014, "Analytical Investigation of Aerosol Jet Printing," Aerosol Science and Technology, 48(9), pp. 924-929.
[20] Gupta, A. A., Bolduc, A., Cloutier, S. G., and Izquierdo, R., "Aerosol Jet Printing for printed electronics rapid prototyping," Proc. 2016 IEEE International Symposium on Circuits and Systems (ISCAS), pp. 866-869.
[21] Mahajan, A., Frisbie, C. D., and Francis, L. F., 2013, "Optimization of Aerosol Jet Printing for High-Resolution, High-Aspect Ratio Silver Lines," ACS Applied Materials & Interfaces, 5(11), pp. 4856-4864.
[22] Zhao, D., Liu, T., Park, J. G., Zhang, M., Chen, J.-M., and Wang, B., 2012, "Conductivity enhancement of aerosol-jet printed electronics by using silver nanoparticles ink with carbon nanotubes," Microelectronic Engineering, 96, pp. 71-75.
[23] Jabari, E., and Toyserkani, E., 2016, "Aerosol-Jet printing of highly flexible and conductive graphene/silver patterns," Materials Letters, 174, pp. 40-43.
[24] Tait, J. G., Witkowska, E., Hirade, M., Ke, T.-H., Malinowski, P. E., Steudel, S., Adachi, C., and Heremans, P., 2015, "Uniform Aerosol Jet printed polymer lines with 30µm width for 140ppi resolution RGB organic light emitting diodes," Organic Electronics, 22, pp. 40-43.
[25] Williams, N. X., Watson, N., Joh, D. Y., Chilkoti, A., and Franklin, A. D., 2020, "Aerosol jet printing of biological inks by ultrasonic delivery," Biofabrication, 12(2), p. 025004.
[26] Bruneaux, J., Therriault, D., and Heuzey, M.-C., 2008, "Micro-extrusion of organic inks for direct-write assembly," Journal of Micromechanics and Microengineering, 18(11), p. 115020.
[27] Li, B., Clark, P. A., and Church, K. H., "Robust Direct-Write Dispensing Tool and Solutions for Micro/Meso-Scale Manufacturing and Packaging," Proc. ASME 2007 International Manufacturing Science and Engineering Conference, pp. 715-721.
[28] Gibson, I., Rosen, D., and Stucker, B., 2015, "Direct Write Technologies," Additive Manufacturing Technologies: 3D Printing, Rapid Prototyping, and Direct Digital Manufacturing, I. Gibson, D. Rosen, and B. Stucker, eds., Springer New York, New York, NY, pp. 269-291.
[29] Hutchings, I. M., and Martin, G. D., 2012, Inkjet technology for digital fabrication, John Wiley & Sons.
[30] Derby, B., 2010, "Inkjet Printing of Functional and Structural Materials: Fluid Property Requirements, Feature Stability, and Resolution," Annual Review of Materials Research, 40(1), pp. 395-414.
[31] Delrot, P., Modestino, M. A., Gallaire, F., Psaltis, D., and Moser, C., 2016, "Inkjet Printing of Viscous Monodisperse Microdroplets by Laser-Induced Flow Focusing," Physical Review Applied, 6(2), p. 024003.
[32] Lee, T., Baac, H. W., Ok, J. G., Youn, H. S., and Guo, L. J., 2015, "Nozzle-Free Liquid Microjetting via Homogeneous Bubble Nucleation," Physical Review Applied, 3(4), p. 044007.
[33] Piqué, A., Auyeung, R., Fitzgerald, J., Chrisey, D. B., Wu, H.-D., Kydd, P., and Richard, D. L., 2006, "Direct-write laser transfer and processing," Google Patents, U.S.A.
[34] Schoner, C., Tuchscherer, A., Blaudeck, T., Jahn, S. F., Baumann, R. R., and Lang, H., 2013, "Particle-free gold metal–organic decomposition ink for inkjet printing of gold structures," Thin Solid Films, 531, pp. 147-151.
[35] Choi, Y., Seong, K.-d., and Piao, Y., 2019, "Metal–Organic Decomposition Ink for Printed Electronics," Advanced Materials Interfaces, 6(20), p. 1901002.
[36] Shen, A., Caldwell, D., Ma, A. W. K., and Dardona, S., 2018, "Direct write fabrication of high-density parallel silver interconnects," Additive Manufacturing, 22, pp. 343-350.

[37] Ahn, B. Y., Duoss, E. B., Motala, M. J., Guo, X., Park, S.-I., Xiong, Y., Yoon, J., Nuzzo, R. G., Rogers, J. A., and Lewis, J. A., 2009, "Omnidirectional Printing of Flexible, Stretchable, and Spanning Silver Microelectrodes," Science, 323(5921), p. 1590.
[38] Ladd, C., So, J.-H., Muth, J., and Dickey, M. D., 2013, "3D Printing of Free Standing Liquid Metal Microstructures," Advanced Materials, 25(36), pp. 5081-5085.
[39] Ren, L., Zhou, X., Song, Z., Zhao, C., Liu, Q., Xue, J., and Li, X., 2017, "Process Parameter Optimization of Extrusion-Based 3D Metal Printing Utilizing PW–LDPE–SA Binder System," MDPI, 10.
[40] Fu, K., Wang, Y., Yan, C., Yao, Y., Chen, Y., Dai, J., Lacey, S., Wang, Y., Wan, J., Li, T., Wang, Z., Xu, Y., and Hu, L., 2016, "Graphene Oxide-Based Electrode Inks for 3D-Printed Lithium-Ion Batteries," Advanced Materials, 28(13), pp. 2587-2594.
[41] Secor, E. B., and Hersam, M. C., 2015, "Emerging Carbon and Post-Carbon Nanomaterial Inks for Printed Electronics," The Journal of Physical Chemistry Letters, 6(4), pp. 620-626.
[42] Zhou, N., Liu, C., Lewis, J. A., and Ham, D., 2017, "Gigahertz Electromagnetic Structures via Direct Ink Writing for Radio-Frequency Oscillator and Transmitter Applications," Advanced Materials, 29(15), p. 1605198.
[43] Adams, J. J., Duoss, E. B., Malkowski, T. F., Motala, M. J., Ahn, B. Y., Nuzzo, R. G., Bernhard, J. T., and Lewis, J. A., 2011, "Conformal Printing of Electrically Small Antennas on Three-Dimensional Surfaces," Advanced Materials, 23(11), pp. 1335-1340.
[44] Seifert, T., Sowade, E., Roscher, F., Wiemer, M., Gessner, T., and Baumann, R. R., 2015, "Additive Manufacturing Technologies Compared: Morphology of Deposits of Silver Ink Using Inkjet and Aerosol Jet Printing," Industrial & Engineering Chemistry Research, 54(2), pp. 769-779.
[45] Eckstein, R., Hernandez-Sosa, G., Lemmer, U., and Mechau, N., 2014, "Aerosol jet printed top grids for organic optoelectronic devices," Organic Electronics, 15(9), pp. 2135-2140.
[46] Jabari, E., and Toyserkani, E., 2015, "Micro-scale aerosol-jet printing of graphene interconnects," Carbon, 91, pp. 321-329.
[47] Renn, M. J., Schrandt, M., Renn, J., and Feng, J. Q., 2017, "Localized Laser Sintering of Metal Nanoparticle Inks Printed with Aerosol Jet® Technology for Flexible Electronics," Journal of Microelectronics and Electronic Packaging, 14(4), pp. 132-139.
[48] Navratil, J., Hamacek, A., Reboun, J., and Soukup, R., "Perspective methods of creating conductive paths by Aerosol Jet Printing technology," Proc. 2015 38th International Spring Seminar on Electronics Technology (ISSE), pp. 36-39.
[49] Kopola, P., Zimmermann, B., Filipovic, A., Schleiermacher, H.-F., Greulich, J., Rousu, S., Hast, J., Myllylä, R., and Würfel, U., 2012, "Aerosol jet printed grid for ITO-free inverted organic solar cells," Solar Energy Materials and Solar Cells, 107, pp. 252-258.
[50] Magdassi, S., Grouchko, M., and Kamyshny, A., 2010, "Copper Nanoparticles for Printed Electronics: Routes Towards Achieving Oxidation Stability," Materials, 3(9), pp. 4626-4638.
[51] Zhang, H., Choi, J. P., Moon, S. K., and Ngo, T. H., 2020, "A hybrid multi-objective optimization of aerosol jet printing process via response surface methodology," Additive Manufacturing, 33, p. 101096.
[52] Padovani, S., Sinesi, S., Priante, S., Antonipieri, M., Negro, A. D., Zoellmer, V., Maiwald, M., and Hedges, M., "New method for head-up display realization by mean of Chip On Board and Aerosol Jet process," Proc. 3rd Electronics System Integration Technology Conference ESTC, pp. 1-3.
[53] Xu, B. L., Zhao, Y., Yu, L. K., Xu, B., Zhang, H. E., Lv, W. L., and Sun, D. H., 2013, "Aerosol Jet Printing on Radio Frequency IDentification Tag Applications," Key Engineering Materials, 562-565, pp. 1417-1421.
[54] Zhao, D., Liu, T., Zhang, M., Liang, R., and Wang, B., 2012, "Fabrication and characterization of aerosol-jet printed strain sensors for multifunctional composite structures," Smart Materials and Structures, 21(11), p. 115008.

[55] Wilkinson, N. J., Smith, M. A. A., Kay, R. W., and Harris, R. A., 2019, "A review of aerosol jet printing—a non-traditional hybrid process for micro-manufacturing," The International Journal of Advanced Manufacturing Technology, 105(11), pp. 4599-4619.
[56] Paulsen, J. A., Renn, M., Christenson, K., and Plourde, R., "Printing conformal electronics on 3D structures with Aerosol Jet technology," Proc. 2012 Future of Instrumentation International Workshop (FIIW) Proceedings, pp. 1-4.
[57] Gu, Y., Hines, D. R., Yun, V., Antoniak, M., and Das, S., 2017, "Aerosol-Jet Printed Fillets for Well-Formed Electrical Connections between Different Leveled Surfaces," Advanced Materials Technologies, 2(11), p. 1700178.
[58] Joe Lopes, A., MacDonald, E., and Wicker Ryan, B., 2012, "Integrating stereolithography and direct print technologies for 3D structural electronics fabrication," Rapid Prototyping Journal, 18(2), pp. 129-143.
[59] MacDonald, E., and Wicker, R., 2016, "Multiprocess 3D printing for increasing component functionality," Science, 353(6307), p. aaf2093.
[60] Lu, Y., Vatani, M., and Choi, J.-W., 2013, "Direct-write/cure conductive polymer nanocomposites for 3D structural electronics," Journal of Mechanical Science and Technology, 27(10), pp. 2929-2934.
[61] Jang, S. H., Oh, S. T., Lee, I. H., Kim, H.-C., and Cho, H. Y., 2015, "3-dimensional circuit device fabrication process using stereolithography and direct writing," International Journal of Precision Engineering and Manufacturing, 16(7), pp. 1361-1367.
[62] Flowers, P. F., Reyes, C., Ye, S., Kim, M. J., and Wiley, B. J., 2017, "3D printing electronic components and circuits with conductive thermoplastic filament," Additive Manufacturing, 18, pp. 156-163.
[63] Roach, D. J., Hamel, C. M., Dunn, C. K., Johnson, M. V., Kuang, X., and Qi, H. J., 2019, "The m4 3D printer: A multi-material multi-method additive manufacturing platform for future 3D printed structures," Additive Manufacturing, 29, p. 100819.
[64] 2018, "DragonFly Pro System Precision Additive Manufacturing of Printed Electronics."
[65] Schleicher, M., Matthes, M., and Platz, H., "Potential and challenges of additive manufactured substrates and auxiliary material for electronics," Proc. PCIM Europe digital days 2020; International Exhibition and Conference for Power Electronics, Intelligent Motion, Renewable Energy and Energy Management, pp. 1-6.
[66] 2020, "Image Gallery DragonFly System," https://www.nano-di.com/image-gallery-of-3d-printing-on-the-dragonfly-pro.
[67] Mannoor, M. S., Jiang, Z., James, T., Kong, Y. L., Malatesta, K. A., Soboyejo, W. O., Verma, N., Gracias, D. H., and McAlpine, M. C., 2013, "3D Printed Bionic Ears," Nano Letters, 13(6), pp. 2634-2639.
[68] Ketterl, T. P., Vega, Y., Arnal, N. C., Stratton, J. W. I., Rojas-Nastrucci, E. A., Córdoba-Erazo, M. F., Abdin, M. M., Perkowski, C. W., Deffenbaugh, P. I., Church, K. H., and Weller, T. M., 2015, "A 2.45 GHz Phased Array Antenna Unit Cell Fabricated Using 3-D Multi-Layer Direct Digital Manufacturing," IEEE Transactions on Microwave Theory and Techniques, 63(12), pp. 4382-4394.
[69] Liang, M., Shemelya, C., MacDonald, E., Wicker, R., and Xin, H., 2015, "3-D Printed Microwave Patch Antenna via Fused Deposition Method and Ultrasonic Wire Mesh Embedding Technique," IEEE Antennas and Wireless Propagation Letters, 14, pp. 1346-1349.
[70] Pa, P., Larimore, Z., Parsons, P., and Mirotznik, M., 2015, "Multi-material additive manufacturing of embedded low-profile antennas," Electronics Letters, 51(20), pp. 1561-1562.
[71] Shemelya, C., Zemba, M., Liang, M., Yu, X., Espalin, D., Wicker, R., Xin, H., and MacDonald, E., 2016, "Multi-layer archimedean spiral antenna fabricated using polymer extrusion 3D printing," Microwave and Optical Technology Letters, 58(7), pp. 1662-1666.
[72] Muth, J. T., Vogt, D. M., Truby, R. L., Mengüç, Y., Kolesky, D. B., Wood, R. J., and Lewis, J. A., 2014, "Embedded 3D Printing of Strain Sensors within Highly Stretchable Elastomers," Advanced Materials, 26(36), pp. 6307-6312.

[73] Shemelya, C., Cedillos, F., Aguilera, E., Espalin, D., Muse, D., Wicker, R., and MacDonald, E., 2015, "Encapsulated Copper Wire and Copper Mesh Capacitive Sensing for 3-D Printing Applications," IEEE Sensors Journal, 15(2), pp. 1280-1286.
[74] Wu, S.-Y., Yang, C., Hsu, W., and Lin, L., 2015, "3D-printed microelectronics for integrated circuitry and passive wireless sensors," Microsystems & Nanoengineering, 1(1), p. 15013.
[75] Sun, K., Wei, T.-S., Ahn, B. Y., Seo, J. Y., Dillon, S. J., and Lewis, J. A., 2013, "3D Printing of Interdigitated Li-Ion Microbattery Architectures," Advanced Materials, 25(33), pp. 4539-4543.
[76] Saleh, M. S., Li, J., Park, J., and Panat, R., 2018, "3D printed hierarchically-porous microlattice electrode materials for exceptionally high specific capacity and areal capacity lithium ion batteries," Additive Manufacturing, 23, pp. 70-78.
[77] Pang, Y., Cao, Y., Chu, Y., Liu, M., Snyder, K., MacKenzie, D., and Cao, C., 2020, "Additive Manufacturing of Batteries," Advanced Functional Materials, 30(1), p. 1906244.
[78] Marshall, W. M., Stegeman, J. D., Zemba, M., MacDonald, E., Shemelya, C., Wicker, R., Kwas, A., and Kief, C., 2015, "Using Additive Manufacturing to Print a CubeSat Propulsion System," 51st AIAA/SAE/ASEE Joint Propulsion Conference, American Institute of Aeronautics and Astronautics.
[79] Cai, F., Pavlidis, S., Papapolymerou, J., Chang, Y. H., Wang, K., Zhang, C., and Wang, B., "Aerosol jet printing for 3-D multilayer passive microwave circuitry," Proc. 2014 44th European Microwave Conference, pp. 512-515.
[80] Deffenbaugh, P. I., Weller, T. M., and Church, K. H., 2015, "Fabrication and Microwave Characterization of 3-D Printed Transmission Lines," IEEE Microwave and Wireless Components Letters, 25(12), pp. 823-825.
[81] Qayyum, J. A., Abt, M., Roch, A., Ulusoy, A. C., and Papapolymerou, J., "Ultra wideband 3D interconnects using aerosol jet printing up to 110 GHz," Proc. 2017 12th European Microwave Integrated Circuits Conference (EuMIC), pp. 372-375.
[82] Macdonald, E., Salas, R., Espalin, D., Perez, M., Aguilera, E., Muse, D., and Wicker, R. B., 2014, "3D Printing for the Rapid Prototyping of Structural Electronics," IEEE Access, 2, pp. 234-242.
[83] Allen, G. L., Bayles, R. A., Gile, W. W., and Jesser, W. A., 1986, "Small particle melting of pure metals," Thin Solid Films, 144(2), pp. 297-308.
[84] Buffat, P., and Borel, J. P., 1976, "Size effect on the melting temperature of gold particles," Physical Review A, 13(6), pp. 2287-2298.
[85] Perelaer, J., Smith, P. J., Mager, D., Soltman, D., Volkman, S. K., Subramanian, V., Korvink, J. G., and Schubert, U. S., 2010, "Printed electronics: the challenges involved in printing devices, interconnects, and contacts based on inorganic materials," Royal Society of Chemistry, 20, pp. 8446-8453.
[86] Degtyarev, M. V., Chashchukhina, T. I., Voronova, L. M., Patselov, A. M., and Pilyugin, V. P., 2007, "Influence of the relaxation processes on the structure formation in pure metals and alloys under high-pressure torsion," Acta Materialia, 55(18), pp. 6039-6050.
[87] Merilampi, S., Laine-Ma, T., and Ruuskanen, P., 2009, "The characterization of electrically conductive silver ink patterns on flexible substrates," Microelectronics Reliability, 49(7), pp. 782-790.
[88] Jang, Y.-R., Joo, S.-J., Chu, J.-H., Uhm, H.-J., Park, J.-W., Ryu, C.-H., Yu, M.-H., and Kim, H.-S., 2020, "A Review on Intense Pulsed Light Sintering Technologies for Conductive Electrodes in Printed Electronics," International Journal of Precision Engineering and Manufacturing-Green Technology.
[89] Jang, Y.-R., Ryu, C.-H., Hwang, Y.-T., and Kim, H.-S., 2020, "Optimization of Intense Pulsed Light Sintering Considering Dimensions of Printed Cu Nano/Micro-paste Patterns for Printed Electronics," International Journal of Precision Engineering and Manufacturing-Green Technology.
[90] Mireles, J., Kim, H.-C., Hwan Lee, I., Espalin, D., Medina, F., MacDonald, E., and Wicker, R., 2013, "Development of a Fused Deposition Modeling System for Low Melting Temperature Metal Alloys," Journal of Electronic Packaging, 135(1).

[91] Wild, A., 2014, "Integration of Functional Circuits into FDM Parts," Advanced Materials Research, 1038, pp. 29-33.
[92] H, L. B., B, L. H., and Z, L. H., 2018, "Additive manufacturing frontier: 3D printing electronics," Opto-Electronic Advances, 1(1).
[93] Kim, J.-H., Kim, K.-S., Jang, K.-R., Jung, S.-B., and Kim, T.-S., 2015, "Enhancing Adhesion of Screen-Printed Silver Nanopaste Films," Advanced Materials Interfaces, 2(13), p. 1500283.
[94] Jeon, E.-B., Joo, S.-J., Ahn, H., and Kim, H.-S., 2016, "Two-step flash light sintering process for enhanced adhesion between copper complex ion/silane ink and a flexible substrate," Thin Solid Films, 603, pp. 382-390.
[95] Anton Georgiev, D. D., Erinche Spassova, Jacob Assa, Peter Dineff and Gencho Danev, 2012, "Chemical and Physical Properties of Polyimides: Biomedical and Engineering Applications," https://www.intechopen.com/books/high-performance-polymers-polyimides-based-from-chemistry-to-applications/chemical-and-physical-properties-of-polyimides-biomedical-and-engineering-applications.
[96] "Kapton Polyimide Films Kapton HN," https://www.dupont.com/products/kapton-hn.html.
[97] Takahashi, Y., Iijima, M., Inagawa, K., and Itoh, A., 1987, "Synthesis of aromatic polyimide film by vacuum deposition polymerization," Journal of Vacuum Science & Technology A, 5(4), pp. 2253-2256.
[98] "Sunshield Membrane Coatings," https://jwst.nasa.gov/content/about/innovations/coating.html.
[99] Deng, D., Chen, Y., and Zhou, C., "Investigation on PEEK fabrication using Mask-image-projection-based Stereolithography," Proc. Annual Solid Free Form Fabrication Symposium.
[100] Bagsik, A., Schöppner, V., and Klemp, E., "FDM part quality manufactured with Ultem* 9085," Proc. 14th international scientific conference on polymeric materials, pp. 307-315.
[101] Kishore, V., Chen, X., Ajinjeru, C., Hassen, A. A., Lindahl, J. M., Failla, J., Kunc, V., and Duty, C. E., 2016, "Additive manufacturing of high performance semicrystalline thermoplastics and their composites," Oak Ridge National Lab.(ORNL), Oak Ridge, TN (United States).
[102] Shrivastava, A., 2018, "3 - Plastic Properties and Testing," Introduction to Plastics Engineering, A. Shrivastava, ed., William Andrew Publishing, pp. 49-110.
[103] Chou, Y.-H., Jeng, M.-J., Lee, Y.-H., and Jan, Y.-G., 2008, "Measurement of RF PCB dielectric properties and losses," Progress In Electromagnetics Research, 4, pp. 139-148.
[104] Yamacli, S., Ozdemir, C., and Akdagli, A., 2008, "A method for determining the dielectric constant of microwave PCB substrates," International Journal of Infrared and Millimeter Waves, 29(2), pp. 207-216.
[105] Huntsberger, J. R., 1964, "The Relationship between Wetting and Adhesion," Contact Angle, Wettability, and Adhesion, AMERICAN CHEMICAL SOCIETY, pp. 180-188.
[106] Dang, M. C., Dang, T. M. D., and Fribourg-Blanc, E., 2014, "Silver nanoparticles ink synthesis for conductive patterns fabrication using inkjet printing technology," Advances in Natural Sciences: Nanoscience and Nanotechnology, 6(1), p. 015003.
[107] Perez, K. B., and Williams, C. B., "Characterization of in-situ conductive paste extrusion on polyjet substrates," Proc. International solid freeform fabrication symposium, Austin (TX).
[108] Singh, Y., 2013, "Electrical Resistivity Measurements: a Review," International Journal of Modern Physics Conference Series, 22, pp. 745-756.
[109] King, B., and Renn, M., "Aerosol Jet direct write printing for mil-aero electronic applications," Proc. Lockheed Martin Palo Alto Colloquia, Palo Alto, CA.
[110] Rahman, M. T., McCloy, J., Ramana, C. V., and Panat, R., 2016, "Structure, electrical characteristics, and high-temperature stability of aerosol jet printed silver nanoparticle films," Journal of Applied Physics, 120(7), p. 075305.
[111] Campo, E. A., "4.4.6 Dielectric Strength (ASTM D-149)," Selection of Polymeric Materials - How to Select Design Properties from Different Standards, William Andrew Publishing/Plastics Design Library, p. 143.

[112] Honeychurch, K. C., 2012, "13 - Printed thick-film biosensors," Printed Films, M. Prudenziati, and J. Hormadaly, eds., Woodhead Publishing, pp. 366-409.
[113] Joshi, J. H., Kanchan, D. K., Joshi, M. J., Jethva, H. O., and Parikh, K. D., 2017, "Dielectric relaxation, complex impedance and modulus spectroscopic studies of mix phase rod like cobalt sulfide nanoparticles," Materials Research Bulletin, 93, pp. 63-73.
[114] Lanfredi, S., Gênova, D. H. M., Brito, I. A. O., Lima, A. R. F., and Nobre, M. A. L., 2011, "Structural characterization and Curie temperature determination of a sodium strontium niobate ferroelectric nanostructured powder," Journal of Solid State Chemistry, 184(5), pp. 990-1000.
[115] Nobre, M. A. L., and Lanfredi, S., 2003, "Dielectric spectroscopy on Bi3Zn2Sb3O14 ceramic: an approach based on the complex impedance," Journal of Physics and Chemistry of Solids, 64(12), pp. 2457-2464.
[116] Oh, J., Moon, T., Kim, T.-G., Kim, C., Lee, J. H., Lee, S. Y., and Park, B., 2007, "The dependence of dielectric properties on the thickness of (Ba,Sr)TiO3 thin films," Current Applied Physics, 7(2), pp. 168-171.
[117] 2017, "ULTEM RESIN 1010."
[118] "Microstrip and Stripline Design, Analog Devices MT-094 Tutorial."

Appendix A

Table A.1: Full resistivity data of the heat treated DIW printed silver ink traces.

Trial Temperature (°C)	Resistance (Ω)	Trace Length (mm)	Area 25% (mm^2)	Area 50% (mm^2)	Area 75% (mm^2)	Area Avg (mm^2)	Resistivity (Ohm-m)	Resistivity X Bulk Silver
160-1	0.330	35.0	0.0242	0.0242	0.0238	0.0241	2.27E-07	14.27
160-2	0.343	35.0	0.0250	0.0237	0.0240	0.0242	2.37E-07	14.93
160-3	0.352	35.0	0.0252	0.0246	0.0243	0.0247	2.48E-07	15.61
200-1	0.266	35.0	0.0270	0.0249	0.0245	0.0255	1.94E-07	12.19
200-2	0.258	35.0	0.0259	0.0251	0.0252	0.0254	1.87E-07	11.77
200-3	0.265	35.0	0.0260	0.0254	0.0258	0.0257	1.95E-07	12.26
250-1	0.190	35.0	0.0243	0.0238	0.0234	0.0238	1.29E-07	8.13
250-2	0.170	35.0	0.0231	0.0231	0.0231	0.0231	1.12E-07	7.06
250-3	0.173	35.0	0.0242	0.0238	0.0238	0.0240	1.18E-07	7.45
300-1	0.070	35.0	0.0198	0.0197	0.0205	0.0200	4.00E-08	2.52
300-2	0.067	35.0	0.0213	0.0203	0.0199	0.0205	3.92E-08	2.47
300-3	0.078	35.0	0.0201	0.0204	0.0203	0.0203	4.52E-08	2.84
350-1	0.063	35.0	0.0208	0.0211	0.0206	0.0209	3.76E-08	2.36
350-2	0.067	35.0	0.0203	0.0198	0.0199	0.0200	3.82E-08	2.41
350-3	0.067	35.0	0.0199	0.0199	0.0196	0.0198	3.79E-08	2.38
400-1	0.068	35.0	0.0183	0.0195	0.0187	0.0189	3.66E-08	2.30
400-2	0.073	35.0	0.0179	0.0170	0.0166	0.0171	3.57E-08	2.25
400-3	0.067	35.0	0.0188	0.0192	0.0196	0.0192	3.67E-08	2.31

Table A.2 Full resistivity data of the heat-treated AJ silver ink traces.

Trial Temperature (°C)	Resistance (Ω)	Trace Length	Area 25% (mm^2)	Area 50% (mm^2)	Area 75% (mm^2)	Area Avg (mm^2)	Resistivity (Ohm-m)	Resistivity X Bulk Silver
200-1	41.543	35.0	6.496E-05	7.682E-05	6.963E-05	7.047E-05	8.364E-08	5.261
200-2	37.209	35.0	6.656E-05	8.623E-05	8.429E-05	7.903E-05	8.401E-08	5.284
200-3	37.422	35.0	6.773E-05	7.988E-05	8.674E-05	7.812E-05	8.352E-08	5.253
250-1	18.439	35.0	8.314E-05	9.420E-05	7.607E-05	8.447E-05	4.450E-08	2.799
250-2	18.268	35.0	7.590E-05	8.730E-05	7.330E-05	7.883E-05	4.115E-08	2.588
250-3	19.93	35.0	1.034E-04	6.707E-05	8.040E-05	8.363E-05	4.762E-08	2.995
300-1	13.056	35.0	7.706E-05	7.055E-05	8.047E-05	7.603E-05	2.836E-08	1.784
300-2	12.501	35.0	7.248E-05	9.067E-05	5.011E-05	7.109E-05	2.539E-08	1.597
300-3	12.601	35.0	7.328E-05	6.859E-05	1.184E-04	8.676E-05	3.124E-08	1.965
350-1	13.182	35.0	7.093E-05	8.161E-05	6.346E-05	7.200E-05	2.712E-08	1.705
350-2	31.712	35.0	2.792E-05	3.360E-05	3.463E-05	3.205E-05	2.904E-08	1.826
350-3	17.023	35.0	6.036E-05	6.438E-05	6.073E-05	6.182E-05	3.007E-08	1.891
400-1	17.835	35.0	5.452E-05	6.841E-05	7.375E-05	6.556E-05	3.341E-08	2.101
400-2	17.094	35.0	6.864E-05	7.631E-05	6.383E-05	6.959E-05	3.399E-08	2.138
400-3	15.888	35.0	7.916E-05	6.517E-05	8.526E-05	7.653E-05	3.474E-08	2.185

Table A.3 Full resistivity data of the heat-treated DIW printed silver ink traces on all-aromatic polyimide film.

Trial Temperatu	Resistance (Ω)	Trace Length	Area 25% (mm^2)	Area 50% (mm^2)	Area 75% (mm^2)	Area Avg (mm^2)	Resistivity (Ohm-m)	Resistivity X Bulk Silver
300-1	0.068	35.0	0.0184	0.0187	0.0190	0.0187	3.63E-08	2.286
300-2	0.068	35.0	0.0172	0.0192	0.0190	0.0187	3.63E-08	2.286
300-3	0.070	35.0	0.0170	0.0177	0.0176	0.0174	3.48E-08	2.191
325-1	0.061	35.0	0.0205	0.0202	0.0191	0.0199	3.48E-08	2.186
325-2	0.062	35.0	0.0195	0.0198	0.0194	0.0195	3.46E-08	2.178
325-3	0.062	35.0	0.0183	0.0178	0.0184	0.0182	3.22E-08	2.027
350-1	0.069	35.0	0.0192	0.0192	0.0188	0.0191	3.76E-08	2.364
350-2	0.068	35.0	0.0194	0.0185	0.0189	0.0189	3.68E-08	2.315
350-3	0.070	35.0	0.0173	0.0186	0.0182	0.0180	3.60E-08	2.266
375-1	0.087	35.0	0.0131	0.0125	0.0151	0.0136	3.37E-08	2.119
375-2	0.083	35.0	0.0147	0.0142	0.0149	0.0146	3.47E-08	2.180
375-3	0.083	35.0	0.0146	0.0146	0.0146	0.0146	3.46E-08	2.177

Table A.4 Full resistivity data of the heat-treated AJ printed silver ink traces on all-aromatic polyimide film.

Trial Temperature (°C)	Resistance (Ω)	Trace Length	Area 25% (mm^2)	Area 50% (mm^2)	Area 75% (mm^2)	Area Avg (mm^2)	Resistivity (Ohm-m)	Resistivity X Bulk Silver
275-b	150.000	35.0	1.246E-05	1.044E-05	1.280E-05	1.190E-05	5.099E-08	3.207
275-m	45.865	35.0	3.516E-05	3.532E-05	3.500E-05	3.516E-05	4.607E-08	2.898
275-t	28.330	35.0	5.222E-05	4.683E-05	5.109E-05	5.005E-05	4.051E-08	2.548
300-1	45.212	35.0	2.608E-05	2.701E-05	2.536E-05	2.615E-05	3.378E-08	2.125
300-2	72.440	35.0	1.946E-05	1.623E-05	1.608E-05	1.726E-05	3.572E-08	2.247
300-3	34.950	35.0	3.362E-05	3.781E-05	4.192E-05	3.778E-05	3.773E-08	2.373
325-b	50.000	35.0	2.291E-05	3.147E-05	2.693E-05	2.710E-05	3.872E-08	2.435
325-m	38.124	35.0	4.101E-05	3.704E-05	3.970E-05	3.925E-05	4.275E-08	2.689
325-t	19.924	35.0	6.775E-05	6.244E-05	6.187E-05	6.402E-05	3.644E-08	2.292
350-b	21.020	35.0	4.484E-05	6.076E-05	5.972E-05	5.511E-05	3.310E-08	2.081
350-t	19.516	35.0	4.682E-05	5.140E-05	6.330E-05	5.384E-05	3.002E-08	1.888
350-t	16.890	35.0	5.953E-05	5.889E-05	6.777E-05	6.206E-05	2.995E-08	1.884

Table A.5 Contact angle measurements of CB028 silver ink on Dupont Kapton film and polyimide film.

Droplet #	Kapton Film After 1 Minute	Polyimide Film After 1 Minute	Kapton Film After 5 Minutes	Polyimide Film After 5 Minutes
1	64.9	54.4	53.6	54.8
2	52.2	51.5	51.6	50.9
3	52.8	49.7	50.6	49.5
4	60.4	51.5	54.7	49.0
5	53.7	49.8	52.0	46.4
6	52.2	55.6	51.5	55.4
7	52.4	52.6	50.3	55.5
8	51.3	54.8	51.6	52.6
9	52.7	56.3	52.4	54.6
10	52.8	51.9	51.8	52.9
Average	54.548	52.813	52.008	52.153
Std. Dev.	4.213	2.213	1.255	2.942

Appendix B

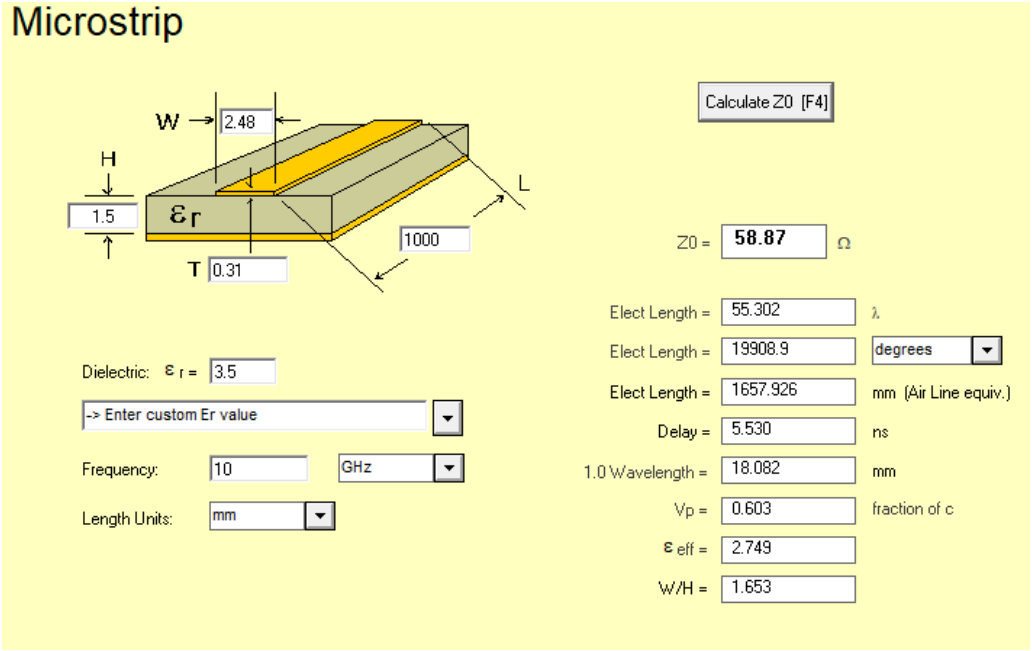

Figure B.1: AppCAD calculation of the characteristic impedance of the UV-DIW polyimide substrate microstrip processed at 200 °C.

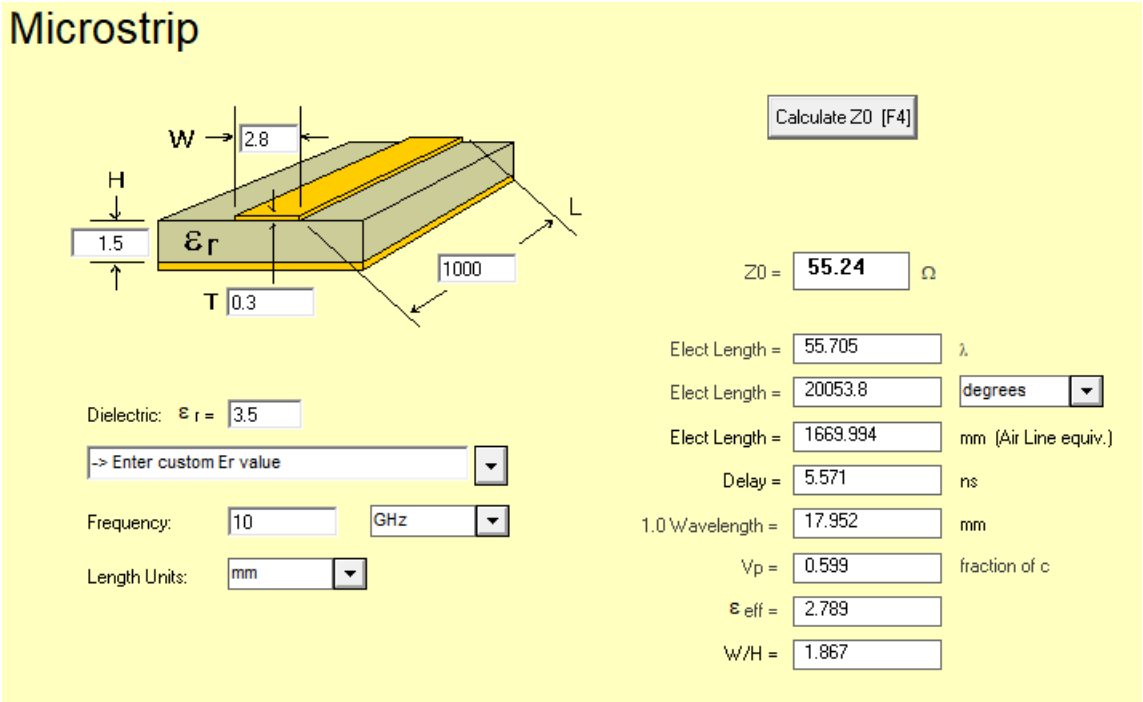

Figure B.2: AppCAD calculation of the characteristic impedance of the UV-DIW polyimide substrate microstrip processed at 400 °C.

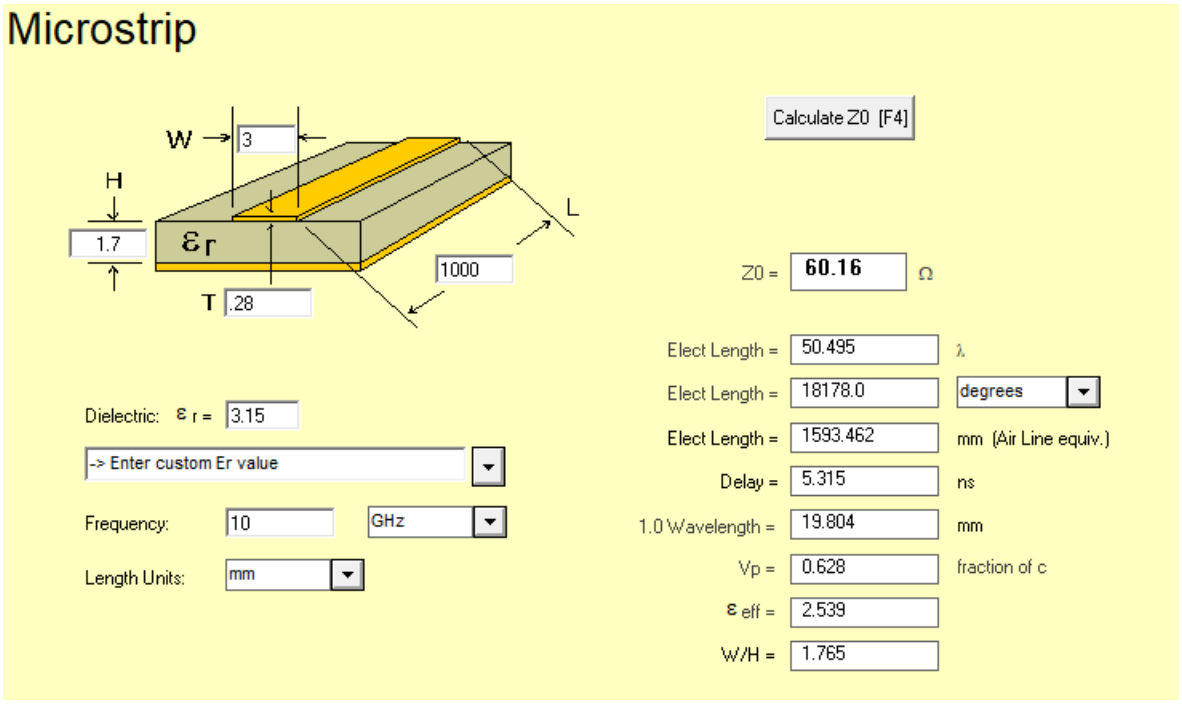

Figure B.3: AppCAD calculation of the characteristic impedance of the ULTEM 1010 substrate microstrip processed at 200 °C.